



This is a repository copy of *Recent progress in low-carbon binders*.

White Rose Research Online URL for this paper:
<http://eprints.whiterose.ac.uk/150089/>

Version: Accepted Version

Article:

Shi, C., Qu, B. and Provis, J.L. orcid.org/0000-0003-3372-8922 (2019) Recent progress in low-carbon binders. *Cement and Concrete Research*, 122. pp. 227-250. ISSN 0008-8846

<https://doi.org/10.1016/j.cemconres.2019.05.009>

Article available under the terms of the CC-BY-NC-ND licence
(<https://creativecommons.org/licenses/by-nc-nd/4.0/>).

Reuse

This article is distributed under the terms of the Creative Commons Attribution-NonCommercial-NoDerivs (CC BY-NC-ND) licence. This licence only allows you to download this work and share it with others as long as you credit the authors, but you can't change the article in any way or use it commercially. More information and the full terms of the licence here: <https://creativecommons.org/licenses/>

Takedown

If you consider content in White Rose Research Online to be in breach of UK law, please notify us by emailing eprints@whiterose.ac.uk including the URL of the record and the reason for the withdrawal request.



eprints@whiterose.ac.uk
<https://eprints.whiterose.ac.uk/>

1 **Recent Progress in Low-Carbon Binders**

2

3 Caijun Shi^{1*}, Bo Qu¹, John L. Provis²

4 ¹ College of Civil Engineering, Hunan University, Changsha 410082, China

5 ² Department of Materials Science & Engineering, University of Sheffield, Sheffield S1 3JD, UK

6

7

8 **Abstract:**

9

10 The development of low-carbon binders has been recognized as a means of reducing the carbon
11 footprint of the Portland cement industry, in response to growing global concerns over CO₂
12 emissions from the construction sector. This paper reviews recent progress in the three most
13 attractive low-carbon binders: alkali-activated, carbonate, and belite-ye'elimite-based binders.
14 Alkali-activated binders/materials were reviewed at the past two ICCC congresses, so this paper
15 focuses on some key developments of alkali-activated binders/materials since the last keynote
16 paper was published in 2015. Recent progress on carbonate and belite-ye'elimite-based binders
17 are also reviewed and discussed, as they are attracting more and more attention as essential
18 alternative low-carbon cementitious materials. These classes of binders have a clear role to play
19 in providing a sustainable future for global construction, as part of the available toolkit of cements.

20

21 **Keywords:** low-carbon cementitious binders; alkali-activated material; carbonated binders;
22 belite-ye'elimite binders; sustainability

23

24 *corresponding author: C. Shi (cshi@hnu.edu.cn)

25

26 **1. Introduction**

27 Growing concerns over the greenhouse emissions profile of the Portland cement and concrete
28 industry have led to a very high level of recent interest in the development of low-carbon binders
29 as alternatives to Portland-based cements. This paper reviews recent progress in the three most
30 prominent classes of low-carbon binders: alkali-activated or geopolymer, carbonate, and belite-
31 ye’elimite-based binders. Alkali-activated binders/materials were reviewed at the past two (13th
32 and 14th) International Congresses on the Chemistry of Cement (ICCC) [1, 2], and in discussing
33 these materials, this paper focuses on some of their key developments since the last keynote paper
34 was published in 2015 [2]. These include rheological properties, setting behavior, structural
35 characterization, dimensional stability, durability, and their applications. However, this paper does
36 not aim to provide a detailed overview with respect to all existing insights into these materials,
37 which can be obtained in other references including [3-5], but rather focuses on the most important
38 new information that has been obtained in the past 4 years. Recent progress on carbonate and
39 belite-ye’elimite-based binders will also be reviewed and discussed in detail, as these are
40 attracting more and more attention as essential parts of the ‘toolkit’ of alternative low-carbon
41 cementitious materials.

42

43 **2. Alkali-Activated Binders**

44 **2.1. Raw materials**

45 **2.1.1 Activators**

46 As numerous workers have promoted alkali-activated binders as a potentially low-carbon
47 cementing system during the past decades (see Section 2.11 for more detailed discussion of
48 advances in the environmental assessment of these materials), increased scrutiny has fallen on the
49 selection of the activator for use in these binders. This also has cost implications: the activator is
50 usually the most expensive component of an alkali-activated binder, particularly if it has been
51 produced at high purity for use in other industry sectors (which is the case for most commercial

52 alkali silicate solutions), where such high purity may be less important to its use in alkali-
53 activation. So, alternative routes to alkali-activation that do not require the use of large volumes
54 of commercial sodium silicate solutions have received serious recent attention. The production of
55 silicate activators from olivine [6] or from waste glass [7-10], and the use of biomass ashes as an
56 alkaline activator [11], have been established with some success.

57

58 The use of near-neutral salts as activators has also seen considerable advances in recent years.
59 This appears to be a pathway that is particularly attractive for production of cements based on
60 ground granulated blast furnace slag, which can be made to react and harden in a useful timeframe
61 by the addition of alkali carbonates or sulfates [12, 13]. In some cases, significant benefits can be
62 gained by using a calcined layered double hydroxide as a carbonate-binding mineral additive [14,
63 15], to accelerate the reaction of some slags with a modest magnesia content which would
64 otherwise not react sufficiently rapidly with near-neutral salt activators. The combination of
65 calcium hydroxide and potassium carbonate has also been shown to give very good performance
66 as an activator for kaolinite [16], offering a potentially very low-carbon emissions route to the
67 production of affordable binders without needing a clay calcination step.

68

69 **2.1.2 Precursors**

70 The selection of precursors available for use in alkali-activation has also broadened significantly
71 in recent years, with particular emphasis being placed upon the use of materials for which there
72 is not strong competition in demand from utilization in blends with Portland cement. For example,
73 calcined non-kaolinitic clays [17-20], palm oil fuel ash [21, 22] or other minerals [23-26], have
74 been shown to yield alkali-activated binder systems with technical properties that are attractive in
75 given applications. Various industrial by-products or wastes without current large-scale utilization
76 as supplementary cementitious materials have been tested and validated for use in alkali-activated
77 binders, including red mud [27-29] and various glassy wastes including slags, some of which can
78 benefit from thermal re-processing or modification to improve their reactivity before use [10, 30-
79 35]. Detailed work is also ongoing to better understand the reactivity of fly ashes under alkali-

80 activation conditions [36-39], and to valorize kaolinitic clay resources which are not of sufficient
81 purity for use in other applications such as ceramic whitewares or coatings [40-42]. Common to
82 many of these types of materials, the role of iron in alkali-activation precursors (and in the
83 resulting binders) is beginning to be understood to some degree [19, 43, 44]. However, a detailed
84 description of its reactivity and the structural implications of its inclusion in the binding gel still
85 remain very much elusive. This is an area in which further advances are expected – and needed –
86 in the coming years.

87
88 Some of the potential precursors described here and in the broader literature are only available in
89 commercially viable quantities in limited locations - but in the locations where they are available,
90 utilization in alkali-activated binders can be extremely attractive as a local solution to the needs
91 of the construction industry. This ability to achieve local specificity in materials design and
92 specification highlights one of the key strengths of alkali-activation, which is its ability to make
93 use of a wide (and ever-growing) range of materials as precursors. However, it also raises
94 challenges in standardization and specification, as it is almost impossible to write a prescriptive
95 recipe-based standard that covers such a broad set of potential material chemistries. This
96 highlights the need for performance-based specification of alkali-activated binders rather than
97 relying on a prescriptive approach; discussion will return to this point in Section 2.10 in
98 consideration of durability.

99

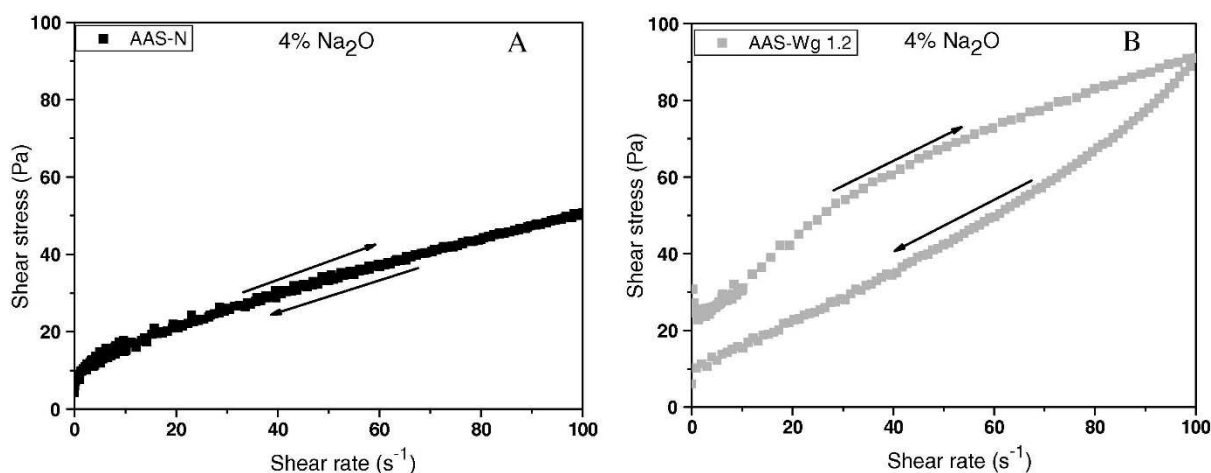
100 **2.2. Rheology**

101 An understanding of the rheological properties of alkali-activated cement pastes, mortars and
102 concretes is essential to ascertaining their consistency and workability, and consequently their
103 ease of casting or placement. In addition, the rheological properties of alkali-activated cement-
104 based materials have a strong influence on their microstructure, mechanical properties, and
105 durability. The identification and modeling of rheological characteristics of alkali-activated
106 materials (pastes, mortars and concretes) have been intensively studied since the last ICCI, as

107 this has been identified as an area with major practical importance (and challenges) for the field
108 application of these materials.

109
110 The rheological behavior of alkali-activated slag (AAS) pastes, activated with NaOH alone or in
111 combination with Na₂CO₃, was similar to the rheology observed in Portland cement pastes and
112 could be fitted by the Bingham model. Conversely, the AAS pastes activated with waterglass
113 (AAS-Wg) required description by the Herschel-Bulkley model, as shown in Fig. 1 [45]. Moreover,
114 their rheology depends on both the SiO₂/Na₂O ratio of waterglass and the Na₂O concentration of
115 the activator. The early-age formation of a C-S-H type gel in silicate-activated AAS due to the
116 reaction between silicate species in waterglass and Ca²⁺ as it dissolves from slag particles, and the
117 effect of this gel formation on the paste rheology, has been confirmed in several publications [3,
118 4].

119



120
121 **Figure 1. Shear stress versus shear rate curves showing paste hysteresis cycles: (A) NaOH-activated**
122 **paste (AASN); (B) waterglass-activated paste (SiO₂/Na₂O=1.2 in the activator; AAS-Wg).**
123 **Reproduced from [45].**

124
125 The high viscosity of alkali silicate-activated cements, sometimes also accompanied by a high
126 yield stress, is one of the critical challenges that hinder their wide application. Favier et al. [46]
127 identified that this high viscosity was intrinsically due to the use of a viscous alkaline silicate
128 activating solution, not controlled by interparticle contacts. Yang et al. [47] focused on
129 ameliorating the rheological performance of sodium silicate-activated fly ash/slag pastes using fly

130 ash microspheres as an inorganic dispersing agent. Rheology is also temperature-dependent;
131 Mehdizadeh and Najafi Kani [48] determined an “apparent activation energy” parameter from the
132 temperature dependence of the rheology of alkali-activated phosphorous slag (AAPS) paste, based
133 on the Arrhenius viscosity model, and determined an activation energy of $42 (\pm 3)$ kJ/mol for the
134 temperature range 10-40°C, which was of a similar magnitude to the equivalent parameter
135 determined for Portland cement pastes.

136

137 The nature of the mixing protocol has been identified to be a key determinant in AAS mortar and
138 concrete rheology. In a series of studies, the Bingham model gave a good fit for all the PC and
139 AAS mortars and concretes tested [49, 50]. A longer time of mixing had an adverse effect on
140 rheology, but gave a slight improvement in hardened performance. In AAS-Wg concrete, the
141 application of a longer mixing time can enhance the rheological behaviour and improve the
142 mechanical properties, as the input of mixing energy can partially break down the early-stage
143 microstructure to allow further reaction to continue. A longer mixing time raised the degree of
144 thixotropy in PC and in NaOH-activated slag concretes, which can be attributed to the formation
145 of fine particles induced by over-mixing, but decreased flocculation and lowered the degree of
146 thixotropy in sodium silicate-activated slag concrete.

147

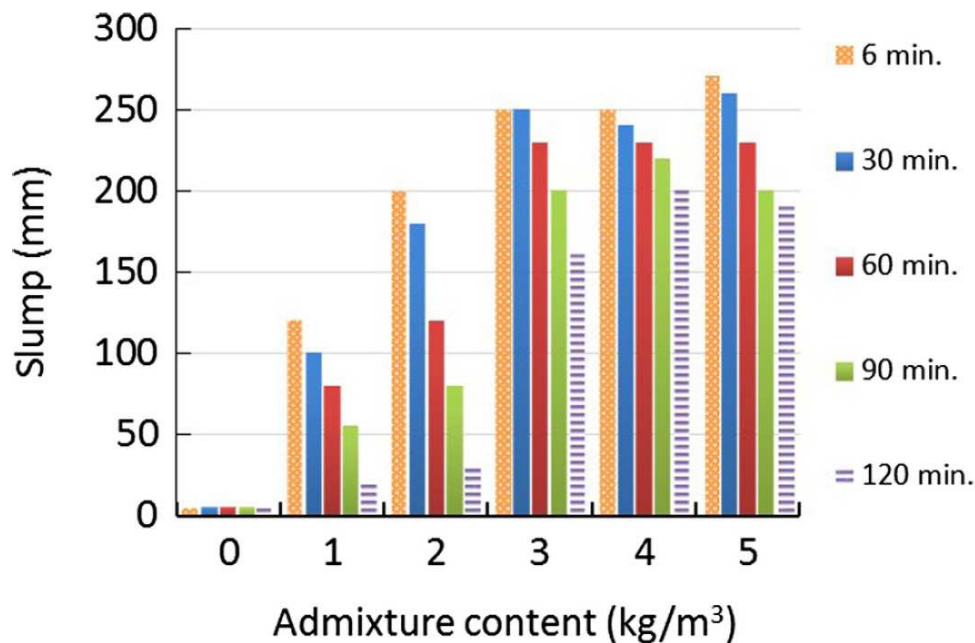
148 Alkali-activated materials (AAMs) have also been proven as useful model systems for the testing
149 and validation of mini-slump [51] and creeping sphere [52] rheological measurement methods.
150 Each different approach to rheological testing, including but not limited to these methods, brings
151 access to different shear rate regimes and different shear histories in the sample, which can enrich
152 the understanding of time-dependent rheological processes in a complex fluid. Understanding the
153 time-dependence of the rheology of alkali-activated pastes is not straightforward [53, 54], as these
154 materials tend to be thixotropic in addition to the reversible non-Newtonian aspects of their
155 behavior, but it is often challenging to distinguish true thixotropy from the gel structural evolution
156 that is also taking place during the rheological measurements.

157

158 **2.3. Chemical Admixtures**

159 Related to the challenges of rheology control in AAMs, it has been identified that it is critically
160 important to improve the use and applicability of admixtures to improve rheology under alkali-
161 activation conditions. Due to the very significant differences in surface chemistry, zeta potential
162 and dissolution mechanisms when comparing alkali-activation to Portland cement hydration [55,
163 56], it is important to design organic molecular architectures that are specifically applicable in
164 alkali-activated binders. Recent efforts [57, 58] have demonstrated important progress in this
165 regard, including demonstration of an allyl ether-based PCE with short side chains that gave
166 extremely effective plasticizing performance in an NaOH-activated slag paste at a dose as low as
167 0.05 wt.% [57]. Keulen et al. [59] also showed that a proprietary PCE admixture could
168 dramatically increase both the slump and the slump retention of alkali-activated fly ash-slag
169 blended concretes, as shown in Fig. 2.

170



171
172 **Figure 2. Slump and slump retention of alkali-activated concretes (binder 73.7% fly ash, 25% BFS,**
173 **1.3% $\text{Na}_2\text{SiO}_3 \cdot 5\text{H}_2\text{O}$ powder; activator 3 M NaOH) as a function of PCE admixture dose.**
174 **Reproduced from [59].**

175

176 There has also been important work aimed at improving the open working time of alkali-activated

177 concretes and grouts, which is problematic in some applications due to the relatively rapid
178 workability loss that is shown by some alkali-activated mixes (including in cases where
179 workability can be lost even though setting is not unduly rapid). This will be discussed further in
180 Section 2.4. Many chemical retarders for PC are not compatible with AAMs [60], but citric acid
181 [61], *d*-gluconic acid [62], borate and phosphate [63] have all been described to give useful
182 retardation in specific cases. However, the appropriate selection of a retarder depends critically
183 on the role and content of calcium within the alkali-activation process; high-calcium mixes tend
184 to be more effectively retarded by small organics that can complex Ca^{2+} as it is released from the
185 solid precursor and thus delay the precipitation of C-A-S-H type gels, whereas low-calcium mixes
186 appear to be more amenable to the use of inorganic retarders. Although care is required to select
187 admixtures that can give retardation without loss of some percentage of the final strength
188 development, it is not always straightforward.

189

190 **2.4. Setting time**

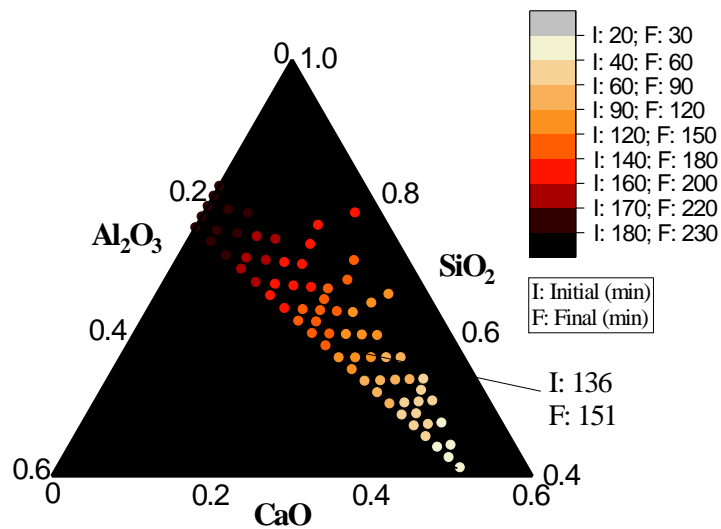
191 The setting time of an alkali-activated material (AAM) is a critical performance parameter that
192 affects its practical application. The practical ability to control setting time of alkali-activated
193 binders can determine the time window available for mixing, transportation, and casting of
194 concrete. However, fast setting is a feature of AAS-Wg based materials; the setting time of this
195 type of binder is often less than 30 min [64]. Setting behavior is affected by many factors, such as
196 raw materials, specimen preparation and process conditions, as well as the use of additives as
197 discussed in section 2.3. Lower-calcium alkali-activated binders have been identified to set
198 through a gel percolation process [65], distinct from the localized precipitation of C-A-S-H type
199 gels that characterizes the early stages of slag alkali-activation. This distinction brings important
200 new abilities to understand and manipulate the setting processes of each binder type.

201

202 Li et al. [66, 67] found that the setting times of alkali-activated slag-fly ash and alkali-activated
203 slag-metakaolin pastes were prolonged with increased fly ash or metakaolin contents. Li et al. [64]

204 summarized the setting times of slag-based AAMs designed in the $\text{SiO}_2\text{-Al}_2\text{O}_3\text{-CaO}$ system with
 205 a single activator (sodium silicate of modulus 1.4), as shown in Fig. 3. They found a general trend
 206 that the setting time decreased with increasing CaO content in the $\text{SiO}_2\text{-Al}_2\text{O}_3\text{-CaO}$ system. The
 207 role of Ca (and correspondingly also Mg) as a network modifier in the slag glass leads to more
 208 rapid dissolution of these precursors, whereas fly ash does not show the same degree of reactivity
 209 as it is a more chemically durable glass. However, when comparing blast furnace slags of different
 210 chemistry, the ability to use a single indexing parameter to predict reaction kinetics (as measured
 211 by isothermal calorimetry) remains elusive [68, 69], as it is becoming clear that many parameters
 212 beyond simple glass chemistry play important roles in determining the rate of slag reaction under
 213 alkali-activation. An indexing approach that also includes particle size distribution parameters has
 214 been proposed for fly ash activation [37], but this will also require further development before it
 215 could be considered in any way broadly applicable.

216



217

218 **Figure 3 Setting times of AAMs (color scale, in minutes) in the $\text{SiO}_2\text{-Al}_2\text{O}_3\text{-CaO}$ solid precursor**
 219 **system [64]**

220

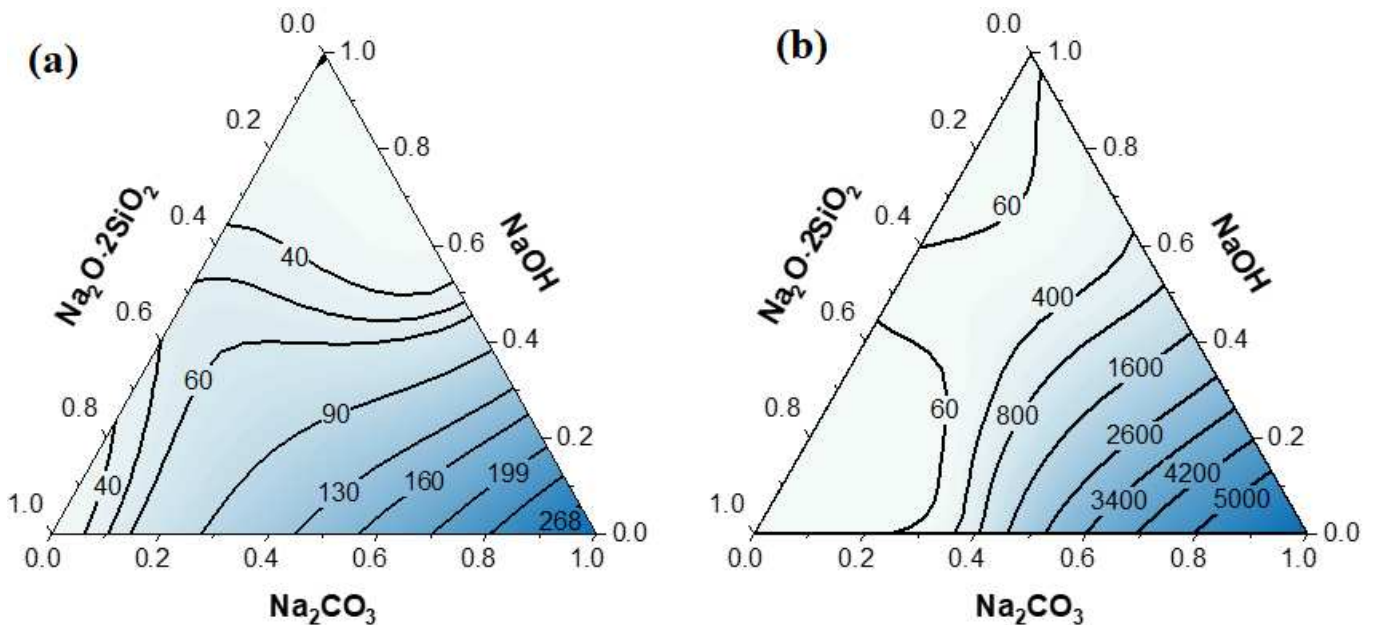
221 Careful selection and/or combination of activators is another way to manipulate the setting times
 222 of AAMs. Shi & Day [70] and Bernal et al. [13, 71] have illustrated that a prolonged induction
 223 period, which can take up to 3-5 days in some slag-based AAM systems, can be obtained when
 224 sodium carbonate is used as the activator. They showed that the Na_2CO_3 promotes the formation

225 of calcite and mixed sodium-calcium carbonates prior to C-(A)-S-H; and that the fairly modest
 226 pH (between 11 and 12) generated from this activator gives a low rate of initial dissolution of the
 227 slag [70]. However, high-magnesia blast furnace slags do react relatively rapidly with Na_2CO_3 as
 228 an activator [14], and can under some conditions give higher early strength with this activator
 229 than with sodium silicate, when using a sufficiently high-MgO slag [72].

230

231 Li et al. [66, 67] further investigated the setting time of alkali-activated slags, and found that the
 232 setting time was prolonged with an increase in the dose of Na_2CO_3 as activator, especially when
 233 considering the final setting time and a slag of moderate MgO content, as shown in Fig. 4. The
 234 initial setting time of Na_2CO_3 -AAS in that study was more than 300 min, while the final setting
 235 time was about 6 days. A wide range of setting time results were also shown in the work of
 236 Fernández-Jiménez & Puertas [73] (mortar setting time above 3 d), Kovtun et al. [74] (concrete
 237 setting time about 8 h), and Atiş et al. [75] (paste setting time about 3 h). However, a well-balanced
 238 mixture of Na_2CO_3 , $\text{Na}_2\text{O}\cdot r\text{SiO}_2\cdot n\text{H}_2\text{O}$, and/or NaOH can take advantage of the influence of each
 239 of the respective anion groups present, leading to the ability to control and tailor setting time,
 240 workability and mechanical properties [71, 76].

241



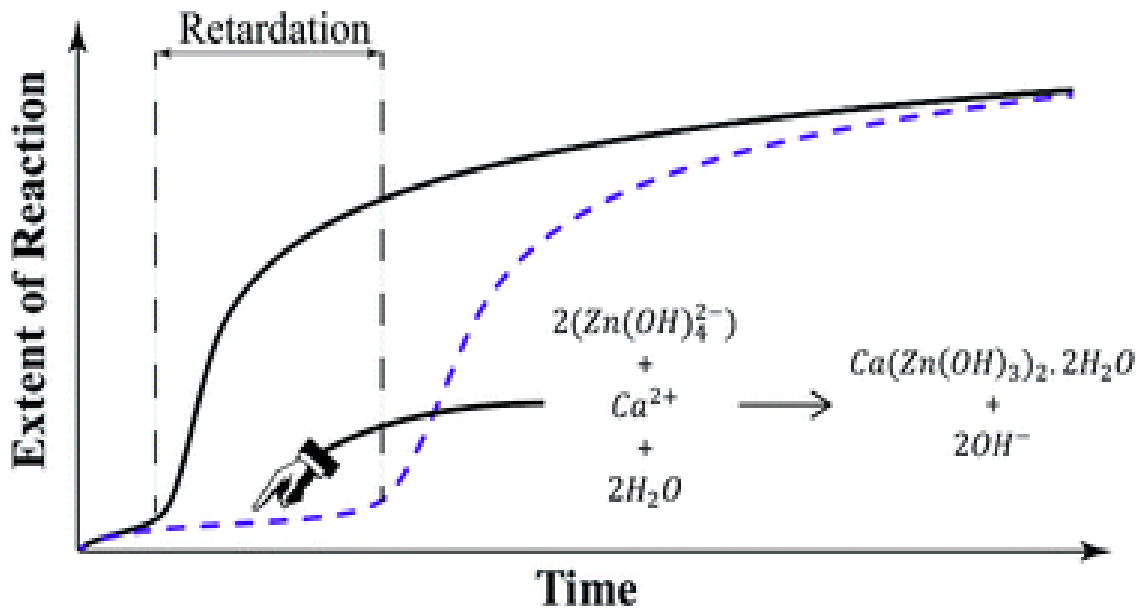
242

243 **Figure 4. Contours of setting time (min) of alkali-activated slag with Na_2CO_3 -NaOH- Na_2SiO_3**

244
245
246
247
248
249
250
251
252
253

activators: (a) Initial setting time, (b) Final setting time [66, 67]

Garg and White [77] investigated how nano-ZnO retards the setting of alkali-activated materials, by pair distribution function (PDF) analysis and isothermal calorimetry. Fig. 5 illustrates the reaction between tetrahydroxozincate ions ($Zn(OH)_4^{2-}$) and calcium ions (Ca^{2+}) in the retardation stage, that can affect the nucleation/growth of the C-(A)-S-H type gel because Ca^{2+} is bound into a calcium zincate phase. In the other hand, nano-ZnO does not significantly influence the alkali-activation reaction of metakaolin-based binders [77], as interactions involving calcium play a pivotal role in dictating the effectiveness of nano-ZnO in retardation of AAMs.



254
255
256
257

Figure 5. A schematic outline of the retardation process caused by adding nano-ZnO to alkali-activation of slag, sketched based on the discussions in Reference [77]

258 2.5. Structural characterization

259 2.5.1 Experimental approaches

260 In alkali-activated binder systems, as in Portland-based cements, the disordered, complex and
261 multiphase nature of the reaction products that contribute to the main strength gain means that it
262 is difficult to gain a full understanding of the binder characteristics from any small subset of

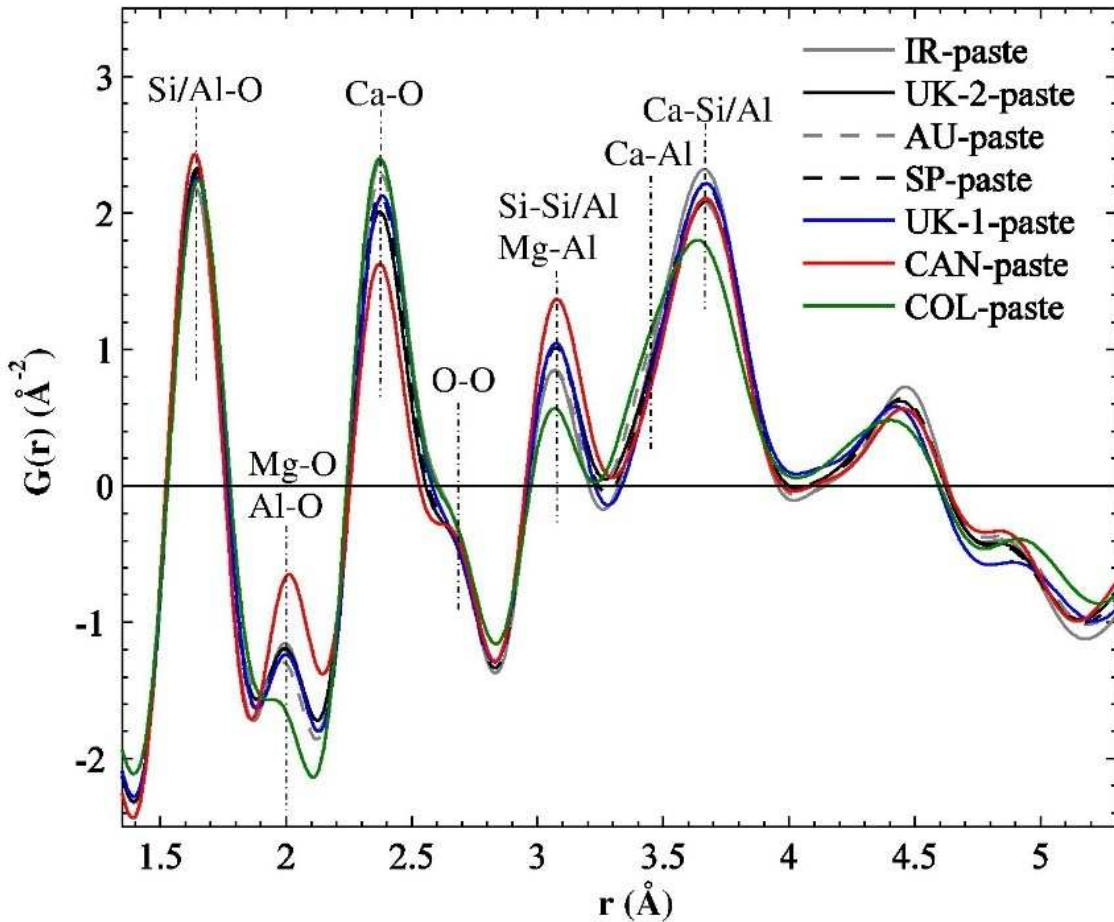
263 common materials science techniques [2]. Therefore, cementitious materials (and AAMs in
264 particular) provide fertile ground for the development and implementation of new approaches to
265 the experimental characterization of complex materials, and the continued structural
266 characterization of alkali-activated materials is still a key field of investigation. The C-S-H type
267 gel (often represented as C-(N)-A-S-H) and layered double hydroxide (LDH) secondary phases
268 that dominate higher-calcium AAMs, and the alkali-aluminosilicate (N-A-S-H) gel formed in
269 lower-calcium AAMs, are all highly complex in chemistry, but are becoming better understood
270 through the application of both conventional and advanced experimental analytical tools. The use
271 of new analytical techniques as well as novel research routes during the past years has provided
272 valuable insight into the structure of alkali-activated binders, and there is no evidence to suggest
273 that major advances in this area are likely to end any time soon.

274
275 There has been much recent focus on the factors affecting aluminum and alkali uptake into the C-
276 S-H structure by analysis of synthetic gels. The full details of this work are beyond the scope of
277 the current review, and an excellent overview was provided in a paper presented at the 2015 ICCB
278 [78]. A low Ca/Si ratio favors the incorporation of Al(IV) into C-S-H gel, whereas a high Ca/Si
279 ratio results in more octahedrally coordinated Al(VI) [79, 80] that is predominately present in
280 “third aluminate hydrate” (TAH) and in AFm phases [81]. High Al and alkali content, as in the
281 case of many AAS binders, leads to co-existence of C-A-S-H and N-A-S-H type products,
282 although these two gels can be very difficult to distinguish and isolate from each other unless
283 detailed structural models are applied to aid in the interpretation of spectroscopic data [82]. Cross-
284 linking within the C-A-S-H type structure has also been identified as playing a key role in the
285 structural description and understanding of the binding phases formed in high-Ca AAMs [82-84]

286
287 Nuclear magnetic resonance (NMR) spectroscopy is now well known as a key technique to track
288 the information on the local bonding environments of silicon and aluminum atoms. The structure
289 of C-(N)-A-S-H gel has been described by various groups [83, 85-88]. However, NMR has a
290 limited capacity to assess medium range ordering. X-ray and neutron pair distribution function

291 (PDF) analysis are now well established as techniques for understanding the gel structure formed
292 in alkali-activated binders, due to the ability of the PDF technique to probe the local atomic
293 structure of disordered materials [89], although the analysis of multi-phase materials by this
294 technique remains very challenging. Gong & White [90] used X-ray total scattering and PDF
295 analysis to study the impact of chemical variability on phase formation in alkali-activated
296 granulated blast-furnace slag (GGBS). The primary reaction product after alkali-activation was
297 C-(N)-A-S-H gel with a highly disordered structure, and PDF analysis revealed that atomic
298 arrangements, as shown in Fig. 6 for the short-range ordering $< 5 \text{ \AA}$, in the C-(N)-A-S-H gel
299 differed depending on the chemical composition, especially the calcium content, of the raw
300 material. The gel connectivity of C-(N)-A-S-H gel increased with decreased calcium content, as
301 shown in Fig. 6, represented to a first approximation by the intensity of the peak just above 3 \AA
302 assigned to Si-Si/Al and Mg-Al correlations. Magnesium in alkali-activated GGBS pastes is
303 primarily incorporated in the secondary reaction product, which is a hydrotalcite-like phase, as
304 will be discussed in more detail below. In-situ X-ray total scattering measurements and PDF
305 analysis are also starting to be widely used in the study of alkali-activated binders, as one of few
306 techniques that can give time-resolved information about gel local structure during setting and
307 hardening [91-93].

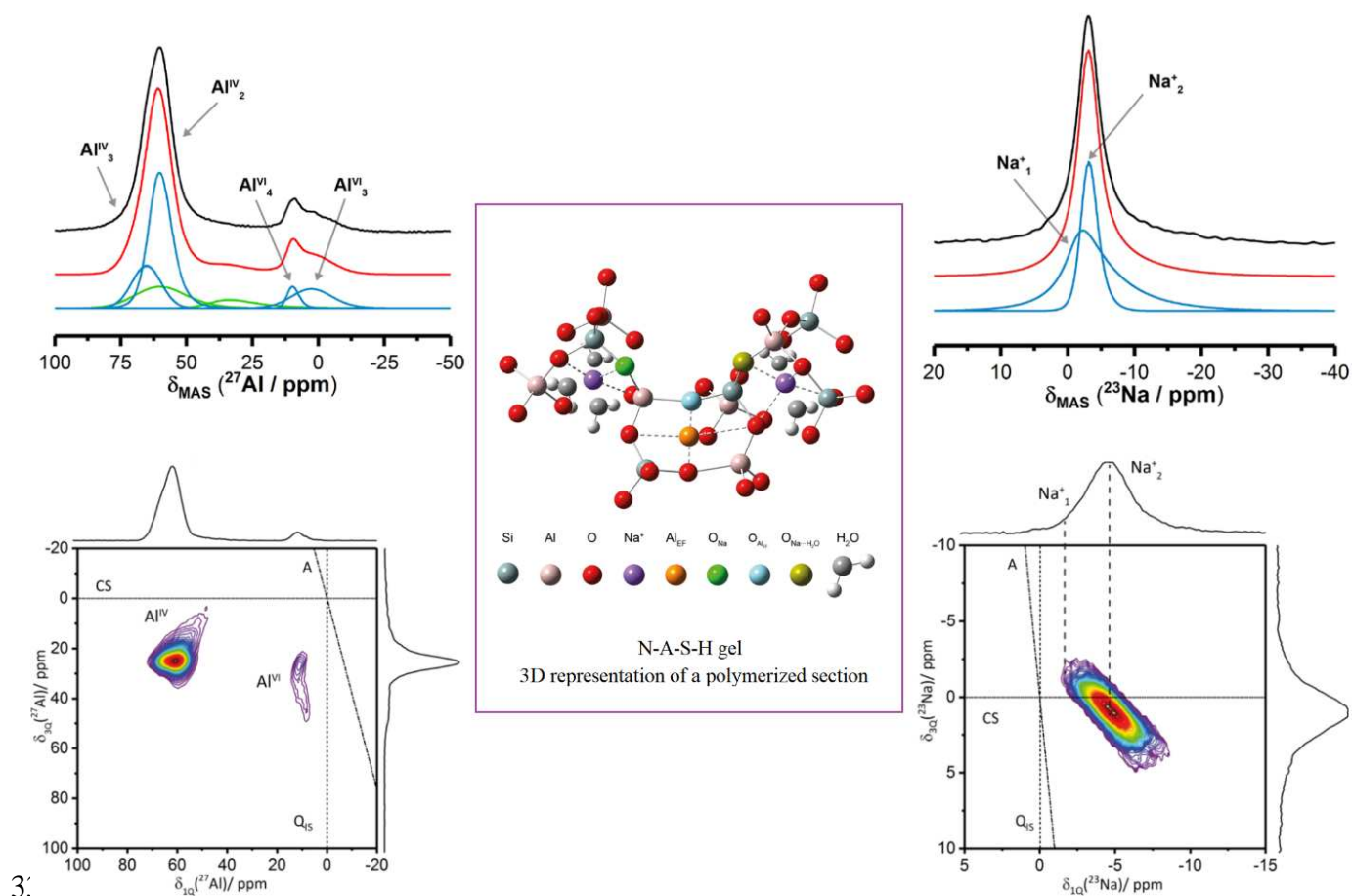
308



309
 310 **Figure 6. X-ray PDFs of pastes produced from hydroxide-activated granulated blast-furnace slags**
 311 **(slags from different sources as noted in the legend), showing the short-range ordering ($< 5 \text{ \AA}$) [90].**
 312

313 A method to investigate the chemistry of aluminosilicate-based cementitious binders by alkali-
 314 activation of high-purity synthetic amorphous aluminosilicate powder has been proposed by
 315 Walkley et al. [94]. The phase evolution and nanostructure development of these materials have
 316 been examined after activation [95, 96]. Using this information, a new structural model of alkali
 317 aluminosilicate gel (N-A-S-H) gel frameworks has been proposed based on data from solid-state
 318 nuclear magnetic resonance spectroscopy (^{17}O , ^{23}Na , and ^{27}Al) [97]. Fig. 7 shows part of the
 319 proposed conceptual model for this gel structure, with charge-balancing of the partial negative
 320 charges on bridging oxygen associated with tetrahedral Al provided by sodium and by extra-
 321 framework Al (Al_{EF}). The alkali aluminosilicate gel predominantly comprises fully coordinated
 322 (Q^4 or q^4) Si and Al units. A considerable proportion of Al^{3+} in tetrahedral coordination exists in

323 sites of lower symmetry, where some of the charge-balancing capacity in the gel is provided by
 324 extra-framework Al species which have not previously been observed in these materials. Greiser
 325 et al. [98] conducted advanced multi-dimensional NMR analysis of N-A-S-H gels derived from
 326 various amorphous silica sources and also identified extra-framework Al sites, although
 327 contended that their results were consistent with tetrahedral Al_{EF} sites, as also noted by Brus et al.
 328 [99] rather than the octahedral Al_{EF} identified by Walkley et al. [97]. There is evidently important
 329 further work required to unravel the nanostructural details of the N-A-S-H gel structure, and multi-
 330 nuclear and multi-dimensional NMR techniques are expected to underpin and inform these efforts
 331 in coming years.
 332

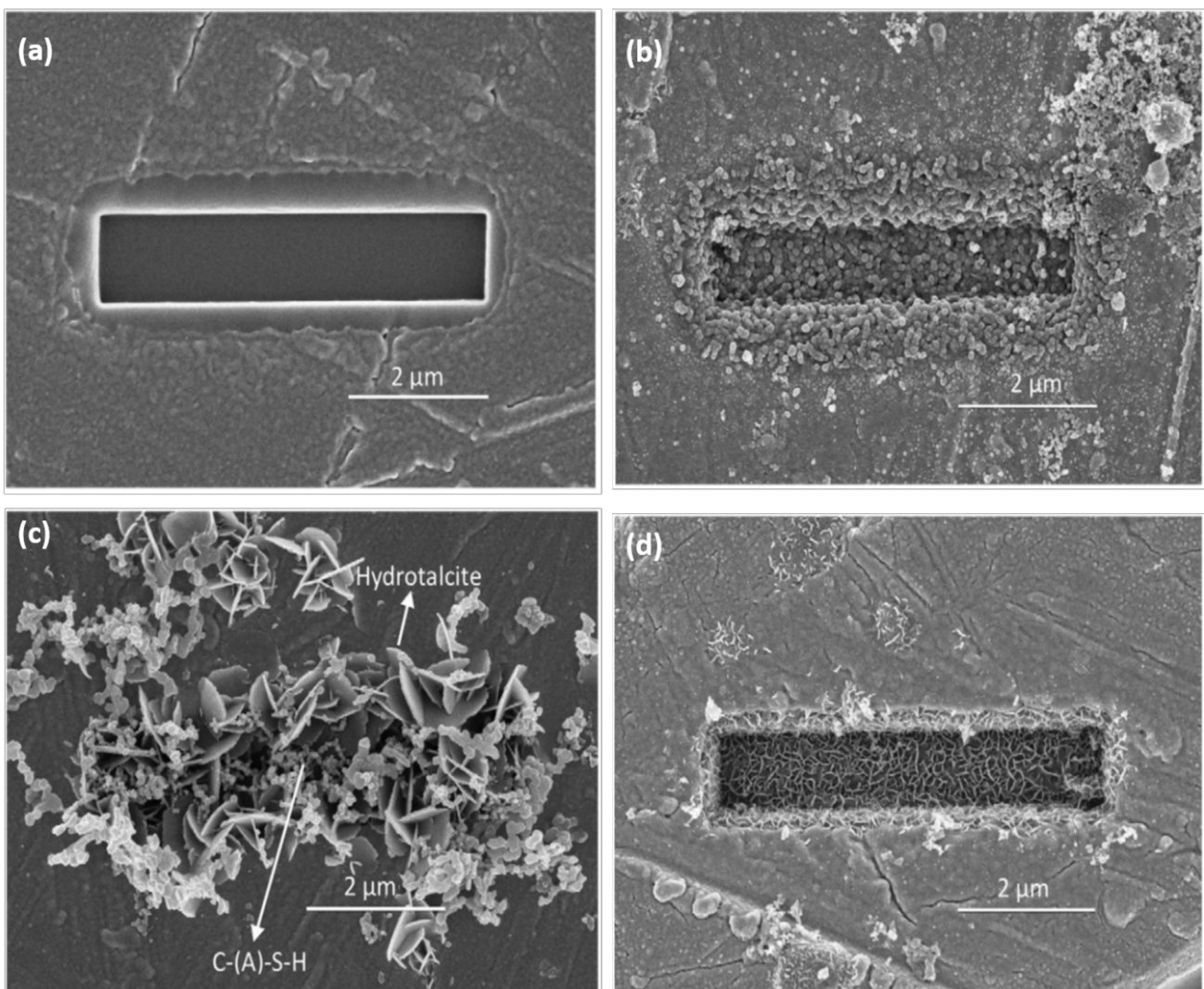


334
 335 **Figure 7.** ²⁷Al and ²³Na MAS and 3QMAS NMR analysis for the gel of alkali-activated synthetic
 336 precursor (Si/Al=2), and a 3D representation of a polymerized section of the N-A-S-H gel showing
 337 various constituent environments as marked, adapted with permission from [97]. Copyright
 338 American Chemical Society.

339

340 Scanning electron microscopy (SEM), together with energy-dispersive X-ray spectroscopy (EDX),
341 has been widely used as a powerful tool by different scholars [91, 100, 101] to track
342 microstructural evolution in alkali-activated binders, including some important work on model
343 systems where “microreactors” were ion-milled into slag grains and the morphology of the
344 reaction products formed by their reaction with different alkaline solutions monitored [102]. Fig.
345 8 shows examples of the data that were obtained using this approach, where both the concentration
346 and the nature of the alkaline solution led to remarkable differences in the appearance of the
347 reaction products formed. The large platelets of hydrotalcite-like minerals and the globular C-S-
348 H type gel are particularly evident at the highest concentration of KOH tested, but there is a clear
349 progress of the alkali-activation reaction under all conditions depicted.

350



351

352 **Figure 8 (a) A microreactor ion-milled into a GGBS grain; and microreactors exposed for 2 days to:**
353 **(b) 0.1 M KOH; (c) 10 M KOH; (d) 1 M NaOH. Reproduced from [102]**

354

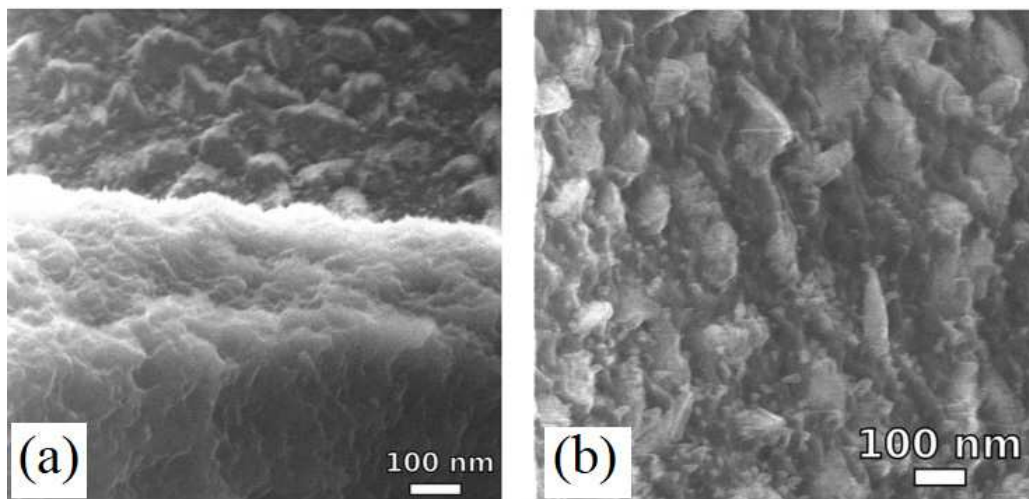
355 The use of SEM as an analytical technique is very well established in the field of cementitious
356 materials, both for imaging and for determination of elemental compositions. Particularly
357 important information has recently been obtained regarding the Mg-Al layered double hydroxide
358 (hydrotalcite-like) phase in alkali-activated slags. Richardson & Li [103] used SEM-EDX to
359 determine the Mg/Al ratio in KOH-activated blast furnace slag paste after 18 years of curing; a
360 ratio of 2.6 was determined, in excellent agreement with calculations based on XRD data for that
361 binder. Ke et al. determined Mg/Al ratios closer to 2.0 for the corresponding Mg-Al LDH phases
362 in Na₂CO₃-activated slag binders [14] and in Na₂SiO₃-activated slag binders [104], also using
363 SEM-EDX, and consistent with older literature including [105] and others. This phase is often
364 described in the cements literature as being simply “hydrotalcite”, but in a mineralogical sense,
365 true hydrotalcite has Mg/Al = 3.0 and contains carbonate in its interlayer [106], whereas the LDH
366 phases formed in many alkali-activated binders will be carbonate-free. The carbonate-containing
367 member of the hydrotalcite family with Mg/Al = 2 is correctly called meixnerite, whereas the
368 carbonate-free “M₄AH₁₃” hydrotalcite-group composition, which is probably the most relevant to
369 most alkali-activated binding systems, does not have a formal mineral name. So, the continued
370 description of the Mg-Al LDH phase formed in alkali-activated binders as “hydrotalcite-like”
371 seems satisfactory, but it does need to be clearly identified that this is not true hydrotalcite in the
372 mineralogical sense.

373

374 Transmission electron microscopy (TEM) has also been applied to the analysis of alkali-activated
375 binders with some success [103], but sample preparation for this technique remains challenging
376 and the samples are prone to beam damage. Helium ion microscopy (HIM), a technique with some
377 resemblances to SEM but potentially offering higher spatial resolution, was proposed by
378 Morandau et al. [107] for studying the nanoscale structure of alkali-activated materials. HIM
379 involves imaging of sample surfaces by detecting secondary electrons that are excited from the

380 sample surface by bombardment with helium ions. Spatial resolution is high due to the specific
381 nature of the beam-sample interaction [108]. Hence, in comparison with SEM, this method is
382 well-suited for resolving nanometer-scale surface morphologies and porosity present in rough and
383 irregular fractured samples, including alkali-activated binders. Fig. 9 shows a selection of HIM
384 images of AAS obtained by Morandea et al. [107]. Finer heterogeneous morphological details
385 have been captured. Two types of C-(N)-A-S-H gel have been identified, with the ‘inner’ gel
386 showing a foil-like morphology while the ‘outer’ gel appearing more globular. The use of HIM
387 with EDX analysis can provide new insight into the structure of alkali-activated materials as well
388 as other binder systems, and although the HIM instruments are still expensive, this technique is
389 becoming more widely available in the international community.

390



391

392

393 **Figure 9. HIM images (a) GGBS particle covered by ‘foil-like’ C-(N)-A-S-H gel; (b) the surface of**
394 **the concave spherical void: C-(N)-A-S-H gel. Reproduced from [107].**

395

396 Scattering and diffraction-based techniques have been used to provide insight into AAMs during
397 the initial [109-111], medium-term [112], and later-age [113] evolution of gel, crystallite, and pore
398 structure in AAMs. The combination of neutron and X-ray scattering, applied in parallel to provide
399 different aspects of the required information, has also given important new insight into the highly-
400 connected nature of the pore structure in metakaolin-based AAMs [114]. The marked differences

401 in pore geometry and its evolution with curing as a function of the nature of the alkali cation
402 present have also been examined using the combination of PDF, small-angle X-ray scattering and
403 electrical impedance methods [115]: the structure-forming (kosmotropic) Na^+ leads to a pore
404 network structure that evolves considerably over a 5-year curing duration, while the pore networks
405 generated through the use of chaotropic (K^+ or Cs^+) alkali cations are much more stable during
406 extended curing periods [115].

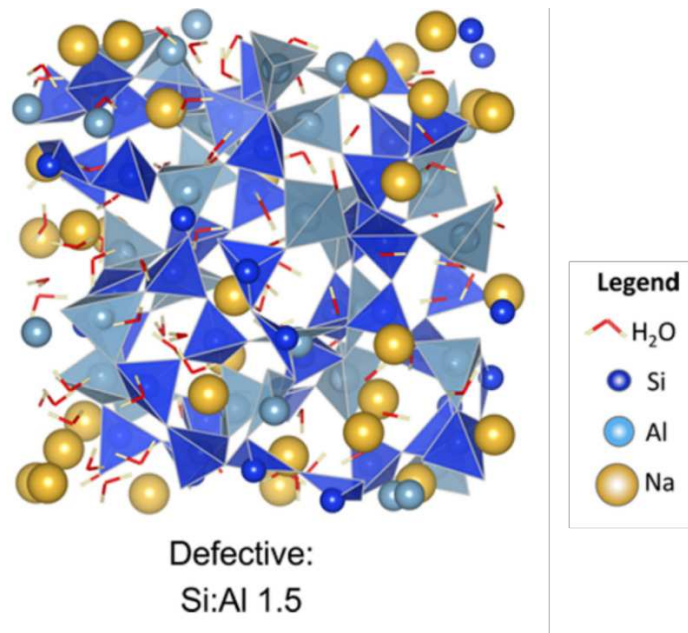
407
408 Another essential aspect of alkali-activated binder chemistry that has received attention – and
409 answers to some key outstanding questions – in recent years is the exact chemical nature of the
410 green coloration in alkali-activated slag binders (and similarly in high volume Portland-slag
411 blends). There has been much speculation in the past that this coloration is due to the presence of
412 polysulfide species (resulting from the release of sulfide by slag dissolution), but the previous
413 spectroscopic evidence was far from sufficient to fully substantiate this argument. However,
414 Chaouche et al. [118] have recently used synchrotron-based X-ray absorption near edge
415 spectroscopy (XANES) to demonstrate that the blue/green regions of alkali-activated (and
416 Portland cement-blended) slag binders contain the characteristic spectroscopic features of the
417 trisulfur (thiozonide) radical anion S_3^- , the same species that gives color to ultramarine pigments.
418 Consistent with this, Le Cornec et al. [119] have also recently applied vibrational spectroscopy to
419 the analysis of greening effects in 70% GGBS-30% PC blended cements, and identified
420 spectroscopic features consistent with the confinement of various sulfur radical ions (S_2^- , S_3^- and
421 S_4^-) within the interlayer space of LDH phases, proposed to be of the AFm family. They claimed
422 that all three of these polysulfide species were present at similar ratios in the hydration products
423 of various slags tested, which modifies the characteristically blue pigmentation of the S_3^- radical
424 anion (which is the most prominent species in their spectra also), to instead give a green color
425 [119]. This is clearly an important step forward in understanding the fundamental science of
426 AAMs, but also has implications for understanding the role of binder redox chemistry in
427 controlling steel corrosion processes.

428

429 **2.5.2 Modelling approaches**

430 There have also been notable recent advances made in the modelling of AAM binder chemistry
431 by a variety of modelling approaches at different length scales. At an atomistic level, a number of
432 molecular dynamics (MD) studies have generated model structures claiming to represent N-A-S-
433 H gels. However, the majority of these studies have not included water in a realistic or reasonable
434 manner, and so have generated structures of anhydrous or partially-hydrated glasses rather than
435 anything representative of a N-A-S-H structure that could form by precipitation from an aqueous
436 solution. Features such as edge-sharing tetrahedra and extensive $\text{Al}^{\text{IV}}\text{-O-Al}^{\text{IV}}$ bonding, which are
437 not observed to any significant degree in hydrous aluminosilicate minerals, can be viewed as
438 indicators of such an unrealistic structure. An exception to this trend is the work of Lolli et al.
439 [120], who used MD to generate correctly hydrated N-A-S-H gel structures based on three
440 approaches: a “crystalline” structure based on adjusting the sodalite framework to the desired N-
441 A-S-H stoichiometry; a “defective” structure generated by introducing defects into the sodalite
442 framework and allowing this to relax (in the presence of water) using MD, and an “amorphous”
443 structure based on SiO_2 glass adjusted to the desired N-A-S-H stoichiometry. Among these three
444 models, the “defective” structure (Fig. 10) gave the best match to experimental PDF data, and also
445 yielded predictions of nanoscale mechanical properties and porosity that are consistent with the
446 available literature, while complying with the requirements for predominantly Q^4 bonding, the
447 absence of edge-sharing tetrahedra, and agreement with Loewenstein’s principle of Al-O-Al
448 avoidance [121]. This can therefore be considered to be a reasonably representative structural
449 model for N-A-S-H gel at this length scale, and is consistent at a chemical level with the schematic
450 description of the potential site types that was shown in Figure 7.

451



452

453 **Figure 10. Representation of part of the N-A-S-H gel structure generated by application of molecular**
 454 **dynamics to relax a defective sodalite framework. Reproduced with permission from [120].**
 455 **Copyright American Chemical Society.**

456

457 At the mesoscale, Valentini [92] adapted an established code designed for Portland cement
 458 hydration simulations to describe the activation of metakaolin by different alkaline solutions,
 459 while Yang & White [122] advanced the use of on-lattice coarse-grained Monte Carlo simulations
 460 to describe activation of different aluminosilicate precursors. Modeling approaches such as these
 461 are computationally intensive and need care in parameterization and specification to ensure that
 462 atomic-scale interactions are replicated as accurately as possible on the mesoscale, but also
 463 provide unparalleled access to mechanistic and microstructural information on a length scale of
 464 up to hundreds of nanometers, which is very difficult to access experimentally in real-time.

465

466 Thermodynamic modeling of phase assemblages in AAMs has been an area of particularly
 467 important recent developments, where the application of a detailed ideal solid solution model for
 468 the C-(N,K)-A-S-H system [123] supported by the availability of improved solubility data [124]
 469 has significantly moved forward the state of the art. This has enabled advances in phase
 470 assemblage predictions for alkali-activation of blast furnace slag [125-127], including prediction

471 of phase diagrams for a wide range of slag and activator compositions [128]. Solubility
472 information for N-A-S-H gels [129], and improved information for aqueous species in the N-K-
473 A-S-H-Cl system [130], are bringing the opportunity for modelling of some lower-calcium binder
474 systems [131], although much work is still required to develop and validate the necessary range
475 of model constituents to enable full description of the phase assemblages in these binders. In
476 particular, the database of zeolite phases available for inclusion in models of the (N,K)-A-S-H
477 system requires expansion, as there are significant gaps in the literature here, although constrained
478 to some degree by issues of metastability and difficulties in actually defining “solubility” in many
479 instances.

480

481 **2.6. Microstructure and mechanical properties**

482 The development of a detailed understanding of the microstructure and mechanical properties of
483 AAMs is obviously key to the application of these materials in civil and infrastructure applications.
484 In particular, it is essential to understand whether the engineering design equations that have been
485 established for conventional concretes are also broadly applicable to AAM concretes. A detailed
486 review of the mechanical properties of AAM concretes has been provided recently by Ding et al.
487 [132], and the full scope of that review will not be repeated here. However, it should be noted that
488 in many cases, the general functional forms of relationships that work well in describing the
489 characteristics of Portland cement-based concretes also appear valid for AAM concretes, but some
490 re-fitting of parameters seems necessary.

491

492 Analysis of the stress-strain characteristics of AAM concretes has tended to show that these
493 materials show a higher tensile strength, lower modulus of elasticity, and lower Poisson’s ratio
494 than conventional Portland cement concretes, as reported by e.g. [133-135] and many others.
495 Thomas and Peethamparan [136] also showed that the specimen size effect in compressive
496 strength testing of AAM concrete cylinders was well described by the established models for
497 Portland cement in the case of AAMs based on GGBS, but observed an unexpectedly strong size

498 effect in AAMs based on fly ash. This was attributed to microcracking effects in the fly ash-based
499 binders; microcracking of AAMs is certainly an area requiring more detailed analysis, and will be
500 revisited below (section 2.8) in the discussion of dimensional stability. The creep of AAM
501 concretes also requires further attention. There are indications that although the early-age creep
502 of these materials resembles that of Portland cement-based concretes, the deceleration of creep
503 over extended timeframes may be less dramatic in AAM concretes, meaning that longer-term
504 creep processes must be taken into account in structural design procedures [137]. AAMs have also
505 been observed to have a higher fracture energy [138, 139] and a more compact interfacial
506 transition zone [138, 140] than comparable Portland cement-based materials, and undergo a more
507 localized cracking process [141]. The strong aggregate-paste bond also gives relatively high
508 fatigue resistance [142, 143].

509
510 An important finding underpinning much of the analysis of AAM property-microstructure
511 relationships was the identification by Winnefeld et al. [68] that the degree of reaction of the blast
512 furnace slag precursor appears to be a characteristic parameter which controls strength, across a
513 range of slag sources and activators. It is quite probable that this relationship is critically
514 dependent on the pore structure of the AAM binder; Ranjbar et al. [144] obtained strengths of
515 over 130 MPa by hot-pressing fly ash-based AAMs to reduce porosity, while Rouyer et al. [145]
516 showed a clear relationship between Young's modulus and pore volume of a range of metakaolin-
517 based AAMs. Blyth et al. [146] also showed orders-of-magnitude differences in intrinsic
518 permeability between hydroxide-activated and silicate-activated slag binders, but without a
519 corresponding difference in the Young's modulus, which was attributed to a very marked
520 reduction in the characteristic pore diameter upon silicate activation. Bernal et al. [147] also
521 reported a surprisingly low dependence of mechanical properties on total pore volume in alkali-
522 activated slag mortars, where water/binder ratios of 0.40 and 0.44 gave similar 28-day strengths
523 and identical 56-day strengths. Babae and Castel [148] used water vapor sorption as a sensitive
524 probe of pore structure in blended fly ash-slag AAMs, distinguishing the very fine pores which
525 dominate slag-rich pastes from the mesoporous nature of fly ash-rich binders. Hu et al. [149]

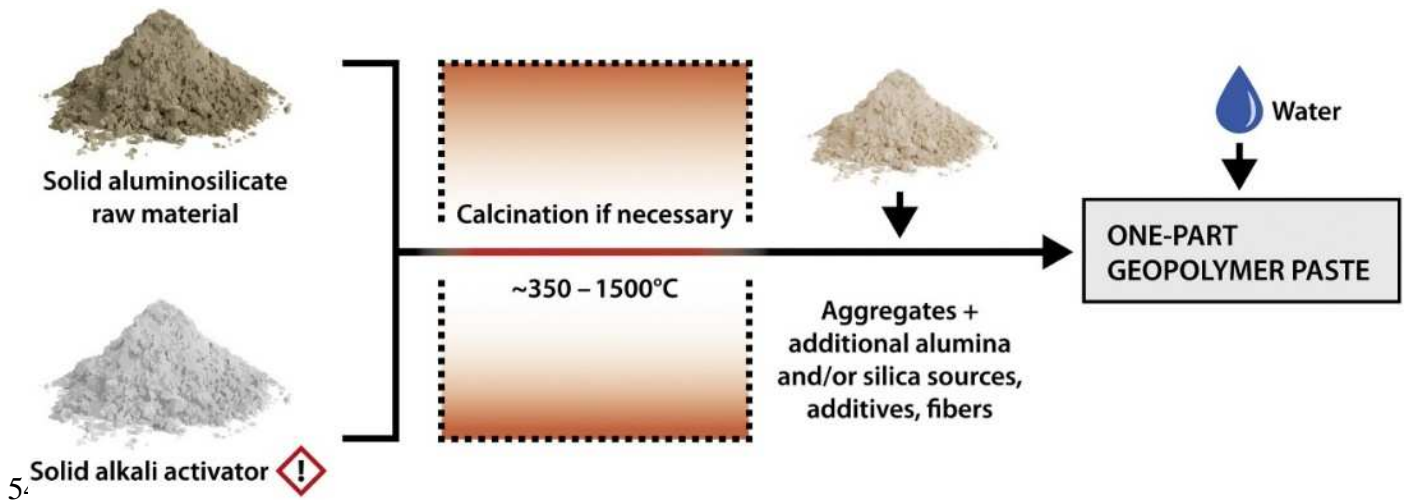
526 reported that the compressive strength of alkali-activated slag/fly ash mortar is mainly affected by
527 total porosity and porosity of capillary pores, with sizes ranging from 10 to 10^4 nm. The change
528 of pore structure in the mortar was strongly influenced by the activator silicate modulus, alkali
529 dosage and fly ash content.

530

531 **2.7. One-part alkali-activated binders**

532 One-part ('just add water') alkali-activated materials can be treated as an important step towards
533 to the commercial-scale development of these low-carbon binders. A new review on one-part
534 AAMs has been published [150] which included systematic analysis of the available literature, so
535 the current paper will not attempt to repeat the full scope of that review, which covered one-part
536 AAMs in respect of raw materials, admixtures, optimum calcination, composition, curing
537 conditions, and mechanical strength. Fig. 11 illustrates the general procedure to prepare one-part
538 AAMs by adding water to a dry mixture of solid alkali-activator and a solid aluminosilicate
539 precursor, including a calcination step if necessary. This technology has been considered as a
540 method to face some technical challenges related to conventional (two-part) AAMs, in particular
541 the question of how to handle large amounts of activator solutions which may be viscous,
542 corrosive, and/or hazardous, on site in a construction application. It should be noted that the pH
543 of most alkali-silicate activators is actually similar to that of fresh Portland cement paste, but the
544 fact that these may need to be stored and handled in large quantities by personnel who are not
545 specialized in chemical handling is nonetheless an important reason to drive forward the
546 development of one-part AAMs.

547



549 **Figure 11. The general procedure of one-part AAM (geopolymer) preparation. From [150].**

550

551 In one-part alkali-activated binders, any substance that dissolves sufficiently rapidly, and offers
 552 alkali cations and provides a high pH environment to facilitate dissolution of the aluminosilicate
 553 precursor, can in principle be used as an activator [151]. Sodium metasilicate powders
 554 ($\text{Na}_2\text{SiO}_3 \cdot x\text{H}_2\text{O}$, $0 \leq x \leq 5$) has been studied as a solid activator in one-part alkali-activated binders
 555 [152-154]. Anhydrous sodium metasilicate was reported to contribute to higher compressive
 556 strength and better workability than its hydrous counterparts when used to activate fly ash and
 557 blast furnace slag-based binders, and is available commercially in the form of spray-dried powders
 558 that appear quite amenable to use in alkali-activation processes at an acceptable cost.

559

560 Hybrid alkaline cement, where Portland cement and an alkaline activator are added in parallel,
 561 can also be regarded as a type of one-part AAM binder. The nanostructural evolution of these
 562 cements has been presented by García-Lodeiro et al. [155] via a descriptive model. Fernández-
 563 Jiménez et al. [156] investigated the hydration mechanisms of fly ash-based alkaline hybrid
 564 cement as a function of the nature of the activator as it was supplied in different forms (solid and
 565 liquid). When solid sodium sulfate was used as the activator in hybrid binder systems, slightly
 566 higher mechanical strength and less AFt and AFm phases were obtained than when it was added
 567 as a liquid. Both early age reaction kinetics and the nature of reaction products were influenced
 568 by the form of addition of the activator.

569

570 Various different precursors, and combinations of precursors, have been validated for use in one-
571 part AAM binders. In addition to the more commonly used GGBS [157, 158], fly ash [159, 160]
572 and calcined clays [161], there has also been meaningful work dedicated to the development of
573 one-part AAMs from industrial waste silicas and NaAlO_2 [162][163], and red mud [164, 165]. In
574 many of these binder systems, a careful balance needs to be drawn between adding sufficient
575 alkalis to enable rapid strength development, and avoiding the excessive alkali levels that may
576 lead to efflorescence. Ongoing work to understand the causes and implications of efflorescence
577 in both one-part and two-part AAM binder systems [166-168] is certainly necessary to underpin
578 the development and deployment of one-part AAMs.

579

580 Qu et al. [169] produced a pre-industrial hybrid alkaline cement, manufactured in a Latin
581 American plant on a scale of around 20 tons. The proportions used were 30 % Portland clinker +
582 32.5 % blast furnace slag + 32.5% fly ash + 5% solid activator (the main salt is Na_2SO_4). This
583 hybrid alkaline cement was showed to react with water at ambient temperature and reached a
584 compressive strength around 32 MPa at 28 days, with acceptable setting time and early strength.
585 Further, the cement paste was tested at up to 1000°C , and showed better high-temperature
586 resistance than Portland cement due to the recrystallization of new poorly hydraulic phases,
587 mainly in gehlenite- and rankinite-type phases [170, 171]. Velandia et al. [172] also demonstrated
588 the production of concretes with good performance using a hybrid fly ash-Portland- Na_2SO_4 binder,
589 and provided extensive data about the durability performance of these concretes, including
590 correlations between key durability parameters and compressive strength at ages of up to 1 year.

591

592 **2.8. Dimensional stability**

593 The dimensional stability of any cementitious binder is a critical factor in determining its use in
594 engineering applications, as concretes are required to neither shrink nor expand excessively in
595 service. The relatively low level of bound water present in AAMs, particularly those with low

596 calcium content, has been observed to cause some susceptibility to drying shrinkage, as has
597 recently been reviewed by Mastali et al. [173]. This area has attracted a high degree of attention
598 in the literature in recent years, as the importance of understanding and controlling shrinkage has
599 become more and more evident. Low-calcium AAMs do not self-desiccate during curing in the
600 same manner as does Portland cement during its hydration [174], as there is not such a strong
601 chemical driving force withdrawing water from the pore fluid into solid phases. However, they do
602 undergo autogenous shrinkage which can lead to early-age cracking if not appropriately controlled
603 [175].

604

605 Higher-calcium AAMs such as sodium-silicate activated GGBS can self-desiccate, in part due to
606 the formation of hydration products, and also because the high ionic strength of their pore solution
607 reduces water activity to draw the relative humidity below 100% [176]; this latter effect is likely
608 to be the cause of any observed self-desiccation effects in lower-calcium binders that do not
609 chemically incorporate water of hydration. Ye & Radlińska [177] proposed that the drying
610 shrinkage of alkali-activated GGBS involves densification of the C-(N)-A-S-H as its structure is
611 damaged by reductions in relative humidity, as neither the moisture loss nor the drying shrinkage
612 were reversible upon soaking of dried specimens. Shrinkage mitigation strategies similar to those
613 that are implemented in conventional Portland cement have been evaluated recently for
614 application in AAS {Ye, 2017 #741}. Chemical shrinkage of alkali-activated GGBS and GGBS-
615 rich blends has been studied experimentally [178] and also identified through thermodynamic
616 modeling [125, 127]. Thomas et al. [179] identified a beneficial role for heat curing in reduction
617 of drying shrinkage, while Gao et al. [180] applied a particle packing model at paste scale to
618 optimize blends of GGBS and fly ash for minimum porosity and shrinkage. The shrinkage
619 properties of alkali-activated binders based on different blended precursors have also been
620 reported [181, 182]. Shrinkage-reducing admixtures [183-186] and super-absorbent polymers
621 [187-189] have also shown some effectiveness in reducing drying shrinkage, as has the tailored
622 design of blended activators [190]. While shrinkage control in AAMs does remain an area of open
623 research, with many questions yet to be answered, the fact that this broad range of approaches

624 have all shown some potential for success is a strong indication that this is not an intractable issue.
625

626 **2.9. Durability**

627 The durability of alkali-activated binders, and concretes produced from them, has been reviewed
628 in various publications [151, 191-193]. In most cases, AAMs have been tested according to
629 methods devised and validated for the testing of Portland cement-based binders; there are ongoing
630 discussions around whether this is entirely appropriate, including through the work of a RILEM
631 Technical Committee [194, 195], and it appears that in the majority of cases there are details of
632 the standard testing methodologies that will require modification if they are to give truly
633 meaningful results for AAMs. Sample preconditioning has been highlighted as an area requiring
634 particular care when designing tests for AAMs, as some of these materials can be damaged by the
635 preconditioning regimes that are often applied to Portland cement-based materials before testing,
636 particularly when very vigorous drying is applied [93, 196-198]. A performance-based
637 specification designed specifically for application to AAMs has been released in the UK, based
638 on minimal adaptations to established Portland cement testing methodologies [199], and efforts
639 are also ongoing in other countries and through multinational collaborative programs; it is
640 expected that this will be an area of rapid development in the coming years.

641
642 It has long been identified that binder carbonation under exposure to CO₂ is an area of durability
643 that requires careful consideration when designing and specifying AAMs. Early accelerated
644 testing at high CO₂ partial pressures appeared to show that alkali-activated binders would be very
645 susceptible to carbonation, but this was not directly matched by observations under natural
646 conditions. The reasons for the sometimes very poor performance of AAMs under accelerated
647 carbonation exposure is now understood to be related to specific changes in the carbonate-
648 bicarbonate equilibrium of the AAM pore solution at elevated CO₂ partial pressures [200]. This
649 can give an unrepresentative reduction in pH compared to natural carbonation exposure, which
650 has been shown to give a much less marked reductions in pH [201, 202]. Relative humidity control

651 during carbonation testing has also been shown to be highly influential in determining the
652 observed rate of carbonation [203].

653

654 The carbonation of AAMs has been shown to be strongly dependent on binder microstructure, and
655 particularly the degree of microstructural evolution and pore network refinement achieved prior
656 to the start of carbonation exposure, which can be influenced by curing, as well as various mix
657 design parameters such as the activator dose [204-207]. The presence of hydrotalcite-type LDH
658 phases has been identified as being particularly crucial in enabling carbonation resistance, whether
659 these are produced directly as a result of activation of an Mg-containing precursor, or due to the
660 addition of a supplemental Mg source (or calcined LDH as a seeding/templating agent) [208] [15,
661 209, 210]. The mechanisms of carbonation shrinkage in alkali-activated slag binders have also
662 been identified [211]. Together, these new aspects of insight provide essential steps toward
663 designing AAMs that can appropriately resist carbonation in service, and also in understanding
664 the connections between accelerated and natural carbonation mechanisms to enable the design of
665 appropriate laboratory tests for the prediction of field performance. Electrochemical examinations
666 of carbonated AAM concrete showed that the binders have been capable of keeping the
667 reinforcement in a passive condition even with the lowered pH caused by the accelerated
668 carbonation [212, 213], but this does necessitate further investigation.

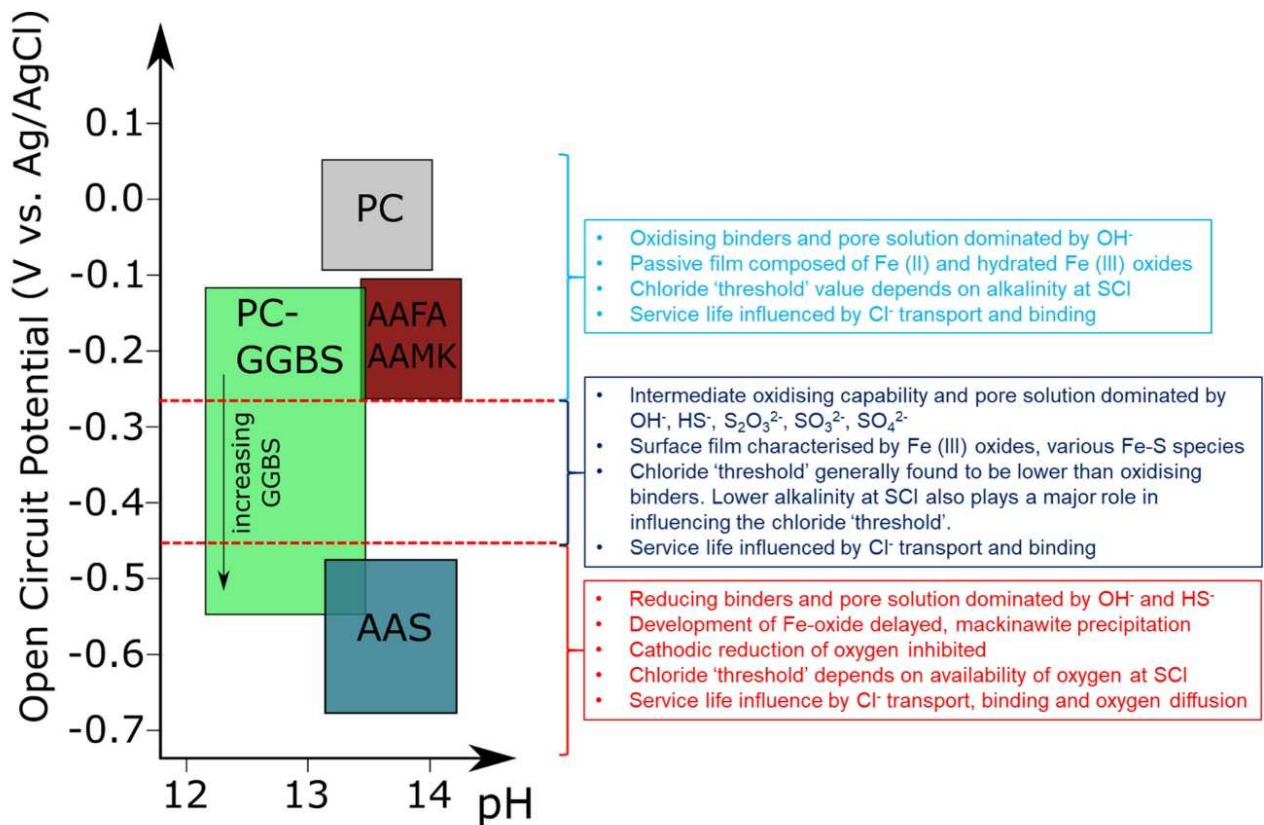
669

670 In many steel-reinforced concrete applications, the service life of a structure or element is
671 governed by the ability of the concrete to protect the steel from chloride-induced corrosion. The
672 rate and mechanisms of chloride transport in AAMs have been reviewed in detail by Osio-
673 Norgaard et al. [214]. Thomas et al. [215, 216] have provided a comparison of chloride test
674 methods as applied to these materials. Hu et al. [144] found that some alkali could leach out during
675 specimen saturation before the electrically accelerated chloride transport test, and that the water-
676 to-specimen ratio could have a critical effect on the passed charges, but not on the chloride
677 migration coefficient of the specimens. This is an active area of work in international
678 organizations including RILEM and the European Federation for Corrosion, who have established

679 working groups to investigate chloride transport and corrosion initiation in AAMs, with a
680 particular view toward the development of more appropriate testing methods. Noushini and Castel
681 [217] have recently discussed the development of performance-based criteria for AAM concretes
682 based on chloride ponding and electrochemically accelerated tests, which is an essential step
683 toward performance-based standardization of AAMs. For electrochemical testing, it also appears
684 likely that the proportionality constants applied in the relationships that are commonly used to
685 obtain material parameters from polarization curves (Tafel slopes) for Portland cement will need
686 to be re-assessed for AAMs, as there appear to be significant deviations from the classical
687 electrochemistry of Portland cement when considering the particular pore fluid chemistry of
688 AAMs [218].

689
690 Chloride binding, particularly by hydrotalcite-type LDH phases, has been identified by some
691 authors to be very influential in determining chloride transport through AAMs [219, 220],
692 although other authors did not identify strong evidence for chloride binding in alkali-activated
693 slag concretes [215, 221]. There is a clear need for further developments to resolve this open
694 question, which is of fundamental importance to service life prediction for reinforced AAMs
695 under chloride exposure.

696
697 Ma et al. [222] linked chloride diffusivity, electrical resistivity, and corrosion testing of reinforced
698 alkali-activated concretes, and highlighted the importance of sulfide (provided by blast furnace
699 slag when used as a precursor in AAMs) in defining the corrosion rate post-initiation. The role of
700 sulfide has also been identified in studies of steel corrosion in simulated alkali-activated slag pore
701 solutions [223-225] [226], and in various types of mortar specimens [227-229]. The very high
702 pore solution pH of some AAM binders has also been shown to generate unconventional
703 threshold-like relationships in chloride initiation, and also to give chemical protection of steel
704 reinforcement even at high chloride concentrations [230-232]. Mundra et al. [226] also developed
705 a classification scheme for alkali-activated and slag-blended binders as shown in Fig. 12.



706

707 **Figure 12. Overview of the classification of cements, particularly of AAMs, based on internal**
 708 **redox conditions, and the parameters influencing the onset of steel pitting and the service-**
 709 **life of these binders. AAFA = alkali-activated fly ashes, AAMK = alkali-activated metakaolin.**

710 **Adapted from [226], under Creative Commons license conditions.**

711

712 Questions around alkali-silica reactions, analogous to those which can lead to damaging
 713 expansion in Portland cement binders with reactive aggregates, also arise regularly in discussions
 714 of AAMs because of the high levels of alkali present in these binders. However, the results of
 715 testing with a broad range of binder-aggregate combinations have shown that alkali-silica
 716 reactions do not appear to be particularly problematic in AAMs with aggregates of 'normal'
 717 reactivity [233]. It is possible to induce alkali-silica reaction expansion under accelerated
 718 conditions and with the use of a reactive aggregate [234, 235], but in the majority of cases, AAM
 719 mortars show less expansion than plain PC mortars with the same reactive aggregates [234, 236-
 720 238]. The relatively high Al concentration in the pore solution of AAMs, and in some cases also

721 the lack or near-absence of dissolved Ca, appears to be important in restricting alkali-silica
722 damage [234, 237, 239].

723

724 The freeze-thaw and frost-salt resistance of AAMs do appear to merit further attention, as the
725 literature on this topic contains many case studies but lacks consistent or systematic analysis
726 across the class of materials in general. Sulfate attack on AAMs has also been studied according
727 to a number of test methods, largely because such testing is often requested by specifiers or end-
728 users as sulfate attack can be problematic for Portland cement-based materials. However, the
729 fundamental mechanism of Portland cement sulfate attack, with expansive processes involving
730 the monosulfate-AFm phase, is not possible in most AAMs as this phase is absent from the hydrate
731 products. Sulfuric acid attack on AAMs is, however, a relevant mechanism related to use in sewer
732 infrastructure and other highly aggressive environments [240, 241], and the performance of
733 AAMs (particularly those with low Ca content [242, 243]) under such conditions has been
734 observed to significantly exceed that of most other cementitious binders [242, 244]. Organic acid
735 resistance has also been reported to be a strength of low-calcium AAMs, as small organic acids
736 damage calcium-rich binders through complexation and removal of Ca^{2+} ions, but this mechanism
737 is much less significant for AAMs that do not rely on calcium as a key binder constituent [245,
738 246].

739

740 Testing of AAM durability in the field has generally shown results that are consistent with
741 laboratory trials under non-accelerated or minimally-accelerated conditions; the materials that
742 have been put into service under varying conditions have in many cases served very well,
743 including concretes dating back to the 1950s [151, 247, 248], and more recent demonstration or
744 full-scale infrastructure projects [249-252] including an airport in Australia that was constructed
745 largely from alkali-activated concretes [253]. Such projects are essential in building stakeholder
746 acceptance of AAM technology, and in using the experience gained to guide standards
747 development, to ensure that the materials selected, specified and used are fully fit for purpose
748 [254].

749 **2.10. Applications of alkali-activated materials**

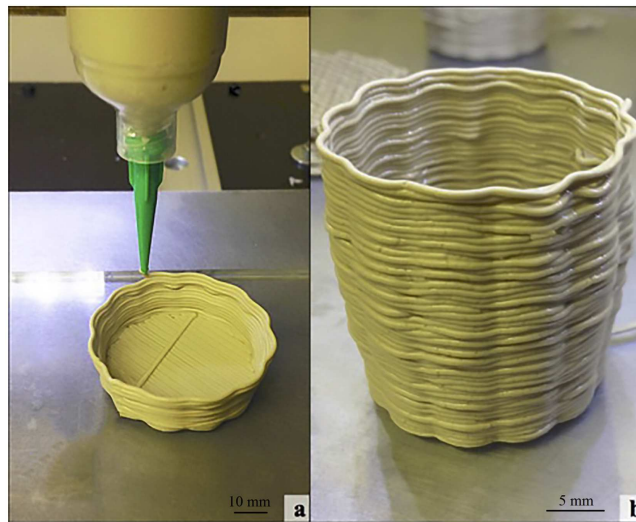
750 Alkali-activated binders are finding rapidly increasing uptake in a growing range of applications,
751 and this section will provide a very brief overview of some of these. The primary route to market
752 for these materials in the short term will almost certainly be as a binder in concretes, and
753 increasingly sophisticated approaches to the design and use of AAM concretes (rather than just
754 directly applying protocols used for Portland cement concretes) are being published for concretes
755 based on alkali-activated GGBS [60, 255-257], fly ash [258-260], metakaolin [261], and various
756 blends of these materials [259].

757
758 AAMs, including particularly the lower-calcium “geopolymer”-type materials, are also attracting
759 attention as matrices for the conditioning and immobilization of radioactive wastes; the ability of
760 these materials to host, and bind, radioisotopes of cesium and strontium has been demonstrated
761 and analyzed in some detail [262-264]. The effective immobilization of cesium in Portland
762 cement-based matrices is well known to be challenging, and so the availability of a cementing
763 system that can restrict its movement is highly desirable. There have been important recent
764 investigations of the potential for compatibility of AAM matrices with complex waste streams
765 containing multiple radioisotopes [265, 266], with oily wastes [267, 268], with ion exchange
766 media [269, 270], and with graphitic or metallic wastes [271-273]. AAM matrices have also been
767 demonstrated to show generally good stability under irradiation [274-276], and a hydrogen
768 radiolytic yield that depends on water content and pore structure [274].

769
770 The ability to produce lightweight AAMs has been investigated by numerous groups, as reviewed
771 recently by Bai & Colombo [277] and by Zhang et al. [278]. Successful approaches have included
772 various types of templating by organic foams or emulsions [160, 267, 268, 279-281], foaming by
773 peroxide addition [282] or by metal powders [283] and the use of lightweight aggregates [284]

774
775 AAMs have also been tested – and in some cases validated – in a broad range of ‘niche’
776 applications in recent years; a non-exhaustive selection of these includes:

- 777 - Well cementing in hydrocarbon and geothermal industries [285-287]
778 - Chromatographic substrates [288]
779 - Manufacture of composites [289, 290], including strain-hardening and/or ductile
780 “engineered composite” materials [291-293]
781 - Repair mortars [294]
782 - Materials for additive manufacturing or “3D printing” through various extrusion-based
783 and powder bed processes (Fig.13 [295]) [296-298]
784 - Moderate-temperature refractories or fire-resistant construction materials [299-302]
785



786
787 **Figure 13. Additive manufacture of a vase from a metakaolin-based AAM, by extrusion. Reproduced**
788 **from [295].**

789

790 **2.11. LCA and environmental aspects**

791 When considering any type of cement as a potentially “eco-friendly” or “low-carbon” alternative
792 to established technologies, it is essential that the actual environmental footprint of both the
793 conventional and innovative materials are sufficiently well understood and quantified, to enable
794 a fair comparison to be made. However, this is an area in which most current research publication
795 practice in the field of alternative cements falls well short of providing the information needed for
796 informed decision-making. This is potentially in part because of the trend for technical authors to

797 justify the importance of their work (to funders, editors or other stakeholders) by ‘advertising’ the
798 class of materials they prefer to study, and in part because the rigorous comparative environmental
799 assessment of two construction materials is actually a highly specialized and challenging research
800 task in itself. In the specific context of AAMs, Habert & Ouellet-Plamondon [303] have provided
801 some very insightful discussion and assessment of data sources, and highlighted in particular the
802 importance of understanding and controlling the environmental footprint of the alkali activator
803 when designing and specifying an AAM mix design.

804

805 Another critical aspect of the assessment of sustainability is the need to conduct a locally-specific
806 determination of energy supply and transport options, and their costs and environmental footprints,
807 as these will differ very strongly between locations worldwide. This means that it is impossible to
808 conduct a valid, generic assessment of the emissions footprint of an AAM at a useful level of
809 precision, without knowing where in the world it will be used. The emissions attributed to
810 electricity generation differ widely from (e.g.) hydroelectric to nuclear to coal sources, and AAMs
811 are much more dependent on electrical energy in production than is Portland cement. This opens
812 some attractive possibilities when considering binder production using a decarbonized electricity
813 supply [304], which may be a strong point in favor of the use of AAMs in regions where low-
814 carbon electricity is available.

815

816 The trend in the academic literature recently has therefore been toward regionally-specific (or
817 very localized) assessments of AAMs for use in particular applications or concrete/mortar
818 products in the Americas [305-307], Europe [308-310], and Australasia [311, 312]. The general
819 trend observed in these studies is that AAMs offer greenhouse emissions savings compared to a
820 Portland cement baseline, and usually on the order of 40-60%, but somewhat increased the
821 environmental impact in other non-greenhouse categories, such as abiotic depletion, ozone layer
822 depletion, fresh and marine water ecotoxicity, and human toxicity, that are considered in the life-
823 cycle assessment process. It has also been identified that there is a strong need for more refined
824 and updated life-cycle inventory data for activator constituents including sodium silicate [303,

825 305, 313], as the currently available international databases do not reflect current production
826 practice or processes. The assessment of recyclability [314, 315] and release of potentially
827 problematic elements (toxic or naturally occurring radioactive materials) [316-318] from AAMs
828 in service has also received some attention as an essential constituent of a full cradle-to-grave or
829 cradle-to-cradle environmental assessment. This will doubtless gain further importance as non-
830 carbon emissions become more of a focus in material and product assessments worldwide, while
831 the sources and characteristics of waste materials used in AAM production become ever more
832 diverse.

833

834 The other critical aspect that needs to be considered in environmental analysis of AAMs is
835 durability (at both material and element/structure scale), and this was discussed in Section 2.9
836 above. Considering all of these aspects together, and to conclude the discussion of AAMs, it
837 should be identified that AAMs are becoming a mature class of materials whose nature and
838 properties are increasingly well understood, and which offer numerous attractive opportunities to
839 exercise their desirable technical and environmental characteristics for the benefit of society. They
840 should not in any way be viewed as a panacea for all problems in the construction materials sector,
841 and nor are they likely to be universally suitable as a replacement for Portland cement-based
842 binders across the full range of applications in which cements are used, for both technical and
843 logistical (materials-supply) reasons. However, as a constituent of the future toolkit of cements,
844 AAMs do bring very significant value.

845

846 In the following sections, the focus of this review will turn to some other types of cementing
847 systems, which are not yet as widely deployed as AAMs, but which can also form valuable
848 components of the cements toolkit.

849

850 **3. Carbonate Binders**

851 The concept of carbonatable binders is based on the fact that some raw materials can harden

852 through carbonation. Carbonated cementitious binders have attracted wide attention in recent
853 years, attributed to their rapid strength gain and the sequestration of CO₂ when exposed to a CO₂
854 rich environment [319, 320]. This section will discuss carbonated calcium silicate, carbonated
855 Portland cement, MgO-based cement and carbonated waste-derived binders. These four binder
856 types react with water and CO₂, yielding strong cementing materials.

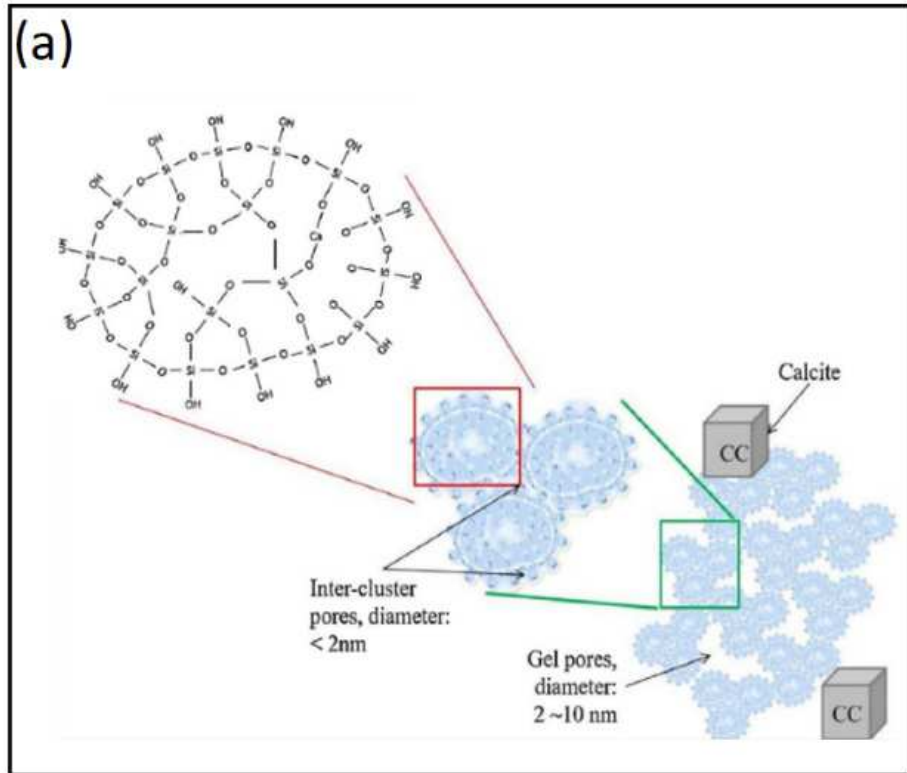
857 **3.1. Carbonated calcium silicate binders**

858 Tricalcium silicate (C₃S), β-dicalcium silicate (β-C₂S), γ-dicalcium silicate (γ-C₂S), tricalcium
859 disilicate (C₃S₂) and monocalcium silicate (CS) can react with CO₂ and form strong monolithic
860 matrices [321-323]. Ashraf & Olek [324] reported that the carbonation of pure calcium silicates
861 consists of two distinct processes: an initial phase-boundary controlled process, and then a
862 subsequent product layer diffusion controlled process. The reaction rate constant was found to
863 vary based on the calcium silicate phases; β-C₂S has the highest reaction rate, followed by C₃S,
864 γ-C₂S, C₃S₂ and finally CS.

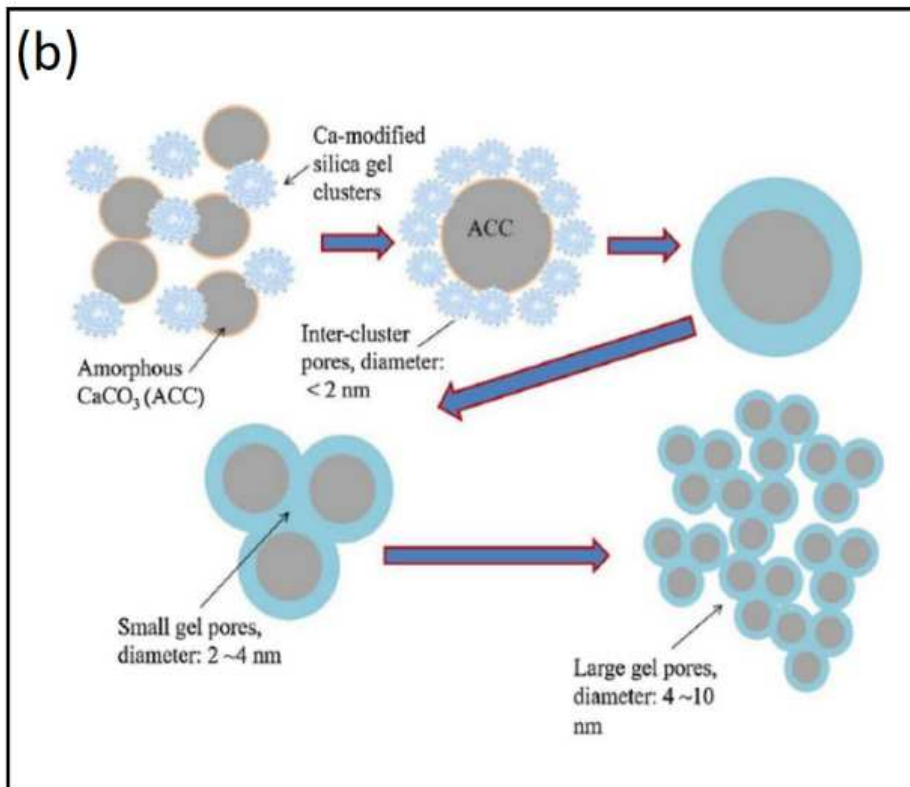
865

866 The carbonation products of pure calcium silicate are calcium carbonate and Ca-modified silica
867 gel or silica gel [323, 325, 326]. The calcium carbonate crystals resulting from carbonation of C₃S,
868 C₂S, C₃S₂ and CS include the polymorphs calcite, aragonite, and vaterite [326, 327]. The presence
869 of a ¹³C CP/MAS NMR signal in carbonated C₃S, C₂S, and C₃S₂ phases can be attributed to the
870 additional formation of amorphous calcium carbonate (ACC), as shown schematically in Fig. 14.
871 However, ACC is not formed in carbonated CS under the same environmental conditions, Fig.14
872 [326]. The presence of poorly crystallized forms of CaCO₃ tends to increase the strength of the
873 carbonated calcium silicate matrices [328]. Furthermore, the values of the elastic modulus of
874 CaCO₃-rich binders can vary over a relatively wide range due to the presence of different
875 polymorphs of CaCO₃ crystals [327].

876



877



878

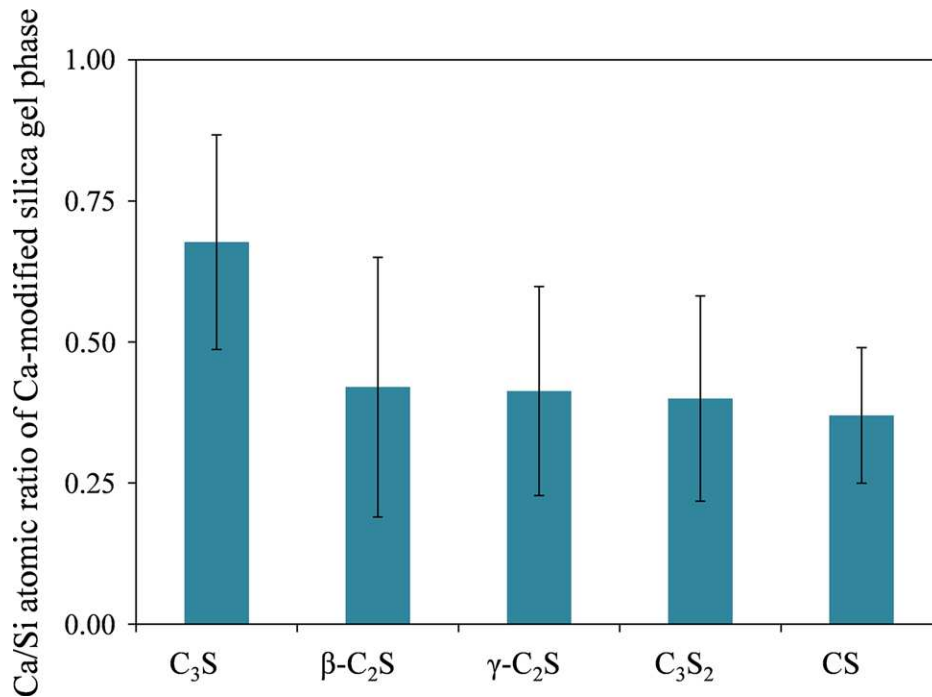
879 **Figure 14. Proposed distribution of the pores (smaller than 10 nm) in carbonated calcium silicate**
 880 **matrixes a) without the presence of amorphous calcium carbonate (ACC) and b) in the presence of**

881 **amorphous calcium carbonate (ACC), adapted from [319].**

882

883 As shown in Fig. 15, the degree of polymerization of Ca-modified silica gel (which is essentially
884 defined by the inverse of the Ca/Si ratio) is nearly the same for all the carbonated calcium silicates
885 discussed, except for the carbonated C_3S , which has a slightly lower degree [326]. However, all
886 the calcium silicates reach a similar overall carbonation level due to the retardation of the
887 carbonation reaction after formation of nearly the same amounts of $CaCO_3$ (Fig. 16), indicating
888 that effect is related to blockage of the surfaces of potentially reactive particles by the precipitated
889 carbonates.

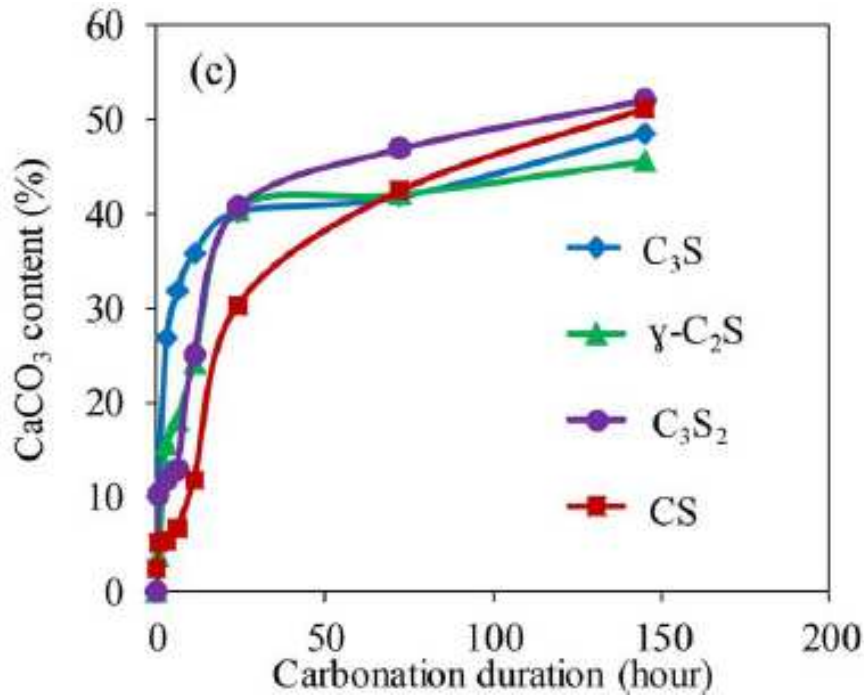
890



891

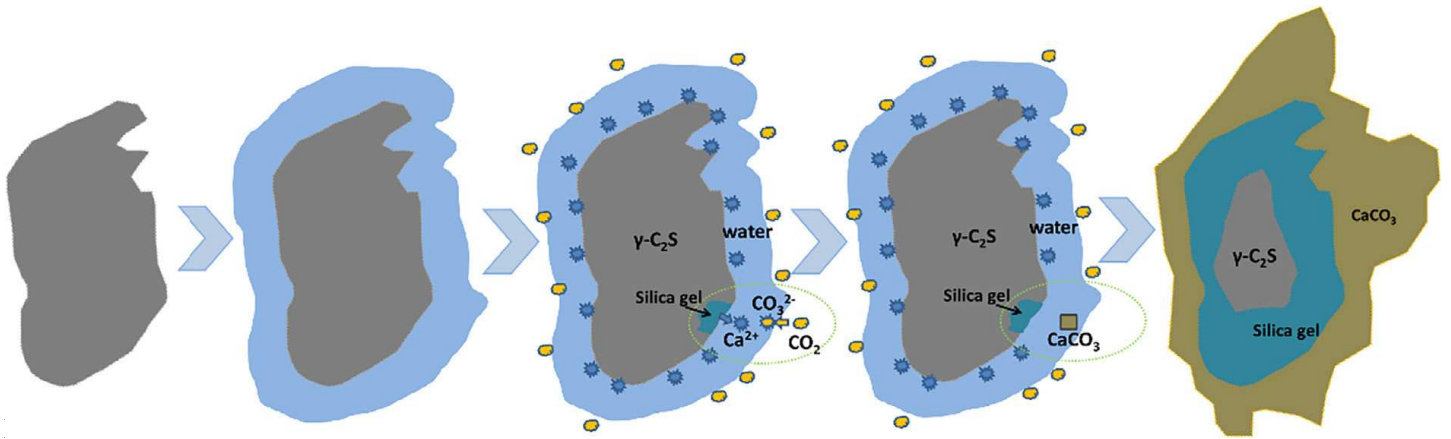
892 **Figure 15. Average Ca/Si atomic ratios of Ca-modified silica gel phase formed during the**
893 **carbonation reaction of the calcium silicate samples [321].**

894



895
 896 **Figure 16. $CaCO_3$ contents (by mass, %) as a function of carbonation duration for different**
 897 **calcium silicate phases [326].**

898
 899 Among these calcium silicates, carbonation of C_2S has attracted more attention due to the different
 900 crystal polymorphs that it can take, particularly $\beta-C_2S$ and $\gamma-C_2S$, as $\gamma-C_2S$ can be produced at
 901 much lower synthesis temperatures than the conventional hydraulic calcium silicate phases.
 902 Chang et al. found $\beta-C_2S$ and $\gamma-C_2S$ to absorb 9.2% and 18.3% of their theoretical levels of CO_2
 903 after 2 h of carbonation, respectively [328], but $\beta-C_2S$ showed the twice the compressive strength
 904 compared to $\gamma-C_2S$. A similar result was reported by Guan et al., who found that the compressive
 905 strength of carbonated $\gamma-C_2S$ was 52.4 MPa after 2 h carbonation [329]. Calcite and aragonite are
 906 the main crystals formed by carbonation of $\gamma-C_2S$, and amorphous Ca-modified silica gel lacking
 907 long-range order was also formed [329-331]. Mu et al. [327] proposed a conceptual model of the
 908 carbonation process of a $\gamma-C_2S$ particle, as shown in Fig. 17.



9
912 **Figure 17. A conceptual carbonation model diagram of γ -C₂S particle. From [327]**

913

914 **3.2. Carbonated Portland cement (PC) binders**

915 It is well known that accelerated early-age carbonation of Portland cement binders can result in
 916 rapid strength gain and lower permeability. This is because the carbonation reaction leads to a
 917 reduction in total porosity through the formation of carbonation products that occupy more space
 918 than the portlandite that they are replacing. Shi et al. [332] proposed the use of pre-conditioning
 919 to improve the accelerated carbonation of PC binders; the compressive strength of carbonated
 920 concrete after proper pre-conditioning then 2 h of CO₂ exposure is similar to that of the concrete
 921 after 24 h of steam curing. Furthermore, the carbonated concrete exhibits a similar compressive
 922 strength to that of steam-cured concrete during winter weathering exposure [333]. Shi et al. [334,
 923 335] suggested that pre-conditioning environments have the most crucial effect on the
 924 effectiveness of CO₂ curing. Additionally, the temperature of the samples rises very quickly once
 925 the samples are exposed to CO₂; this could reach a peak value of 70 °C during the first 15-20 min,
 926 then goes down gradually with time.

927

928 Kenward et al. [336] studied hydration of an oil-well cement in the presence and the absence of
 929 pure CO₂ gas. The carbonate formed was initially amorphous calcium carbonate that was not
 930 detectable by XRD, but this changed to crystalline calcite detectable by XRD within 24 h. The
 931 addition of carbon dioxide did result in performance benefits.

932

933 Shah et al. [331] have suggested that the precipitation of the three polymorphs of calcium
934 carbonate (calcite, vaterite, and aragonite) takes place in carbonated PC, while Castellote et al.
935 [333] only detected calcite in carbonated PC. CaCO_3 polymorphism is sensitive to pore fluid
936 chemistry, carbonation conditions and duration, and may also involve amorphous phases as noted
937 in Section 3.1, so this is a complex area requiring further analysis. Based on thermogravimetric
938 analysis, the main mass loss from carbonated PC pastes takes place between 600°C and 950°C .
939 The poorly crystalline carbonates, preferentially associated with C-S-H carbonation, decomposed
940 at a temperature below 600°C , while the decomposition temperature of well crystallized CaCO_3
941 is above 600°C [320, 337, 338]. The carbonated PC was strongly decalcified to form these CaCO_3
942 phases along with a Ca-modified silica gel, identified via the decrease of the Q^1 and Q^2 sites, and
943 increase in Q^3 and Q^4 sites, according to ^{29}Si MAS NMR analysis. ^{27}Al MAS NMR spectroscopy
944 confirmed that the aluminum-bearing phases, containing mainly AlO_6 (ettringite and AFm) and
945 AlO_4 sites (C-A-S-H) were dissolved to form an alumino-silicate amorphous gel (with Al as AlO_4),
946 characterized by a broad resonance that was always positioned at the same chemical shift (55 ppm)
947 [339].

948

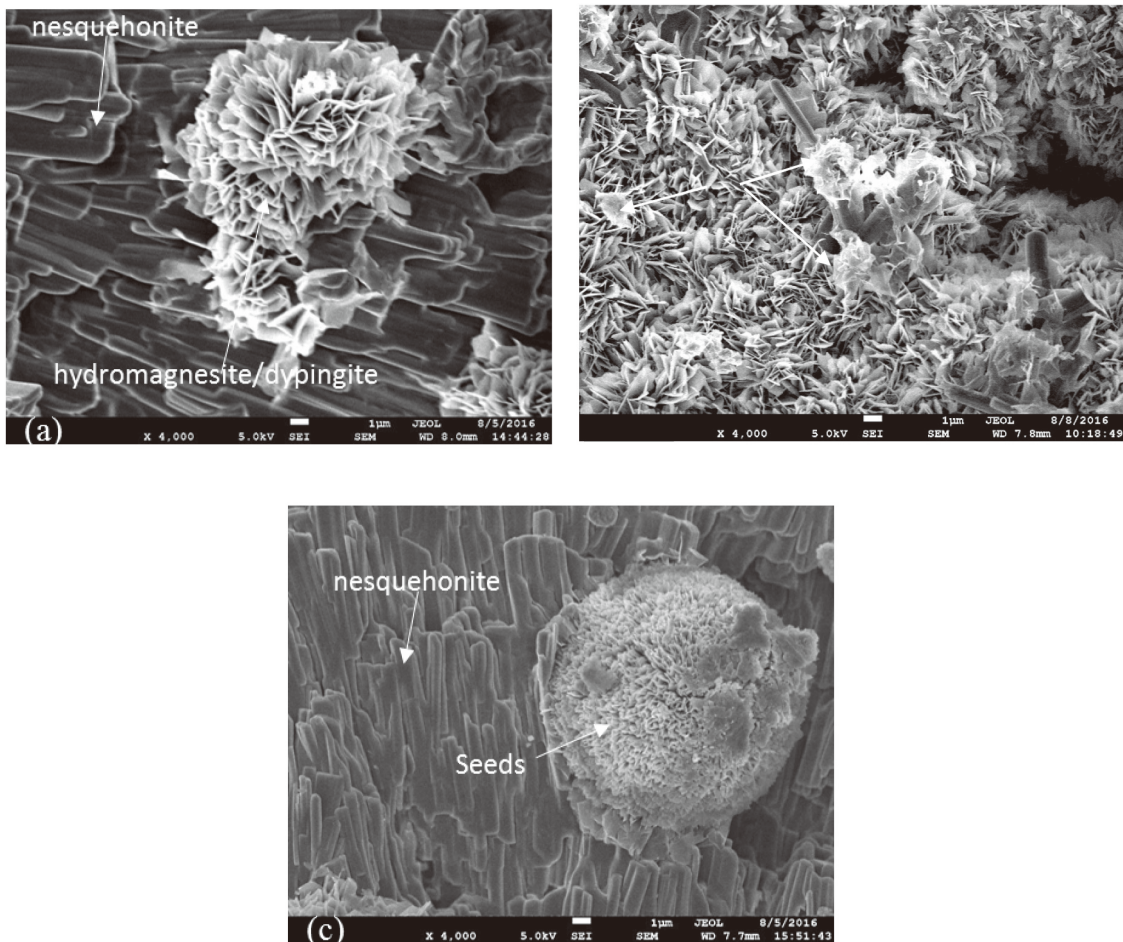
949 **3.3. Magnesium-based cement (MC) binders**

950 In recent decades, the use of reactive magnesium oxide (MgO) in PC has received more and more
951 attention. Carbonation of magnesium-rich cements improves the compressive strength of these
952 cementitious materials, which is attributed to the densification of materials caused by the
953 formation of nesquehonite ($\text{MgCO}_3 \cdot 3\text{H}_2\text{O}$), dypingite ($\text{Mg}_5(\text{CO}_3)_4(\text{OH})_2 \cdot 5\text{H}_2\text{O}$) and artinite
954 ($\text{Mg}_2(\text{OH})_2\text{CO}_3 \cdot 3\text{H}_2\text{O}$) [340, 341]. Mo et al. [342] suggested that a large amount of calcite and a
955 relatively smaller amount of aragonite are the calcium carbonates formed, while magnesian calcite
956 is formed due to the incorporation of Mg^{2+} in the carbonated phase, and nesquehonite is formed
957 only in pastes containing at least 40% reactive MgO. Nesquehonite has been identified as the key
958 binding phase in other potential carbonated magnesia-based binders [343].

959

960 Figure 18 shows the morphology of carbonated magnesia cement [344]. The needle-like
961 nesquehonite and disk/rose-like hydromagnesite/dypingite, which are the main sources of strength
962 development in these cement formulations, are observed. The disk/rose-like
963 hydromagnesite/dypingite crystals that formed due to the carbonation process could be
964 distinguished from the hydromagnesite seeds included within the initial mix, which possesses a
965 ground ball-like morphology.

966



967

968 **Figure 18. SEM images of H₂O samples after carbonation: (a) H₂O·S0, (b) H₂O·S0.5 and (c)**

969

H₂O·S1.0. From [344].

970

971 The area of magnesia-based cements is very diverse, and includes cements which harden and gain
972 strength by various combinations of carbonation and other chemical reactions, as reviewed in
973 detail recently by Walling & Provis [345]. These cements are proposed for use in many
974 applications ranging from large-scale construction to nuclear waste immobilization, and in some

975 cases offer the possibility for notable CO₂ emissions savings compared to conventional Portland
976 cement. The supply of MgO is constrained in some areas due to cost or resource availability, but
977 this is not universally the case, and materials of very good technical and environmental
978 performance can certainly be produced using this chemistry.

979

980 **3.4. Carbonated waste-derived binders**

981 Steel slag is a broad classification for several types of industrial by-products produced during the
982 steel making process, which may be regarded as a waste-derived binder precursor [346-348].
983 Generally, the components of steel slag include hydraulic calcium silicates (C₃S, β-C₂S), non-
984 hydraulic calcium silicates (e.g. γ-C₂S, CS), and free CaO, each of which can react with CO₂.
985 Formation of calcium carbonate in the form of calcite and aragonite in the carbonated steel slag
986 binders causes microstructural densification associated with a reduction in the total porosity, and
987 hence improves the compressive strength. A carbonated steel slag binder was observed to show a
988 shift in its dominant pore diameter from 0.3-3 μm before carbonation, to <0.1 μm in the carbonated
989 paste [349]. The free CaO in the steel slag is partially or completely consumed due to the reaction
990 with CO₂, which improves the volume stability of the binder [350, 351]. Calcium carbonate (as
991 calcite and aragonite) is the main carbonate product formed, and portlandite and calcium silicate
992 seem to be more carbonation-reactive than the Fe-bearing phases that are also present [349].
993 Monkman et al. [352] reported the possibility of using a carbonated ladle slag as a fine aggregate.
994 After carbonation, calcium carbonates and spurrite were detected as new phases by XRD, together
995 with the consumption of hydrogarnet and calcium hydroxide. Mortars made with the slag sand
996 demonstrated strengths comparable to mortars made with conventional river sand.

997

998 High calcium fly ashes have an attractive capacity to be used for mineral sequestration of CO₂
999 under controlled conditions [353, 354]. A recent study show that Ca-rich fly ashes react readily
1000 with gas-phase CO₂ to produce robustly cemented solids which can achieve a compressive
1001 strength of around 35 MPa and take up 9% CO₂ under optimized conditions [355]. Mahoutian and

1002 Shao [356] implemented a low temperature process to produce a binder material from blends of
1003 fly ash and ladle slag. CO₂ gas (99.5% purity) was used for carbonation of the synthesized cement
1004 for 2 hours and showed that the early age carbonation curing increased the subsequent hydration
1005 strength.

1006

1007 **4. Belite-Ye'elimite Binders**

1008 Ye'elimite, or calcium sulfoaluminate (Ca₄Al₆O₁₂SO₄), is the main mineral in CSA cement clinker,
1009 and has a crystallographic structure belonging to the sodalite family [357]. CSA cements have
1010 been developed on a commercial basis and used in real applications, primarily in China, since the
1011 1970s [358]. These cements are normally used as components in specialty applications because
1012 of their higher price compared to Portland cement. However, as low-carbon binders, the interest
1013 in these binders from the cement industry continues to increase because it is closer to the objective
1014 of 'eco-friendly' than many of the other low-carbon binder systems that are still under R&D [359,
1015 360]. The highly innovative production of ye'elimite-containing clinkers burning waste elemental
1016 sulfur as fuel, meeting both energy and materials supply demand in a single step, has also been
1017 demonstrated in a full-scale kiln [361], with the potential for further scale-up.

1018

1019 Ye'elimite reacts very quickly with water and contributes to the development of early strength of
1020 this binder, forming monosulfate, ettringite, and amorphous aluminum hydroxide as major
1021 hydrates. Various other reaction products can be obtained, such as strätlingite,
1022 monocarboaluminate, and gibbsite depending on the minor phases in the CSA cement [362, 363].
1023 Normally calcium sulfates are used to adjust the binder hydration reactions, and to promote the
1024 formation of ettringite rather than monosulfate [364, 365]. Dicalcium silicate (belite) and ferrites
1025 are present as additional main mineralogical components of CSA cements. In this paper, the
1026 authors will focus on some belite-ye'elimite binders containing more belite than ye'elimite, which
1027 is different from CSA cements that contain more ye'elimite than belite. Both belite and ye'elimite
1028 are lower energy minerals compared with tricalcium silicate (alite), which are suitable for low

1029 energy and low-carbon clinker cement production and applications.

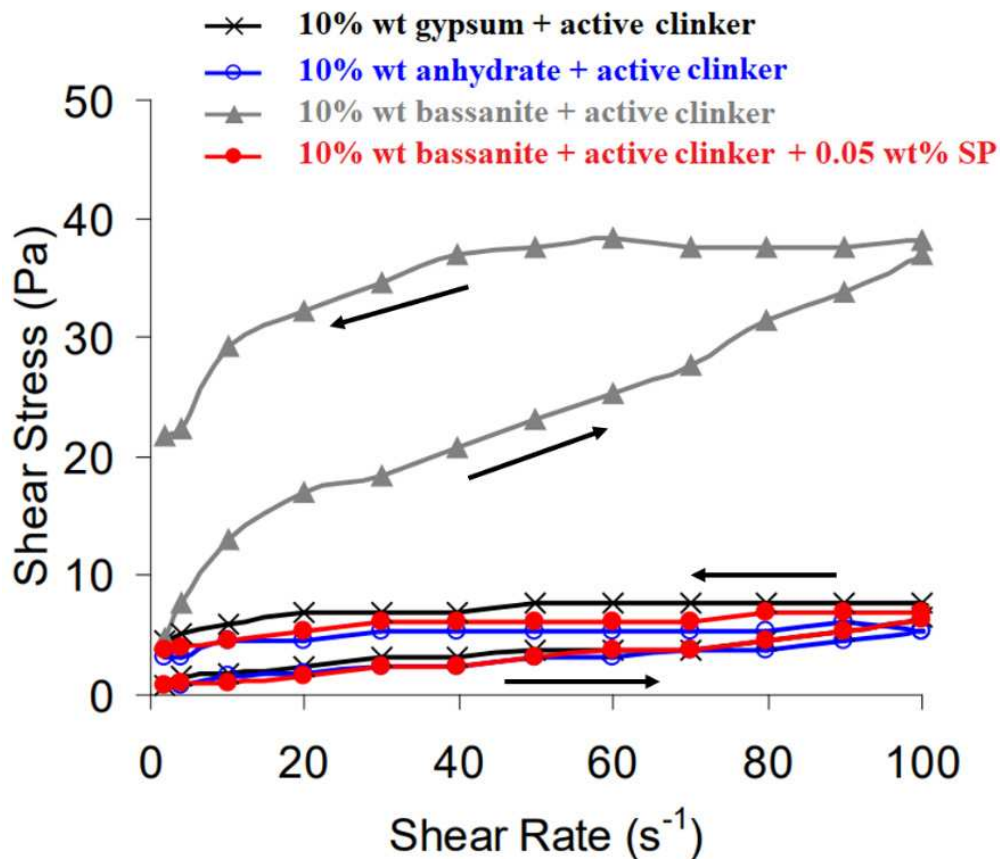
1030 **4.1. Belite-ye'elimite-ferrite binders**

1031 Belite-ye'elimite-ferrite (BYF) binders, also known as calcium sulfoaluminate or sulfobelite
1032 cement [359, 360], have belite as the main phase (45-75%), and ye'elimite as a second component
1033 (20-45%). This approach to manufacturing BYF binders allows the use of less expensive Al-rich
1034 raw materials, due to the lower ye'elimite content in the clinker compared to 'conventional' CSA
1035 cements which require a higher-purity Al source. The recent main research interest in this type of
1036 binder is related to the understanding of ye'elimite hydration, that should be carefully controlled
1037 to achieve desired rheology and setting time, and also on achieving more reactivity of the belite
1038 component that contributes to the later growth in strength. BYF binders are not yet in large-scale
1039 industrial production, but have been developed to pilot scale by some cement companies under
1040 certain national and multi-national projects.

1041
1042 A study by Cuesta et al. [366] on the early hydration mechanisms of synthetic ye'elimite revealed
1043 that the polymorphism of ye'elimite (orthorhombic stoichiometric and pseudo-cubic solid-
1044 solution ye'elimite) influenced the hydration kinetics, together with the w/c ratio and the solubility
1045 of the additional sulfate sources.

1046
1047 Recently, new data on the hydration of BYF cements have been published by Álvarez-Pinazo et
1048 al. [367]. 'Non-active' clinker (containing β -belite and orthorhombic ye'elimite) and 'active
1049 clinker' (containing α'_H -belite and pseudo-cubic ye'elimite) have been studied with different
1050 calcium sulfate sources. The findings of this study showed that the active-clinker mortar
1051 developed higher compressive strengths than non-active-clinker mortars, independent of the
1052 choice of sulfate source, and it formed higher quantities of ettringite during hydration and less
1053 AFm compared to non-active cements. Another interesting finding that should be mentioned is
1054 that the paste with basanite ($\text{CaSO}_4 \cdot 0.5\text{H}_2\text{O}$) as the sulfate source showed the highest viscosity
1055 values and a hysteresis cycle attributed to fast setting, more so than gypsum- and anhydrite-

1056 containing pastes; this behavior can be adjusted by adding a small amount of polycarboxylate-
 1057 based superplasticizer (SP) (0.05 wt%) without changing the phase assemblage [368, 369] (Fig.
 1058 19). This offers a possibility to add a superplasticizer normally used in Portland cement binders
 1059 to control the rheological behaviour of BYF cements.
 1060



1061
 1062 **Figure 19. Flow curves of different BYF clinkers with different additional sulphate sources (re-**
 1063 **drawn based on [367])**

1064
 1065 Morin et al. [370] studied five different BYF cements by experimental analysis and
 1066 thermodynamic modeling to track the hydration kinetics and phase assemblage, which were
 1067 influenced by the quantity of anhydrite, the w/c ratio, and the clinker fineness. The results
 1068 indicated that with increasing addition of anhydrite, belite hydration was delayed, which
 1069 contributed to the formation of a strength plateau between early ye'elite hydration and later
 1070 belite and ferrite hydration. Also, a higher fineness of cement together with increased w/c ratio

1071 leads to higher belite hydration kinetics. Those authors proposed that the question of whether there
1072 is enough water provided to form all hydration products strongly influences the hydration of belite
1073 and ferrite phases.

1074

1075 **4.2. Belite-alite-ye'elinite binder**

1076 Because some belite-ye'elinite-ferrite cements present quite low mechanical strength due to their
1077 high content of belite with slow reactivity, methods to improve early strength have been sought.
1078 One such approach is a clinkering method aiming to introduce a reactive alite phase into the belite-
1079 ye'elinite binder system, as an alternative way to improve the mechanical strength. However, the
1080 temperature incompatibility between alite formation (above ~ 1300 °C) and ye'elinite
1081 decomposition (between 1300 and 1350 °C) brings difficulty in achieving the coexistence of alite
1082 and ye'elinite phases in clinkering processes. However, this problem can be solved and controlled
1083 by addition of minor quantities of CaF_2 [371] or other oxides, such as ZnO , B_2O_3 , or Na_2O , in the
1084 raw meal [372].

1085

1086 Chitvoranund et al. [373] prepared a clinker by firing limestone, tuff, gypsum and calcium fluoride
1087 (used as mineraliser) in a laboratory furnace at 1300 °C for 45 min, which requires a synthesis
1088 temperature 150–200°C lower than traditional PC clinker. The minerals present in the clinker
1089 included alite (48.3%), belite (1.5% α' - C_2S + 10.3 % β - C_2S + 2.2% γ - C_2S), ye'elinite (9.6%),
1090 and ferrite (12.9%). Later, the ground clinker was mixed with 5% anhydrite to make a so-called
1091 alite-calcium sulfoaluminate cement. The hydration products were mainly C-S-H, ettringite,
1092 monosulfate, and portlandite, and hydration rates are rapid. Thermodynamic modeling revealed
1093 that the cement reacted strongly within the first 10 days of hydration, then the reaction process
1094 slowed down and was almost completed by 100 days. Ferrite exhibited reactivity in the presence
1095 of C_3S , and was consumed to give monosulfoaluminate and katoite. The compressive strength of
1096 mortars developed quite rapidly, from 10 MPa at 1 day to 35 MPa at 28 days. The release of CO_2
1097 from this approach to clinker production is estimated at about 11-12 % less than conventional

1098 Portland cement without the consideration of other factors.
1099
1100 In another study by Londono-Zuluaga et al. [374], a novel clinkering process to prepare belite-
1101 alite-ye'elimite (BAY) binders has been optimized (900 °C/30 min – 1300 °C/15 min) and scaled-
1102 up to 2 kg scale. This process involved as raw meal a mix of natural limestone, sand, iron oxide
1103 (a byproduct of the sulfuric acid industry), gypsum, and kaolin. The main mineralogical
1104 composition of their final scaled-up BAY clinker was 60.6 % belite, 14.3 % of alite and 10.4%
1105 ye'elimite, on a mass basis. BAY cements were prepared by mixing the scaled-up clinker with 12
1106 wt.% anhydrite. The analysis of hydration highlighted that the main reaction products are
1107 ettringite, AFm phases (monosulfoaluminate and strätlingite), katoite, and C-S-H. Ye'elimite
1108 reacted with anhydrite to be completely consumed within 1 day, alite and ferrite almost fully
1109 reacted after 7 days, and belite showed a typical slower hydration behavior. Portlandite was not
1110 detected in the pastes at testing ages of 1, 7 and 28 days; it was speculated to be consumed to form
1111 katoite, AFt phases or monosulfoaluminate. The compressive strength of BAY mortars was
1112 recorded to be higher than that of a BYF binder prepared by the same group, at any testing age,
1113 most likely due to the presence of alite. The influence of fly ash blending in BAY cements has
1114 been also reported by the same authors [375]: with the addition of fly ash, the compressive
1115 strengths of mortars increased to 68, 73 and 82 MPa, for mortars with 0, 15 and 30 wt.%
1116 replacement of BAY cement by fly ash respectively, at 180 days. The main hydration products
1117 were AFt, AFm phases, katoite, and C-S-H for all systems studied. Utilizing a small amount of
1118 superplasticizer makes it possible to prepare BAF pastes with low viscosity values. The reactivity
1119 of belite appeared to have been inhibited by the high addition of fly ash, and other than the strength
1120 increase, no clear evidence of pozzolanic chemical reaction with fly ash in BAY systems was
1121 obtained. These do appear to be a promising class of cements for future large-scale utilization.
1122 Zhou et al. [376] investigated the influence of the ferrite phase in a similar binder system on its
1123 hydration and mechanical properties.
1124

1125 **4.3. Belite-ye'elinite-ternesite binder**

1126 Belite-ye'elinite-ternesite binders have been treated as another interesting alternative material for
1127 reducing CO₂ emissions. The HeidelbergCement Technology Center (HTC) has worked for
1128 several years to develop new and innovative techniques of production approaches for this binder,
1129 and have published some patents related to this type of cement in recent years.

1130

1131 Ternesite (C₅S₂Ŝ) was first found in Germany as a natural mineral in the 1990s. It is also found in
1132 the crust covering the areas of Portland cement kilns where the temperature is lower than 1250 °C.
1133 The advantages of ternesite-containing clinkers are quite clear due to the lower clinkering
1134 temperature. For a long time, this phase has been regarded as a non-hydraulic material, until it
1135 was recently found to be reactive with aluminum hydroxide. According to Ben Haha et al. [377],
1136 aluminum hydroxide can be used to activate ternesite to form ettringite, strätlingite and C-S-H in
1137 different proportions, depending on the reactivity and reaction degree. Work by Montes et al. [378],
1138 focusing on how other calcium aluminates activate the hydration of ternesite, has also been
1139 published recently. Synthetic C₃A, C₁₂A₇, CA and C₄A₃Ŝ (ye'elinite) phases were blended with
1140 ternesite separately, then the hydration reactions of the blends were studied through various
1141 techniques. Ternesite was activated in all the blends with aluminates, with descending
1142 effectiveness order C₁₂A₇ ≈ CA > C₃A >>> C₄A₃Ŝ. Also, the presence of ternesite changes the
1143 hydration products of these aluminates. However, ternesite was less consumed in the samples
1144 mixed with ye'elinite due to the sulfate common ion effect. Even though in this study some
1145 calorimetric evidence of an activating effect was recorded, ternesite could not be regarded as
1146 having been activated by ye'elinite as no strätlingite was detected. The characteristics of ternesite
1147 as a component of belite-ye'elinite (sulfobelitic) binders was later discussed by Blanco and
1148 Carmona [379] who noted that ye'elinite and ternesite can co-exist in the CaO-SiO₂-Al₂O₃-
1149 CaSO₄ system.

1150

1151 A single-stage process to produce ternesite-containing clinkers (belite and ternesite-rich calcium
1152 sulphoaluminate) has been proposed by Hanein et al. [380], based on some important new work

1153 in determining and defining the high-temperature thermodynamics of sulfur-containing
1154 clinkerization processes [381]. The clinker was obtained in a pilot plant where the partial pressure
1155 of O₂ and SO₂ was controlled in the kiln. The target operation temperature was set up to 1260 °C
1156 in order to make the process to reach steady state rapidly, corresponding with their thermodynamic
1157 calculations that the upper limit stability temperature for ternesite is ~1290 °C. The results also
1158 clearly confirmed that ternesite can be synthesized in a dry atmosphere.

1159

1160 **5. Conclusions and Final Remarks**

1161 The development and use of low-carbon binders as an alternative to Portland cement-based
1162 materials, aiming to reduce the carbon footprint associated with construction and other
1163 applications, has made notable progress in recent years. In summary:

1164

1165 a) Alkali-activated binders are very important and high-potential alternative materials, which
1166 are now deployed on a commercial scale in several nations in the world. Recently the
1167 development of understanding on the rheological behavior, setting properties and structural
1168 characterization of alkali-activated binders has advanced rapidly. Progress in formulation of
1169 one-part alkali-activated binders has further approached large-scale production and
1170 application. However, the development and optimization of mix designs based on different
1171 raw materials and activators has not yet been systematically understood. Durability
1172 performance appears very good in most areas but needs more detailed work on test method
1173 validation and standardization. Environmental assessment of these materials should also be
1174 improved.

1175 b) Carbonatable binders, regarding as a new approach to address concerns over CO₂ emissions,
1176 still are in a development route. The technology has been advanced recently, especially in the
1177 understanding of accelerating and controlling the carbonation hardening process. The
1178 limitations for these binders in application are also becoming clear, for instance the CO₂-rich
1179 atmospheres required for curing, and the pH reduction that means that use in reinforced

1180 elements will be challenging. However, these binders which may offer very high CO₂ savings
1181 if a circular CO₂ economy develops [360] still deserve serious attention as alternative low-
1182 carbon materials.

1183 c) Belite-ye'elimite binders: this is a relatively new approach to produce alternative
1184 cementitious materials compared to the conventional CSA cements, targeting a high belite
1185 content in the clinkers. Although belite-ye'elimite-based binders are still under development
1186 and have not reached the full scale-up stage, the clinkering process, understanding of
1187 hydration, and the formulation of binders has developed greatly, not only in the scientific
1188 community but also in the cement industry. Good mechanical strength was obtained by
1189 hydrating this type of binder. The control of the rheological behavior and setting time have
1190 also been investigated. However, this binder system and technology is not yet commercialized
1191 or standardized. The clinkering process, which depends on different raw materials, should be
1192 optimized for large-scale production.

1193 **Acknowledgements**

1194 The financial support of this work from the National Natural Science Foundation of China under
1195 contract No. 51638008 is greatly appreciated.

1196

1197 **References**

- 1198 [1] C. Shi, A. Fernández-Jiménez, A. Palomo, New cements for the 21st century: The pursuit of
1199 an alternative to Portland cement, *Cem. Concr. Res.*, 41 (2011) 750-763.
- 1200 [2] J.L. Provis, A. Palomo, C. Shi, Advances in understanding alkali-activated materials, *Cem.*
1201 *Concr. Res.*, 78 (2015) 110-125.
- 1202 [3] C. Shi, D. Roy, P. Krivenko, *Alkali-activated cements and concretes*, Taylor & Francis, 2006.
- 1203 [4] F. Pacheco-Torgal, J. Labrincha, C. Leonelli, A. Palomo, P. Chindaprasit, *Handbook of alkali-*
1204 *activated cements, mortars and concretes*, Elsevier, 2014.
- 1205 [5] J.L. Provis, *Alkali-activated materials*, *Cem. Concr. Res.*, 114 (2018) 40-48.
- 1206 [6] X. Gao, Q.L. Yu, A. Lazaro, H.J.H. Brouwers, Investigation on a green olivine nano-silica
1207 source based activator in alkali activated slag-fly ash blends: Reaction kinetics, gel structure and
1208 carbon footprint, *Cem Concr. Res.*, 100 (2017) 129-139.
- 1209 [7] R. Vinai, M. Soutsos, Production of sodium silicate powder from waste glass cullet for alkali
1210 activation of alternative binders, *Cem Concr. Res.*, 116 (2019) 45-56.
- 1211 [8] N. Toniolo, A. Rincón, J.A. Roether, P. Ercole, E. Bernardo, A.R. Boccaccini, Extensive reuse
1212 of soda-lime waste glass in fly ash-based geopolymers, *Constr. Build. Mater.*, 188 (2018) 1077-
1213 1084.
- 1214 [9] M. Torres-Carrasco, M.T. Tognonvi, A. Tagnit-Hamou, F. Puertas, Durability of alkali-
1215 activated slag concretes prepared using waste glass as alternative activator, *ACI Mater. J.*, 112
1216 (2015) 791-800.
- 1217 [10] Y. Liu, C. Shi, Z. Zhang, N. Li, An overview on the reuse of waste glasses in alkali-activated
1218 materials, *Resourc. Conserv. Recyc.*, Accepted for publication (2019).
- 1219 [11] A. Peys, H. Rahier, Y. Pontikes, Potassium-rich biomass ashes as activators in metakaolin-
1220 based inorganic polymers, *Applied Clay Science*, 119 (2016) 401-409.
- 1221 [12] S.A. Bernal, Advances in near-neutral salts activation of blast furnace slags, *RILEM Tech.*
1222 *Lett.*, 1 (2016) 39-44.
- 1223 [13] S.A. Bernal, J.L. Provis, R.J. Myers, R. San Nicolas, J.S.J. Van Deventer, Role of carbonates
1224 in the chemical evolution of sodium carbonate-activated slag binders, *Mater. Struct.*, 48 (2015)
1225 517-529.
- 1226 [14] X. Ke, S.A. Bernal, J.L. Provis, Controlling the reaction kinetics of sodium carbonate-
1227 activated slag cements using calcined layered double hydroxides, *Cem Concr. Res.*, 81 (2016) 24-
1228 37.
- 1229 [15] X. Ke, M. Criado, J.L. Provis, S.A. Bernal, Slag-based cements that resist damage induced
1230 by carbon dioxide, *ACS Sust. Chem. Eng.*, 6 (2018) 5067-5075.
- 1231 [16] M. Esaifan, H. Khoury, I. Aldabsheh, H. Rahier, M. Hourani, J. Wastiels, Hydrated
1232 lime/potassium carbonate as alkaline activating mixture to produce kaolinitic clay based inorganic
1233 polymer, *Appl. Clay Sci.*, 126 (2016) 278-286.
- 1234 [17] L. Valentini, S. Contessi, M.C. Dalconi, F. Zorzi, E. Garbin, Alkali-activated calcined
1235 smectite clay blended with waste calcium carbonate as a low-carbon binder, *J. Cleaner Prod.*, 184
1236 (2018) 41-49.
- 1237 [18] J. Dietel, L.N. Warr, M. Bertmer, A. Steudel, G.H. Grathoff, K. Emmerich, The importance

- 1238 of specific surface area in the geopolymerization of heated illitic clay, *Appl. Clay Sci.*, 139 (2017)
1239 99-107.
- 1240 [19] R.C. Kaze, L.M. Beleuk à Mougam, M.L. Fonkwe Djouka, A. Nana, E. Kamseu, U.F. Chinje
1241 Melo, C. Leonelli, The corrosion of kaolinite by iron minerals and the effects on
1242 geopolymerization, *Appl. Clay Sci.*, 138 (2017) 48-62.
- 1243 [20] M. Lassinantti Gualtieri, M. Romagnoli, S. Pollastri, A.F. Gualtieri, Inorganic polymers from
1244 laterite using activation with phosphoric acid and alkaline sodium silicate solution: Mechanical
1245 and microstructural properties, *Cem Concr. Res.*, 67 (2015) 259-270.
- 1246 [21] N. Nadziri, I. Ismail, S. Hamdan, Binding gel characterization of alkali-activated binders
1247 based on palm oil fuel ash (POFA) and fly ash, *J. Sust. Cem.-Based Mater.*, 7 (2018) 1-14.
- 1248 [22] G. Sukmak, S. Horpibulsuk, M. Setkit, S. Kassawat, A. Arulrajah, Palm oil fuel ash-soft soil
1249 geopolymer for subgrade applications: strength and microstructural evaluation, *Road Mater. Pave.
1250 Des.*, 20 (2019) 110-131.
- 1251 [23] H. Sreenivasan, P. Kinnunen, E.-P. Heikkinen, M. Illikainen, Thermally treated phlogopite as
1252 magnesium-rich precursor for alkali activation purpose, *Miner. Eng.*, 113 (2017) 47-54.
- 1253 [24] E. Najafi Kani, A. Allahverdi, J.L. Provis, Calorimetric study of geopolymer binders based
1254 on natural pozzolan, *J. Therm. Anal. Calor.*, 127 (2017) 2181-2190.
- 1255 [25] H.S. Hassan, H.A. Abdel-Gawwad, S.R. Vásquez-García, I. Israde-Alcántara, N. Flores-
1256 Ramirez, J.L. Rico, M.S. Mohammed, Cleaner production of one-part white geopolymer cement
1257 using pre-treated wood biomass ash and diatomite, *J. Cleaner Prod.*, 209 (2019) 1420-1428.
- 1258 [26] A. Nana, J. Ngouné, R.C. Kaze, L. Boubakar, S.K. Tchounang, H.K. Tchakouté, E. Kamseu,
1259 C. Leonelli, Room-temperature alkaline activation of feldspathic solid solutions: Development of
1260 high strength geopolymers, *Constr. Build. Mater.*, 195 (2019) 258-268.
- 1261 [27] P. Krivenko, O. Kovalchuk, A. Pasko, T. Croymans, M. Hult, G. Lutter, N. Vandevenne, S.
1262 Schreurs, W. Schroyers, Development of alkali activated cements and concrete mixture design
1263 with high volumes of red mud, *Constr. Build. Mater.*, 151 (2017) 819-826.
- 1264 [28] Y. Hu, S. Liang, J. Yang, Y. Chen, N. Ye, Y. Ke, S. Tao, K. Xiao, J. Hu, H. Hou, W. Fan, S.
1265 Zhu, Y. Zhang, B. Xiao, Role of Fe species in geopolymer synthesized from alkali-thermal
1266 pretreated Fe-rich Bayer red mud, *Constr. Build. Mater.*, 200 (2019) 398-407.
- 1267 [29] N. Ye, J. Yang, S. Liang, Y. Hu, J. Hu, B. Xiao, Q. Huang, Synthesis and strength optimization
1268 of one-part geopolymer based on red mud, *Constr. Build. Mater.*, 111 (2016) 317-325.
- 1269 [30] A. Peys, C.E. White, D. Olds, H. Rahier, B. Blanpain, Y. Pontikes, Molecular structure of
1270 CaO-FeO_x-SiO₂ glassy slags and resultant inorganic polymer binders, *J. Am. Ceram. Soc.*, 101
1271 (2018) 5846-5857.
- 1272 [31] S. Zhang, A. Keulen, K. Arbi, G. Ye, Waste glass as partial mineral precursor in alkali-
1273 activated slag/fly ash system, *Cem Concr. Res.*, 102 (2017) 29-40.
- 1274 [32] P. Kinnunen, H. Sreenivasan, C.R. Cheeseman, M. Illikainen, Phase separation in alumina-
1275 rich glasses to increase glass reactivity for low-CO₂ alkali-activated cements, *J. Cleaner Prod.*,
1276 213 (2019) 126-133.
- 1277 [33] L. Kriskova, Y. Pontikes, F. Zhang, Ö. Cizer, P.T. Jones, K. Van Balen, B. Blanpain, Influence
1278 of mechanical and chemical activation on the hydraulic properties of gamma dicalcium silicate,
1279 *Cem Concr. Res.*, 55 (2014) 59-68.
- 1280 [34] S. Onisei, A.P. Douvalis, A. Malfliet, A. Peys, Y. Pontikes, Inorganic polymers made of

1281 fayalite slag: On the microstructure and behavior of Fe, *J. Am. Ceram. Soc.*, 101 (2018) 2245-
1282 2257.

1283 [35] P.L. Lopez Gonzalez, R.M. Novais, J. Labrincha, B. Blanpain, Y. Pontikes, Modifications of
1284 basic-oxygen-furnace slag microstructure and their effect on the rheology and the strength of
1285 alkali-activated binders, *Cem. Concr. Compos.*, 97 (2019) 143-153.

1286 [36] J. Shekhovtsova, I. Zhernovskiy, M. Kovtun, N. Kozhukhova, I. Zhernovskaya, E. Kearsley,
1287 Estimation of fly ash reactivity for use in alkali-activated cements - A step towards sustainable
1288 building material and waste utilization, *J. Cleaner Prod.*, 178 (2018) 22-33.

1289 [37] Z. Zhang, J.L. Provis, J. Zou, A. Reid, H. Wang, Toward an indexing approach to evaluate
1290 fly ashes for geopolymer manufacture, *Cem Concr. Res.*, 85 (2016) 163-173.

1291 [38] J.E. Oh, Y. Jun, Y. Jeong, P.J.M. Monteiro, The importance of the network-modifying element
1292 content in fly ash as a simple measure to predict its strength potential for alkali-activation, *Cem.*
1293 *Concr. Compos.*, 57 (2015) 44-54.

1294 [39] C.R. Shearer, J.L. Provis, S.A. Bernal, K.E. Kurtis, Alkali-activation potential of biomass-
1295 coal co-fired fly ash, *Cem. Concr. Compos.*, 73 (2016) 62-74.

1296 [40] M.A. Longhi, E.D. Rodríguez, S.A. Bernal, J.L. Provis, A.P. Kirchheim, Valorisation of a
1297 kaolin mining waste for the production of geopolymers, *J. Cleaner Prod.*, 115 (2016) 265-272.

1298 [41] A. McIntosh, S.E.M. Lawther, J. Kwasny, M.N. Soutsos, D. Cleland, S. Nanukuttan,
1299 Selection and characterisation of geological materials for use as geopolymer precursors, *Adv.*
1300 *Appl. Ceram.*, 114 (2015) 378-385.

1301 [42] I. Balczár, T. Korim, A. Kovács, É. Makó, Mechanochemical and thermal activation of kaolin
1302 for manufacturing geopolymer mortars – comparative study, *Ceram. Int.*, 42 (2016) 15367-15375.

1303 [43] S. Simon, G.J.G. Gluth, A. Peys, S. Onisei, D. Banerjee, Y. Pontikes, The fate of iron during
1304 the alkali-activation of synthetic (CaO-)FeO_x-SiO₂ slags: An Fe K-edge XANES study, *J. Am.*
1305 *Ceram. Soc.*, 101 (2018) 2107-2118.

1306 [44] K.C. Gomes, G.S.T. Lima, S.M. Torres, S. De Barros, I.F. Vasconcelos, N.P. Barbosa, Iron
1307 distribution in geopolymer with ferromagnetic rich precursor, *Mater. Sci. Forum*, 643 (2010) 131-
1308 138.

1309 [45] F. Puertas, C. Varga, M.M. Alonso, Rheology of alkali-activated slag pastes. Effect of the
1310 nature and concentration of the activating solution, *Cem. Concr. Compos.*, 53 (2014) 279-288.

1311 [46] A. Favier, J. Hot, G. Habert, N. Roussel, J.-B. d'Espinose de Lacaillerie, Flow properties of
1312 MK-based geopolymers pastes. A comparative study with standard Portland cement pastes, *Soft*
1313 *Matter*, 10 (2014) 1134-1141.

1314 [47] T. Yang, H. Zhu, Z. Zhang, X. Gao, C. Zhang, Q. Wu, Effect of fly ash microsphere on the
1315 rheology and microstructure of alkali-activated fly ash/slag pastes, *Cem. Concr. Res.*, 109 (2018)
1316 198-207.

1317 [48] H. Mehdizadeh, E. Najafi Kani, Rheology and apparent activation energy of alkali activated
1318 phosphorous slag, *Constr. Build. Mater.*, 171 (2018) 197-204.

1319 [49] M.M. Alonso, S. Gismera, M.T. Blanco, M. Lanzón, F. Puertas, Alkali-activated mortars:
1320 Workability and rheological behaviour, *Constr. Build. Mater.*, 145 (2017) 576-587.

1321 [50] F. Puertas, B. González-Fonteboa, I. González-Taboada, M.M. Alonso, M. Torres-Carrasco,
1322 G. Rojo, F. Martínez-Abella, Alkali-activated slag concrete: Fresh and hardened behaviour, *Cem.*
1323 *Concr. Compos.*, 85 (2018) 22-31.

- 1324 [51] Z. Tan, S.A. Bernal, J.L. Provis, Reproducible mini-slump test procedure for measuring the
1325 yield stress of cementitious pastes, *Mater. Struct.*, 50 (2017) #235.
- 1326 [52] A. Kashani, J.L. Provis, B.B.G. van Deventer, G.G. Qiao, J.S.J. van Deventer, Time-resolved
1327 yield stress measurement of evolving materials using a creeping sphere, *Rheol. Acta*, 54 (2015)
1328 365-376.
- 1329 [53] V. Benavent, P. Steins, I. Sobrados, J. Sanz, D. Lambertin, F. Frizon, S. Rossignol, A.
1330 Poulesquen, Impact of aluminum on the structure of geopolymers from the early stages to
1331 consolidated material, *Cem Concr. Res.*, 90 (2016) 27-35.
- 1332 [54] P. Steins, A. Poulesquen, O. Diat, F. Frizon, Structural evolution during geopolymerization
1333 from an early age to consolidated material, *Langmuir*, 28 (2012) 8502-8510.
- 1334 [55] D. Marchon, U. Sulser, A. Eberhardt, R.J. Flatt, Molecular design of comb-shaped
1335 polycarboxylate dispersants for environmentally friendly concrete, *Soft Matter*, 9 (2013) 10719-
1336 10728.
- 1337 [56] A. Kashani, J.L. Provis, G.G. Qiao, J.S.J. van Deventer, The interrelationship between surface
1338 chemistry and rheology in alkali activated slag paste, *Constr. Build. Mater*, 65 (2014) 583-591.
- 1339 [57] T. Conte, J. Plank, Impact of molecular structure and composition of polycarboxylate comb
1340 polymers on the flow properties of alkali-activated slag, *Cem Concr. Res.*, 116 (2019) 95-101.
- 1341 [58] A. Kashani, J.L. Provis, J. Xu, A.R. Kilcullen, G.G. Qiao, J.S.J. van Deventer, Effect of
1342 molecular architecture of polycarboxylate ethers on plasticizing performance in alkali activated
1343 slag paste, *J. Mater. Sci*, 49 (2014) 2761-2772.
- 1344 [59] A. Keulen, Q.L. Yu, S. Zhang, S. Grünewald, Effect of admixture on the pore structure
1345 refinement and enhanced performance of alkali-activated fly ash-slag concrete, *Constr. Build.*
1346 *Mater*, 162 (2018) 27-36.
- 1347 [60] N. Li, C. Shi, Z. Zhang, D. Zhu, H.-J. Hwang, Y. Zhu, T. Sun, A mixture proportioning method
1348 for the development of performance-based alkali-activated slag-based concrete, *Cem. Concr.*
1349 *Compos.*, 93 (2018) 163-174.
- 1350 [61] L. Xu, F. Matalkah, P. Soroushian, N. Darsanasiri, S. Hamadneh, W. Wu, Effects of citric
1351 acid on the rheology, hydration and strength development of alkali aluminosilicate cement, *Adv.*
1352 *Cem. Res.*, 30 (2018) 75-82.
- 1353 [62] N. Schneider, D. Stephan, The effect of d-gluconic acid as a retarder of ground granulated
1354 blast-furnace slag pastes, *Constr. Build. Mater*, 123 (2016) 99-105.
- 1355 [63] C. Dupuy, J. Havette, A. Gharzouni, N. Texier-Mandoki, X. Bourbon, S. Rossignol,
1356 Metakaolin-based geopolymer: Formation of new phases influencing the setting time with the use
1357 of additives, *Constr. Build. Mater*, 200 (2019) 272-281.
- 1358 [64] N. Li, C. Shi, Q. Wang, Z. Zhang, Z. Ou, Composition design and performance of alkali-
1359 activated cements, *Mater. Struct.*, 50 (2017) #178.
- 1360 [65] J. Rouyer, A. Poulesquen, Evidence of a fractal percolating network during
1361 geopolymerization, *J. Am. Ceram. Soc*, 98 (2015) 1580-1587.
- 1362 [66] Z.Z. Li N, A study on the setting characteristics of alkali-activated slag cement., in: W. H
1363 (Ed.) *The 3rd International Conference on Chemical Activated Materials*, Australia 2017, pp. 65.
- 1364 [67] N. Li, Z. Zhang, C. Shi, J. Zhang, Some progresses in the challenges for geopolymer, *IOP*
1365 *Conf. Series: Mater. Sci. Eng.*, 2018, #022003.
- 1366 [68] F. Winnefeld, M. Ben Haha, G. Le Saout, M. Costoya, S.-C. Ko, B. Lothenbach, Influence

1367 of slag composition on the hydration of alkali-activated slags, *J. Sust. Cem-Based Mater.*, 4 (2015)
1368 85-100.

1369 [69] M. Criado, B. Walkley, X. Ke, J.L. Provis, S.A. Bernal, Slag and activator chemistry control
1370 the reaction kinetics of sodium metasilicate-activated slag cements, *Sustainability*, 10 (2018)
1371 #4709.

1372 [70] C. Shi, R.L. Day, A calorimetric study of early hydration of alkali-slag cements, *Cem Concr.*
1373 *Res.*, 25 (1995) 1333-1346.

1374 [71] S.A. Bernal, R. San Nicolas, J.S.J. van Deventer, J.L. Provis, Alkali-activated slag cements
1375 produced with a blended sodium carbonate/silicate activator, *Adv. Cem. Res.*, 28 (2016) 262-273.

1376 [72] A.M. Humad, J.L. Provis, A. Cwirzen, Alkali-activation of a high MgO GGBS – Fresh and
1377 hardened properties, *Mag. Concr. Res.*, 70 (2018) 1256-1264.

1378 [73] A. Fernández-Jiménez, F. Puertas, Setting of alkali-activated slag cement. Influence of
1379 activator nature, *Advances in Cement Research*, 13 (2001) 115-121.

1380 [74] M. Kovtun, E.P. Kearsley, J. Shekhovtsova, Chemical acceleration of a neutral granulated
1381 blast-furnace slag activated by sodium carbonate, *Cem. Concr. Res.*, 72 (2015) 1-9.

1382 [75] C. Duran Atiş, C. Bilim, Ö. Çelik, O. Karahan, Influence of activator on the strength and
1383 drying shrinkage of alkali-activated slag mortar, *Constr. Build. Mater.*, 23 (2009) 548-555.

1384 [76] A. Fernández-Jiménez, F. Puertas, Effect of activator mix on the hydration and strength
1385 behaviour of alkali-activated slag cements, *Adv. Cem. Res.*, 15 (2003) 129-136.

1386 [77] N. Garg, C.E. White, Mechanism of zinc oxide retardation in alkali-activated materials: an
1387 in situ X-ray pair distribution function investigation, *J. Mater. Chem. A*, 5 (2017) 11794-11804.

1388 [78] B. Lothenbach, A. Nonat, Calcium silicate hydrates: Solid and liquid phase composition,
1389 *Cem Concr. Res.*, 78 (2015) 57-70.

1390 [79] E. L'Hôpital, B. Lothenbach, D.A. Kulik, K. Scrivener, Influence of calcium to silica ratio
1391 on aluminium uptake in calcium silicate hydrate, *Cem. Concr. Res.*, 85 (2016) 111-121.

1392 [80] E. L'Hôpital, B. Lothenbach, K. Scrivener, D.A. Kulik, Alkali uptake in calcium alumina
1393 silicate hydrate (C-A-S-H), *Cem. Concr. Res.*, 85 (2016) 122-136.

1394 [81] E. Kapeluszna, Ł. Kotwica, A. Różycka, Ł. Gołek, Incorporation of Al in C-A-S-H gels with
1395 various Ca/Si and Al/Si ratio: Microstructural and structural characteristics with DTA/TG, XRD,
1396 FTIR and TEM analysis, *Constr. Build. Mater.*, 155 (2017) 643-653.

1397 [82] R.J. Myers, S.A. Bernal, J.L. Provis, J.D. Gehman, J.S.J. van Deventer, The role of Al in
1398 cross-linking of alkali-activated slag cements, *J. Am. Ceram. Soc.*, 98 (2015) 996-1004.

1399 [83] R.J. Myers, S.A. Bernal, R. San Nicolas, J.L. Provis, Generalized structural description of
1400 calcium-sodium aluminosilicate hydrate gels: The crosslinked substituted tobermorite model,
1401 *Langmuir*, 29 (2013) 5294-5306.

1402 [84] J. Yang, D. Hou, Q. Ding, Structure, dynamics, and mechanical properties of cross-linked
1403 calcium aluminosilicate hydrate: A molecular dynamics study, *ACS Sust. Chem. Eng.*, 6 (2018)
1404 9403-9417.

1405 [85] G. Sun, J.F. Young, R.J. Kirkpatrick, The role of Al in C-S-H: NMR, XRD, and
1406 compositional results for precipitated samples, *Cem. Concr. Res.*, 36 (2006) 18-29.

1407 [86] F. Puertas, M. Palacios, H. Manzano, J.S. Dolado, A. Rico, J. Rodríguez, A model for the C-
1408 A-S-H gel formed in alkali-activated slag cements, *J. Eur. Ceram. Soc.*, 31 (2011) 2043-2056.

1409 [87] X. Pardal, F. Brunet, T. Charpentier, I. Pochard, A. Nonat, ²⁷Al and ²⁹Si solid-state NMR

1410 characterization of calcium-aluminosilicate-hydrate, *Inorg. Chem.*, 51 (2012) 1827-1836.
1411 [88] I.G. Richardson, Model structures for C-(A)-S-H (I), *Acta Cryst B*, 70 (2014) 903-923.
1412 [89] T. Egami, S.J.L. Billinge, *Underneath the Bragg peaks: structural analysis of complex*
1413 *materials*, Elsevier 2003.
1414 [90] K. Gong, C.E. White, Impact of chemical variability of ground granulated blast-furnace slag
1415 on the phase formation in alkali-activated slag pastes, *Cem. Concr. Res.*, 89 (2016) 310-319.
1416 [91] R. Si, S. Guo, Q. Dai, Influence of calcium content on the atomic structure and phase
1417 formation of alkali-activated cement binder, *Journal of the American Ceramic Society*, (2018).
1418 [92] L. Valentini, Modeling dissolution–precipitation kinetics of alkali-activated metakaolin, *ACS*
1419 *Omega*, 3 (2018) 18100-18108.
1420 [93] K. Yang, V.O. Özçelik, N. Garg, K. Gong, C.E. White, Drying-induced atomic structural
1421 rearrangements in sodium-based calcium-alumino-silicate-hydrate gel and the mitigating effects
1422 of ZrO₂ nanoparticles, *Phys. Chem. Chem. Phys.*, 20 (2018) 8593-8606.
1423 [94] B. Walkley, R. San Nicolas, M.-A. Sani, J.D. Gehman, J.S.J. van Deventer, J.L. Provis,
1424 Synthesis of stoichiometrically controlled reactive aluminosilicate and calcium-aluminosilicate
1425 powders, *Powder Technol.*, 297 (2016) 17-33.
1426 [95] B. Walkley, R. San Nicolas, M.-A. Sani, J.D. Gehman, J.S.J. van Deventer, J.L. Provis, Phase
1427 evolution of Na₂O–Al₂O₃–SiO₂–H₂O gels in synthetic aluminosilicate binders, *Dalton Trans.*, 45
1428 (2016) 5521-5535.
1429 [96] B. Walkley, R. San Nicolas, M.-A. Sani, G.J. Rees, J.V. Hanna, J.S.J. van Deventer, J.L.
1430 Provis, Phase evolution of C-(N)-A-S-H/N-A-S-H gel blends investigated via alkali-activation of
1431 synthetic calcium aluminosilicate precursors, *Cem. Concr. Res.*, 89 (2016) 120-135.
1432 [97] B. Walkley, G.J. Rees, R. San Nicolas, J.S.J. van Deventer, J.V. Hanna, J.L. Provis, New
1433 structural model of hydrous sodium aluminosilicate gels and the role of charge-balancing extra-
1434 framework Al, *J. Phys. Chem. C*, 122 (2018) 5673-5685.
1435 [98] S. Greiser, G.J.G. Gluth, P. Sturm, C. Jäger, ²⁹Si{²⁷Al}, ²⁷Al{²⁹Si} and ²⁷Al{¹H} double-
1436 resonance NMR spectroscopy study of cementitious sodium aluminosilicate gels (geopolymers)
1437 and gel–zeolite composites, *RSC Adv.*, 8 (2018) 40164-40171.
1438 [99] J. Brus, L. Kobera, M. Urbanová, D. Koloušek, J. Kotek, Insights into the structural
1439 transformations of aluminosilicate inorganic polymers: A comprehensive solid-state NMR study,
1440 *J. Phys. Chem. C*, 116 (2012) 14627-14637.
1441 [100] Q. Wan, F. Rao, S. Song, R.E. García, R.M. Estrella, C.L. Patiño, Y. Zhang,
1442 Geopolymerization reaction, microstructure and simulation of metakaolin-based geopolymers at
1443 extended Si/Al ratios, *Cem. Concr. Compos.*, 79 (2017) 45-52.
1444 [101] Z. Pan, Z. Tao, Y.F. Cao, R. Wuhler, T. Murphy, Compressive strength and microstructure
1445 of alkali-activated fly ash/slag binders at high temperature, *Cem. Concr. Compos.*, 86 (2018) 9-
1446 18.
1447 [102] P. Suraneni, M. Palacios, R.J. Flatt, New insights into the hydration of slag in alkaline media
1448 using a micro-reactor approach, *Cem Concr. Res.*, 79 (2016) 209-216.
1449 [103] I.G. Richardson, S. Li, Composition and structure of an 18-year-old 5M KOH-activated
1450 ground granulated blast-furnace slag paste, *Constr. Build. Mater*, 168 (2018) 404-411.
1451 [104] X. Ke, S.A. Bernal, J.L. Provis, Layered double hydroxides modify the reaction of sodium
1452 silicate-activated slag cements, *Green Mater.*, (2019) in press, DOI 10.1680/jgrma.1618.00024.

1453 [105] S.D. Wang, K.L. Scrivener, Hydration products of alkali-activated slag cement, *Cem Concr.*
1454 *Res.*, 25 (1995) 561-571.

1455 [106] S.J. Mills, A.G. Christy, J.-M.R. Génin, T. Kameda, F. Colombo, Nomenclature of the
1456 hydrotalcite supergroup: natural layered double hydroxides, *Miner. Mag.*, 76 (2012) 1289-1336.

1457 [107] A.E. Morandea, J.P. Fitts, H.D. Lee, S.M. Shubeita, L.C. Feldman, T. Gustafsson, C.E.
1458 White, Nanoscale heterogeneities in a fractured alkali-activated slag binder: A helium ion
1459 microscopy analysis, *Cem. Concr. Res.*, 79 (2016) 45-48.

1460 [108] D. Cohen-Tanugi, N. Yao, Superior imaging resolution in scanning helium-ion microscopy:
1461 A look at beam-sample interactions, *J. Appl. Phys.*, 104 (2008) #063504.

1462 [109] R. Williams, A. Van Riessen, The first 20 hours of geopolymerization: An in situ WAXS
1463 study of flyash-based geopolymers, *Materials*, 9 (2016) #552.

1464 [110] C.E. White, J.L. Provis, B. Bloomer, N.J. Henson, K. Page, In situ X-ray pair distribution
1465 function analysis of geopolymer gel nanostructure formation kinetics, *Phys. Chem. Chem. Phys.*,
1466 15 (2013) 8573-8582.

1467 [111] C.E. White, D.P. Olds, M. Hartl, R.P. Hjelm, K. Page, Evolution of the pore structure during
1468 the early stages of the alkali-activation reaction: an in situ small-angle neutron scattering
1469 investigation, *J. Appl. Cryst.*, 50 (2017) 61-75.

1470 [112] J.P. Gevaudan, K.M. Campbell, T.J. Kane, R.K. Shoemaker, W.V. Sruhar, Mineralization
1471 dynamics of metakaolin-based alkali-activated cements, *Cem Concr. Res.*, 94 (2017) 1-12.

1472 [113] Z. Sun, A. Vollpracht, Isothermal calorimetry and in-situ XRD study of the NaOH activated
1473 fly ash, metakaolin and slag, *Cem. Concr. Res.*, 103 (2018) 110-122.

1474 [114] V. Benavent, F. Frizon, A. Poulesquen, Effect of composition and aging on the porous
1475 structure of metakaolin-based geopolymers, *J. Appl. Cryst.*, 49 (2016) 2116-2128.

1476 [115] J. Melar, G. Renaudin, F. Leroux, A. Hardy-Dessources, J.-M. Nedelec, C. Taviot-Gueho,
1477 E. Petit, P. Steins, A. Poulesquen, F. Frizon, The porous network and its interface inside
1478 geopolymers as a function of alkali cation and aging, *J. Phys. Chem. C*, 119 (2015) 17619-17632.

1479 [116] X. Liu, C. Shi, X. Hu, Study of hydration and microstructure of alkali-activated slag cement
1480 and portland cement by impedance spectroscopy, *Materials Review*, 29 (2015) 130-135 (in
1481 Chinese).

1482 [117] A.F. Sosa Gallardo, J. Provis, D.C. Sinclair, Electrochemical characterisation of cement
1483 hydration and properties by alternating current impedance spectroscopy, *ECI International*
1484 *Conference on Alkali Activated Materials and Geopolymers: Versatile Materials Offering High*
1485 *Performance and Low Emissions*, Tomar, Portugal (2018).

1486 [118] M. Chaouche, X.X. Gao, M. Cyr, M. Cotte, L. Frouin, On the origin of the blue/green color
1487 of blast-furnace slag-based materials: Sulfur K-edge XANES investigation, *J. Am. Ceram. Soc.*,
1488 100 (2017) 1707-1716.

1489 [119] D. Le Cornec, Q. Wang, L. Galois, G. Renaudin, L. Izoret, G. Calas, Greening effect in
1490 slag cement materials, *Cem. Concr. Compos.*, 84 (2017) 93-98.

1491 [120] F. Lolli, H. Manzano, J.L. Provis, M.C. Bignozzi, E. Masoero, Atomistic simulations of
1492 geopolymer models: the impact of disorder on structure and mechanics, *ACS Appl. Mater. Interf.*,
1493 10 (2018) 22809-22820.

1494 [121] W. Loewenstein, The distribution of aluminum in the tetrahedra of silicates and aluminates,
1495 *Am. Miner.*, 39 (1954) 92-96.

1496 [122] K. Yang, C.E. White, Modeling the formation of alkali aluminosilicate gels at the mesoscale
1497 using coarse-grained Monte Carlo, *Langmuir*, 32 (2016) 11580-11590.

1498 [123] R.J. Myers, S.A. Bernal, J.L. Provis, A thermodynamic model for C-(N-)A-S-H gel:
1499 CNASH_{ss}. Derivation and validation, *Cem. Concr. Res.*, 66 (2014) 27-47.

1500 [124] R.J. Myers, E. L'Hopital, J.L. Provis, B. Lothenbach, Composition-solubility-structure
1501 relationships in calcium (alkali) aluminosilicate hydrate (C-(N,K-)A-S-H), *Dalton Trans.*, 44
1502 (2015) 13530-13544.

1503 [125] R.J. Myers, B. Lothenbach, S.A. Bernal, J.L. Provis, Thermodynamic modelling of alkali-
1504 activated slag cements, *Appl. Geochem.*, 61 (2015) 233-247.

1505 [126] Y. Zuo, M. Nedeljković, G. Ye, Coupled thermodynamic modelling and experimental study
1506 of sodium hydroxide activated slag, *Constr. Build. Mater.*, 188 (2018) 262-279.

1507 [127] H. Ye, A. Radlińska, Shrinkage mitigation strategies in alkali-activated slag, *Cem Concr.*
1508 *Res.*, 101 (2017) 131-143.

1509 [128] R.J. Myers, S.A. Bernal, J.L. Provis, Phase diagrams for alkali-activated slag binders, *Cem*
1510 *Concr. Res.*, 95 (2017) 30-38.

1511 [129] L. Gomez-Zamorano, M. Balonis, B. Erdemli, N. Neithalath, G. Sant, C-(N)-S-H and N-
1512 A-S-H gels: Compositions and solubility data at 25°C and 50°C, *J. Am. Ceram. Soc.*, 100 (2017)
1513 2700-2711.

1514 [130] G.D. Miron, T. Wagner, D.A. Kulik, C.A. Heinrich, Internally consistent thermodynamic
1515 data for aqueous species in the system Na-K-Al-Si-O-H-Cl, *Geochim. Cosmochim. Acta*, 187
1516 (2016) 41-78.

1517 [131] M.U. Okoronkwo, M. Balonis, L. Katz, M. Juenger, G. Sant, A thermodynamics-based
1518 approach for examining the suitability of cementitious formulations for solidifying and stabilizing
1519 coal-combustion wastes, *J. Environ. Manag.*, 217 (2018) 278-287.

1520 [132] Y. Ding, J.-G. Dai, C.-J. Shi, Mechanical properties of alkali-activated concrete: A state-of-
1521 the-art review, *Constr. Build. Mater.*, 127 (2016) 68-79.

1522 [133] R.J. Thomas, S. Peethamparan, Alkali-activated concrete: Engineering properties and
1523 stress-strain behavior, *Constr. Build. Mater.*, 93 (2015) 49-56.

1524 [134] A. Noushini, F. Aslani, A. Castel, R.I. Gilbert, B. Uy, S. Foster, Compressive stress-strain
1525 model for low-calcium fly ash-based geopolymer and heat-cured Portland cement concrete, *Cem.*
1526 *Concr. Compos.*, 73 (2016) 136-146.

1527 [135] K.-M. Lee, S. Choi, J.F. Choo, S.-W. Yoo, Y.C. Choi, Flexural and shear behaviors of
1528 reinforced alkali-activated slag concrete beams, *Adv. Mater. Sci. Eng.*, 2017 (2017) #5294290.

1529 [136] R.J. Thomas, S. Peethamparan, Effect of specimen size and curing condition on the
1530 compressive strength of alkali-activated concrete, *Transp. Res. Record*, 2629 (2017) 9-14.

1531 [137] C.H. Un, J.G. Sanjayan, R. San Nicolas, J.S.J. van Deventer, Predictions of long-term
1532 deflection of geopolymer concrete beams, *Constr. Build. Mater.*, 94 (2015) 10-19.

1533 [138] Y. Ding, J.-G. Dai, C.-J. Shi, Fracture properties of alkali-activated slag and ordinary
1534 Portland cement concrete and mortar, *Constr. Build. Mater.*, 165 (2018) 310-320.

1535 [139] P. Nath, P.K. Sarker, Fracture properties of GGBFS-blended fly ash geopolymer concrete
1536 cured in ambient temperature, *Mater. Struct.*, 50 (2017) #32.

1537 [140] R. San Nicolas, J.L. Provis, The interfacial transition zone in alkali-activated slag mortars,
1538 *Front. Mater.*, 2 (2015) #70.

- 1539 [141] A. Dakhane, S. Das, S. Kailas, N. Neithalath, Elucidating the crack resistance of alkali-
1540 activated slag mortars using coupled fracture tests and image correlation, *J. Am. Ceram. Soc.*, 99
1541 (2016) 273-280.
- 1542 [142] V.S. Cândido, A.C.R. da Silva, N.T. Simonassi, E.S. Lima, F.S. da Luz, S.N. Monteiro,
1543 Mechanical and microstructural characterization of geopolymeric concrete subjected to fatigue, *J.*
1544 *Mater. Res. Technol.*, 7 (2018) 566-570.
- 1545 [143] J.-S. Mun, K.-H. Yang, S.-J. Kim, Tests on the compressive fatigue performance of various
1546 concretes, *J. Mater. Civ. Eng.*, (2016) #04016099.
- 1547 [144] N. Ranjbar, M. Mehrli, M.R. Maheri, M. Mehrli, Hot-pressed geopolymer, *Cem Concr.*
1548 *Res.*, 100 (2017) 14-22.
- 1549 [145] J. Rouyer, V. Benavent, F. Frizon, A. Poulesquen, Influence of geopolymer formulation
1550 parameters on the elastic and porous properties over a one-year monitoring, *Mater. Lett.*, 207
1551 (2017) 121-124.
- 1552 [146] A. Blyth, C.A. Eiben, G.W. Scherer, C.E. White, Impact of activator chemistry on
1553 permeability of alkali-activated slags, *J. Am. Ceram. Soc.*, 100 (2017) 4848-4859.
- 1554 [147] S.A. Bernal, R. San Nicolas, J.S.J. van Deventer, J.L. Provis, Water content modifies the
1555 structural development of sodium metasilicate-activated slag binders (El contenido de agua
1556 modifica el desarrollo estructural de cementantes de escoria activada con metasilicato de sodio),
1557 *ALCONPAT J.*, 5 (2015) 30-41.
- 1558 [148] M. Babae, A. Castel, Water vapor sorption isotherms, pore structure, and moisture transport
1559 characteristics of alkali-activated and Portland cement-based binders, *Cem Concr. Res.*, 113 (2018)
1560 99-120.
- 1561 [149] X. Hu, C. Shi, Z. Shi, L. Zhang, Compressive strength, pore structure and chloride transport
1562 properties of alkali-activated slag/fly ash mortars, *Cement and Concrete Composites*, Accepted
1563 for publication (2019), Doi: <https://doi.org/10.1016/j.cemconcomp.2019.01.010>.
- 1564 [150] T. Luukkonen, Z. Abdollahnejad, J. Yliniemi, P. Kinnunen, M. Illikainen, One-part alkali-
1565 activated materials: A review, *Cem. Concr. Res.*, 103 (2018) 21-34.
- 1566 [151] J.L. Provis, J.S.J. van Deventer, *Alkali-Activated Materials: State-of-the-Art Report*,
1567 *RILEM TC 224-AAM*, Springer/RILEM, Dordrecht, 2014.
- 1568 [152] A. Hajimohammadi, J.S.J. van Deventer, Characterisation of one-part geopolymer binders
1569 made from fly ash, *Waste Biomass Valoriz.*, 8 (2017) 225-233.
- 1570 [153] B. Nematollahi, J. Sanjayan, J. Qiu, E.-H. Yang, Micromechanics-based investigation of a
1571 sustainable ambient temperature cured one-part strain hardening geopolymer composite, *Constr.*
1572 *Build. Mater.*, 131 (2017) 552-563.
- 1573 [154] K.-t. Wang, L.-q. Du, X.-s. Lv, Y. He, X.-m. Cui, Preparation of drying powder inorganic
1574 polymer cement based on alkali-activated slag technology, *Powder Technol.*, 312 (2017) 204-209.
- 1575 [155] I. Garcia-Lodeiro, S. Donatello, A. Fernández-Jiménez, Á. Palomo, Hydration of hybrid
1576 alkaline cement containing a very large proportion of fly ash: A descriptive model, *Materials*, 9
1577 (2016) #605.
- 1578 [156] A. Fernández-Jiménez, I. Garcia-Lodeiro, O. Maltseva, A. Palomo, Hydration mechanisms
1579 of hybrid cements as a function of the way of addition of chemicals, *J. Am. Ceram. Soc.*, 102
1580 (2018) 427-436.
- 1581 [157] F. Matalkah, P. Soroushian, Synthesis and characterization of alkali aluminosilicate

1582 hydraulic cement that meets standard requirements for general use, *Constr. Build. Mater*, 158
1583 (2018) 42-49.

1584 [158] T. Luukkonen, Z. Abdollahnejad, J. Yliniemi, P. Kinnunen, M. Illikainen, Comparison of
1585 alkali and silica sources in one-part alkali-activated blast furnace slag mortar, *J. Cleaner Prod.*,
1586 187 (2018) 171-179.

1587 [159] K. Neupane, P. Kidd, D. Chalmers, D. Baweja, R. Shrestha, Investigation on compressive
1588 strength development and drying shrinkage of ambient cured powder-activated geopolymer
1589 concretes, *Aust. J. Civil Eng.*, 14 (2016) 72-83.

1590 [160] A. Hajimohammadi, T. Ngo, A. Kashani, Sustainable one-part geopolymer foams with glass
1591 fines versus sand as aggregates, *Constr. Build. Mater*, 171 (2018) 223-231.

1592 [161] M.X. Peng, Z.H. Wang, Q.G. Xiao, F. Song, W. Xie, L.C. Yu, H.W. Huang, S.J. Yi, Effects
1593 of alkali on one-part alkali-activated cement synthesized by calcining bentonite with dolomite and
1594 Na_2CO_3 , *Appl. Clay Sci.*, 139 (2017) 64-71.

1595 [162] P. Sturm, G.J.G. Gluth, S. Simon, H.J.H. Brouwers, H.C. Kühne, The effect of heat
1596 treatment on the mechanical and structural properties of one-part geopolymer-zeolite composites,
1597 *Thermochim. Acta*, 635 (2016) 41-58.

1598 [163] P. Sturm, G.J.G. Gluth, H.J.H. Brouwers, H.C. Kühne, Synthesizing one-part geopolymers
1599 from rice husk ash, *Constr. Build. Mater*, 124 (2016) 961-966.

1600 [164] X. Ke, S.A. Bernal, N. Ye, J.L. Provis, J. Yang, One-part geopolymers based on thermally
1601 treated red mud/NaOH blends, *J. Am. Ceram. Soc.*, 98 (2015) 5-11.

1602 [165] N. Ye, Y. Chen, J. Yang, S. Liang, Y. Hu, J. Hu, S. Zhu, W. Fan, B. Xiao, Transformations
1603 of Na, Al, Si and Fe species in red mud during synthesis of one-part geopolymers, *Cem Concr.*
1604 *Res.*, 101 (2017) 123-130.

1605 [166] Z. Zhang, J.L. Provis, X. Ma, A. Reid, H. Wang, Efflorescence and subflorescence induced
1606 microstructural and mechanical evolution in fly ash-based geopolymers, *Cem. Concr. Compos.*,
1607 92 (2018) 165-177.

1608 [167] Z. Zhang, J.L. Provis, A. Reid, H. Wang, Fly ash-based geopolymers: The relationship
1609 between composition, pore structure and efflorescence, *Cem. Concr. Res.*, 64 (2014) 30-41.

1610 [168] X. Xue, Y.-L. Liu, J.-G. Dai, C.-S. Poon, W.-D. Zhang, P. Zhang, Inhibiting efflorescence
1611 formation on fly ash-based geopolymer via silane surface modification, *Cem. Concr. Compos.*,
1612 94 (2018) 43-52.

1613 [169] B. Qu, A. Martin, J. Pastor, A. Palomo, A. Fernández-Jiménez, Characterisation of pre-
1614 industrial hybrid cement and effect of pre-curing temperature, *Cem. Concr. Compos.*, 73 (2016)
1615 281-288.

1616 [170] B. Qu, A. Palomo, A. Fernández-Jiménez, A. Martin, J.Y. Pastor, High-temperature effect
1617 on the mechanical behaviour of hybrid cement, *Materiales de Construcción*, MC-133-18, (Under
1618 review) 2018.

1619 [171] B. Qu, Temperature effect on performance of Portland cement versus advanced hybrid
1620 cements and alkali-fly ash cement, PhD thesis, Department of materials science, E.T.S.I. Caminos,
1621 Canales y Puerdos, Universidad Politécnica de Madrid, Madrid, Spain, 2018.

1622 [172] D.F. Velandía, C.J. Lynsdale, J.L. Provis, F. Ramirez, Effect of mix design inputs, curing
1623 and compressive strength on the durability of Na_2SO_4 -activated high volume fly ash concretes,
1624 *Cem. Concr. Compos.*, 91 (2018) 11-20.

1625 [173] M. Mastali, P. Kinnunen, A. Dalvand, R. Mohammadi Firouz, M. Illikainen, Drying
1626 shrinkage in alkali-activated binders – A critical review, *Constr. Build. Mater*, 190 (2018) 533-
1627 550.

1628 [174] Y. Ma, G. Ye, The shrinkage of alkali activated fly ash, *Cem Concr. Res.*, 68 (2015) 75-82.

1629 [175] A. Rodrigue, J. Duchesne, B. Fournier, B. Bissonnette, Influence of added water and fly ash
1630 content on the characteristics, properties and early-age cracking sensitivity of alkali-activated
1631 slag/fly ash concrete cured at ambient temperature, *Constr. Build. Mater*, 171 (2018) 929-941.

1632 [176] D. Ballekere Kumarappa, S. Peethamparan, M. Ngami, Autogenous shrinkage of alkali
1633 activated slag mortars: Basic mechanisms and mitigation methods, *Cem Concr. Res.*, 109 (2018)
1634 1-9.

1635 [177] H. Ye, A. Radlińska, Shrinkage mechanisms of alkali-activated slag, *Cem Concr. Res.*, 88
1636 (2016) 126-135.

1637 [178] G. Fang, H. Bahrami, M. Zhang, Mechanisms of autogenous shrinkage of alkali-activated
1638 fly ash-slag pastes cured at ambient temperature within 24 h, *Constr. Build. Mater*, 171 (2018)
1639 377-387.

1640 [179] R.J. Thomas, D. Lezama, S. Peethamparan, On drying shrinkage in alkali-activated concrete:
1641 Improving dimensional stability by aging or heat-curing, *Cem Concr. Res.*, 91 (2016) 13-23.

1642 [180] X. Gao, Q.L. Yu, H.J.H. Brouwers, Assessing the porosity and shrinkage of alkali activated
1643 slag-fly ash composites designed applying a packing model, *Constr. Build. Mater*, 119 (2016) 175-
1644 184.

1645 [181] G. Wang, Y. Ma, Drying shrinkage of alkali-activated fly ash/slag blended system, *J. Sust.*
1646 *Cement-Based Mater.*, 7 (2018) 203-213.

1647 [182] A.M.A. Aboshia, R.A. Rahmat, M.F.M. Zain, A. Ismail, Early age shrinkage cracking of
1648 restrained metakaolin-slag-palm oil fuel ash binder geopolymer mortars, *J. Sust. Cement-Based*
1649 *Mater.*, 7 (2018) 271-295.

1650 [183] V. Bílek, L. Kalina, R. Novotný, J. Tkacz, L. Pařízek, Some issues of shrinkage-reducing
1651 admixtures application in alkali-activated slag systems, *Materials*, 9 (2016) 462.

1652 [184] L. Kalina, V. Bilek Jr, R. Novotny, Influence of alkali ions on the efficiency of shrinkage
1653 reduction by polypropylene glycol in alkali activated systems, *Adv. Cem. Res.*, 30 (2017) 240-
1654 244.

1655 [185] C. Nguyen, P. Mangat, G. Jones, Effect of shrinkage reducing admixture on the strength and
1656 shrinkage of alkali activated cementitious mortar, *IOP Conf. Series: Mater. Sci. Eng.*, 2018,
1657 #012022.

1658 [186] X. Hu, C. Shi, Z. Zhang, Z. Hu, Autogenous and drying shrinkage of alkali-activated slag
1659 mortars, *J. Am. Ceram. Soc.*, Accepted (2019).

1660 [187] S. Oh, Y.C. Choi, Superabsorbent polymers as internal curing agents in alkali activated slag
1661 mortars, *Constr. Build. Mater*, 159 (2018) 1-8.

1662 [188] W. Tu, Y. Zhu, G. Fang, X. Wang, M. Zhang, Internal curing of alkali-activated fly ash-slag
1663 pastes using superabsorbent polymer, *Cem Concr. Res.*, 116 (2019) 179-190.

1664 [189] C. Song, Y.C. Choi, S. Choi, Effect of internal curing by superabsorbent polymers – Internal
1665 relative humidity and autogenous shrinkage of alkali-activated slag mortars, *Constr. Build. Mater*,
1666 123 (2016) 198-206.

1667 [190] B. Yuan, Q.L. Yu, H.J.H. Brouwers, Phase modification induced drying shrinkage reduction

1668 on Na₂CO₃ activated slag by incorporating Na₂SO₄, *Mater. Struct.*, 50 (2017) 220.

1669 [191] K. Arbi, M. Nedeljković, Y. Zuo, G. Ye, A review on the durability of alkali-activated fly
1670 ash/slag systems: Advances, issues, and perspectives, *Ind. Eng. Chem. Res.*, 55 (2016) 5439-5453.

1671 [192] J.S.J. van Deventer, R. San Nicolas, I. Ismail, S.A. Bernal, D.G. Brice, J.L. Provis,
1672 Microstructure and durability of alkali-activated materials as key parameters for standardisation,
1673 *J. Sust. Cem-Based Mater.*, 4 (2015) 116-128.

1674 [193] S.A. Bernal, J.L. Provis, Durability of alkali-activated materials: progress and perspectives,
1675 *J. Am. Ceram. Soc.*, 97 (2014) 997-1008.

1676 [194] J.L. Provis, Alkali-activated cements and concretes – durability testing to underpin
1677 standardisation, in: P.A.M. Basheer (Ed.) *Proceedings of the Sixth International Conference on*
1678 *the Durability of Concrete Structures*, Leeds, UK, 2018, pp. 16-26.

1679 [195] J.L. Provis, F. Winnefeld, “Testing the test” –the outcomes of the round robin tests of
1680 RILEM TC 247-DTA on the durability of alkali-activated concrete, in: H. Beushausen (Ed.)
1681 *Proceedings of the 5th International Conference on Concrete Repair, Rehabilitation and*
1682 *Retrofitting*, Cape Town, South Africa, 2018.

1683 [196] K. Yang, C. Yang, B. Magee, S. Nanukuttan, J. Ye, Establishment of a preconditioning
1684 regime for air permeability and sorptivity of alkali-activated slag concrete, *Cem. Concr. Compos.*,
1685 73 (2016) 19-28.

1686 [197] I. Ismail, S.A. Bernal, J.L. Provis, S. Hamdan, J.S.J. van Deventer, Drying-induced changes
1687 in the structure of alkali-activated pastes, *J. Mater. Sci.*, 48 (2013) 3566-3577.

1688 [198] Z. Zhang, Y. Zhu, H. Zhu, Y. Zhang, J.L. Provis, H. Wang, Effect of drying procedures on
1689 pore structure and phase evolution of alkali-activated cements, *Cem. Concr. Compos.*, 96 (2019)
1690 194-203.

1691 [199] British Standards Institute, BSI PAS 8820:2016, Construction materials – Alkali-activated
1692 cementitious material and concrete – Specification, London, UK, 2016.

1693 [200] S.A. Bernal, J.L. Provis, D.G. Brice, A. Kilcullen, P. Duxson, J.S.J. van Deventer,
1694 Accelerated carbonation testing of alkali-activated binders significantly underestimates service
1695 life: The role of pore solution chemistry, *Cem Concr. Res.*, 42 (2012) 1317-1326.

1696 [201] R. Pouhet, M. Cyr, Carbonation in the pore solution of metakaolin-based geopolymer, *Cem*
1697 *Concr. Res.*, 88 (2016) 227-235.

1698 [202] M.S.H. Khan, A. Castel, A. Noushini, Carbonation of a low-calcium fly ash geopolymer
1699 concrete, *Mag. Concr. Res.*, 69 (2017) 24-34.

1700 [203] S.A. Bernal, J.L. Provis, R. Mejía de Gutiérrez, J.S.J. van Deventer, Accelerated carbonation
1701 testing of alkali-activated slag/metakaolin blended concretes: effect of exposure conditions, *Mater.*
1702 *Struct.*, 48 (2015) 653-669.

1703 [204] S.A. Bernal, Effect of the activator dose on the compressive strength and accelerated
1704 carbonation resistance of alkali silicate-activated slag/metakaolin blended materials, *Constr. Build.*
1705 *Mater.*, 98 (2015) 217-226.

1706 [205] M. Nedeljković, B. Šavija, Y. Zuo, M. Luković, G. Ye, Effect of natural carbonation on the
1707 pore structure and elastic modulus of the alkali-activated fly ash and slag pastes, *Construction and*
1708 *Building Materials*, 161 (2018) 687-704.

1709 [206] M. Nedeljković, B. Ghiassi, S. van der Laan, Z. Li, G. Ye, Effect of curing conditions on
1710 the pore solution and carbonation resistance of alkali-activated fly ash and slag pastes, *Cem Concr.*

1711 Res., 116 (2019) 146-158.

1712 [207] Z. Shi, C. Shi, S. Wan, N. Li, Z. Zhang, Effect of alkali dosage and silicate modulus on
1713 carbonation of alkali-activated slag mortars, *Cem Concr. Res.*, 113 (2018) 55-64.

1714 [208] M.S.H. Khan, A. Castel, Effect of MgO and Na₂SiO₃ on the carbonation resistance of alkali
1715 activated slag concrete, *Mag. Concr. Res.*, 70 (2018) 685-692.

1716 [209] S.A. Bernal, R. San Nicolas, R.J. Myers, R. Mejía de Gutiérrez, F. Puertas, J.S.J. van
1717 Deventer, J.L. Provis, MgO content of slag controls phase evolution and structural changes
1718 induced by accelerated carbonation in alkali-activated binders, *Cem Concr. Res.*, 57 (2014) 33-
1719 43.

1720 [210] S.M. Park, J.G. Jang, H.K. Lee, Unlocking the role of MgO in the carbonation of alkali-
1721 activated slag cement, *Inorg. Chem. Front.*, 5 (2018) 1661-1670.

1722 [211] H. Ye, A. Radlińska, Carbonation-induced volume change in alkali-activated slag, *Constr.*
1723 *Build. Mater.*, 144 (2017) 635-644.

1724 [212] M. Babae, M.S.H. Khan, A. Castel, Passivity of embedded reinforcement in carbonated
1725 low-calcium fly ash-based geopolymer concrete, *Cem. Concr. Compos.*, 85 (2018) 32-43.

1726 [213] M.S. Badar, K. Kupwade-Patil, S.A. Bernal, J.L. Provis, E.N. Allouche, Corrosion of steel
1727 bars induced by accelerated carbonation in low and high calcium fly ash geopolymer concretes,
1728 *Constr. Build. Mater.*, 61 (2014) 79-89.

1729 [214] J. Osio-Norgaard, J.P. Gevaudan, W.V. Srubar, A review of chloride transport in alkali-
1730 activated cement paste, mortar, and concrete, *Constr. Build. Mater.*, 186 (2018) 191-206.

1731 [215] C. Shi, L. Zhang, J. Zhang, N. Li, Z. Ou, Advances in testing methods and influencing
1732 factors of chloride ion transport properties of alkali-activated materials, *Materials Review*, 31
1733 (2017) 95-100 (in Chinese).

1734 [216] R.J. Thomas, E. Ariyachandra, D. Lezama, S. Peethamparan, Comparison of chloride
1735 permeability methods for alkali-activated concrete, *Constr. Build. Mater.*, 165 (2018) 104-111.

1736 [217] A. Noushini, A. Castel, Performance-based criteria to assess the suitability of geopolymer
1737 concrete in marine environments using modified ASTM C1202 and ASTM C1556 methods, *Mater.*
1738 *Struct.*, 51 (2018) #146.

1739 [218] M. Babae, A. Castel, Chloride-induced corrosion of reinforcement in low-calcium fly ash-
1740 based geopolymer concrete, *Cem Concr. Res.*, 88 (2016) 96-107.

1741 [219] X. Ke, S.A. Bernal, J.L. Provis, Uptake of chloride and carbonate by Mg-Al and Ca-Al
1742 layered double hydroxides in simulated pore solutions of alkali-activated slag cement, *Cem Concr.*
1743 *Res.*, 100 (2017) 1-13.

1744 [220] X. Ke, S.A. Bernal, O.H. Hussein, J.L. Provis, Chloride binding and mobility in sodium
1745 carbonate-activated slag pastes and mortars, *Mater. Struct.*, 50 (2017) #252.

1746 [221] M. Babae, A. Castel, Chloride diffusivity, chloride threshold, and corrosion initiation in
1747 reinforced alkali-activated mortars: Role of calcium, alkali, and silicate content, *Cem Concr. Res.*,
1748 111 (2018) 56-71.

1749 [222] Q. Ma, S.V. Nanukuttan, P.A.M. Basheer, Y. Bai, C. Yang, Chloride transport and the
1750 resulting corrosion of steel bars in alkali activated slag concretes, *Mater. Struct.*, 49 (2016) 3663-
1751 3677.

1752 [223] X. Yu, L. Jiang, J. Xu, Electrochemical and semiconducting properties of passive films on
1753 steel surfaces in alkali-activated slag extraction solution, *J. Mater. Civ. Eng.*, 30 (2018) 04018146.

1754 [224] J. Shi, J. Ming, W. Sun, Electrochemical performance of reinforcing steel in alkali-activated
1755 slag extract in the presence of chlorides, *Corros. Sci.*, 133 (2018) 288-299.

1756 [225] W. Wang, H. Chen, X. Li, Z. Zhu, Corrosion behavior of steel bars immersed in simulated
1757 pore solutions of alkali-activated slag mortar, *Constr. Build. Mater*, 143 (2017) 289-297.

1758 [226] S. Mundra, S.A. Bernal, M. Criado, P. Hlaváček, G. Ebell, S. Reinemann, G.J.G. Gluth, J.L.
1759 Provis, Steel corrosion in reinforced alkali-activated materials, *RILEM Tech. Lett.*, 2 (2017) 33-
1760 39.

1761 [227] M. Holloway, J.M. Sykes, Studies of the corrosion of mild steel in alkali-activated slag
1762 cement mortars with sodium chloride admixtures by a galvanostatic pulse method, *Corros. Sci.*,
1763 47 (2005) 3097-3110.

1764 [228] M. Criado, J.L. Provis, Alkali activated slag mortars provide high resistance to chloride-
1765 induced corrosion of steel, *Front. Mater.*, 5 (2018) #34.

1766 [229] M. Criado, S.A. Bernal, P. Garcia-Triñanes, J.L. Provis, Influence of slag composition on
1767 the stability of steel in alkali-activated cementitious materials, *J. Mater. Sci*, 53 (2018) 5016-5035.

1768 [230] S. Mundra, M. Criado, S.A. Bernal, J.L. Provis, Chloride-induced corrosion of steel rebars
1769 in simulated pore solutions of alkali-activated concretes, *Cem Concr. Res.*, 100 (2017) 385-397.

1770 [231] C. Tennakoon, A. Shayan, J.G. Sanjayan, A. Xu, Chloride ingress and steel corrosion in
1771 geopolymer concrete based on long term tests, *Mater. Des.*, 116 (2017) 287-299.

1772 [232] C. Monticelli, M.E. Natali, A. Balbo, C. Chiavari, F. Zanotto, S. Manzi, M.C. Bignozzi,
1773 Corrosion behavior of steel in alkali-activated fly ash mortars in the light of their microstructural,
1774 mechanical and chemical characterization, *Cem Concr. Res.*, 80 (2016) 60-68.

1775 [233] C. Shi, Z.G. Shi, X. Hu, R. Zhao, L. Chong, A review on alkali-aggregate reactions in alkali-
1776 activated mortars/ concretes made with alkali-reactive aggregates, *Mater. Struct.*, 48 (2015) 621-
1777 628.

1778 [234] R. Pouhet, M. Cyr, Alkali-silica reaction in metakaolin-based geopolymer mortar, *Mater.*
1779 *Struct.*, 48 (2015) 571-583.

1780 [235] R. Tänzer, Y. Jin, D. Stephan, Effect of the inherent alkalis of alkali activated slag on the
1781 risk of alkali silica reaction, *Cem Concr. Res.*, 98 (2017) 82-90.

1782 [236] Z. Shi, C. Shi., R. Zhao, S. Wan, Comparison of alkali-silica reactions in alkali-activated
1783 slag and Portland cement mortars, *Mater. Struct.*, 48 (2015) 743-751.

1784 [237] T. Williamson, M.C.G. Juenger, The role of activating solution concentration on alkali-
1785 silica reaction in alkali-activated fly ash concrete, *Cem Concr. Res.*, 83 (2016) 124-130.

1786 [238] Z. Shi, C. Shi, J. Zhang, S. Wan, Z. Zhang, Z. Ou, Alkali-silica reaction in waterglass-
1787 activated slag mortars incorporating fly ash and metakaolin, *Cem Concr Res*, 108 (2018) 10-19.

1788 [239] Z. Shi, C. Shi, S. Wan, Z. Ou, Effect of alkali dosage on alkali-silica reaction in sodium
1789 hydroxide activated slag mortars, *Constr. Build. Mater*, 143 (2017) 16-23.

1790 [240] L. Gu, P. Visintin, T. Bennett, Evaluation of accelerated degradation test methods for
1791 cementitious composites subject to sulfuric acid attack; application to conventional and alkali-
1792 activated concretes, *Cem. Concr. Compos.*, 87 (2018) 187-204.

1793 [241] Y. Xie, X. Lin, W. Pan, T. Ji, Y. Liang, H. Zhang, Study on corrosion mechanism of alkali-
1794 activated concrete with biogenic sulfuric acid, *Constr. Build. Mater*, 188 (2018) 9-16.

1795 [242] T.A. Aiken, J. Kwasny, W. Sha, M.N. Soutsos, Effect of slag content and activator dosage
1796 on the resistance of fly ash geopolymer binders to sulfuric acid attack, *Cem Concr. Res.*, 111 (2018)

1797 23-40.

1798 [243] P. Sturm, G.J.G. Gluth, C. Jäger, H.J.H. Brouwers, H.C. Kühne, Sulfuric acid resistance of
1799 one-part alkali-activated mortars, *Cem Concr. Res.*, 109 (2018) 54-63.

1800 [244] J. Kwasny, T.A. Aiken, M.N. Soutsos, J.A. McIntosh, D.J. Cleland, Sulfate and acid
1801 resistance of lithomarge-based geopolymer mortars, *Constr. Build. Mater.*, 166 (2018) 537-553.

1802 [245] A. Koenig, A. Herrmann, S. Overmann, F. Dehn, Resistance of alkali-activated binders to
1803 organic acid attack: Assessment of evaluation criteria and damage mechanisms, *Constr. Build.*
1804 *Mater.*, 151 (2017) 405-413.

1805 [246] T.A. Aiken, W. Sha, J. Kwasny, M.N. Soutsos, Resistance of geopolymer and Portland
1806 cement based systems to silage effluent attack, *Cem Concr. Res.*, 92 (2017) 56-65.

1807 [247] A. Buchwald, M. Vanooteghem, E. Gruyaert, H. Hilbig, N. Belie, Purdocement: application
1808 of alkali-activated slag cement in Belgium in the 1950s, *Mater. Struct.*, 48 (2015) 501-511.

1809 [248] H. Xu, J.L. Provis, J.S.J. van Deventer, P.V. Krivenko, Characterization of aged slag
1810 concretes, *ACI Mater. J.*, 105 (2008) 131-139.

1811 [249] K. Pasupathy, M. Berndt, J. Sanjayan, P. Rajeev, D.S. Cheema, Durability of low-calcium
1812 fly ash based geopolymer concrete culvert in a saline environment, *Cem Concr. Res.*, 100 (2017)
1813 297-310.

1814 [250] H.A. Khan, M.S.H. Khan, A. Castel, J. Sunarho, Deterioration of alkali-activated mortars
1815 exposed to natural aggressive sewer environment, *Constr. Build. Mater.*, 186 (2018) 577-597.

1816 [251] K. Pasupathy, M. Berndt, J. Sanjayan, P. Rajeev, D.S. Cheema, Durability performance of
1817 precast fly ash-based geopolymer concrete under atmospheric exposure conditions, *J. Mater. Civ.*
1818 *Eng.*, 30 (2018) 04018007.

1819 [252] K. Pasupathy, M. Berndt, A. Castel, J. Sanjayan, R. Pathmanathan, Carbonation of a blended
1820 slag-fly ash geopolymer concrete in field conditions after 8 years, *Constr. Build. Mater.*, 125 (2016)
1821 661-669.

1822 [253] J. Aldred, J. Day, T. Glasby, Geopolymer concrete - No longer labcrete!, 40th Conference
1823 on Our World in Concrete & Structures, Singapore, 2015.

1824 [254] R.D. Hooton, Current developments and future needs in standards for cementitious
1825 materials, *Cem Concr. Res.*, 78 (2015) 165-177.

1826 [255] D. Bondar, Q. Ma, M. Soutsos, M. Basheer, J.L. Provis, S. Nanukuttan, Alkali activated slag
1827 concretes designed for a desired slump, strength and chloride diffusivity, *Constr. Build. Mater.*,
1828 190 (2018) 191-199.

1829 [256] K. Yang, C. Yang, J. Zhang, Q. Pan, L. Yu, Y. Bai, First structural use of site-cast, alkali-
1830 activated slag concrete in China, *Proc. ICE Struct. Build.*, 171 (2018) 800-809.

1831 [257] V. Bilek, J. Hurta, P. Done, L. Zidek, Development of alkali-activated concrete for
1832 structures—mechanical properties and durability, *Persp. Sci.*, 7 (2016) 190-194.

1833 [258] L.N. Assi, E. Deaver, M.K. ElBatanouny, P. Ziehl, Investigation of early compressive
1834 strength of fly ash-based geopolymer concrete, *Constr. Build. Mater.*, 112 (2016) 807-815.

1835 [259] A. Rafeet, R. Vinai, M. Soutsos, W. Sha, Guidelines for mix proportioning of fly ash/GGBS
1836 based alkali activated concretes, *Constr. Build. Mater.*, 147 (2017) 130-142.

1837 [260] B. Tempest, C. Snell, T. Gentry, M. Trejo, K. Isherwood, Manufacture of full-scale
1838 geopolymer cement concrete components: A case study to highlight opportunities and challenges,
1839 *PCI J.*, 60 (2015) 39-50.

1840 [261] R. Pouhet, M. Cyr, Formulation and performance of flash metakaolin geopolymer concretes,
1841 *Constr. Build. Mater.*, 120 (2016) 150-160.

1842 [262] N. Vandevenne, R.I. Iacobescu, Y. Pontikes, R. Carleer, E. Thijssen, K. Gijbels, S. Schreurs,
1843 W. Schroeyers, Incorporating Cs and Sr into blast furnace slag inorganic polymers and their effect
1844 on matrix properties, *J. Nucl. Mater.*, 503 (2018) 1-12.

1845 [263] M. Arbel Haddad, E. Ofer-Rozovsky, G. Bar-Nes, E.J.C. Borojovich, A. Nikolski, D.
1846 Mogiliansky, A. Katz, Formation of zeolites in metakaolin-based geopolymers and their potential
1847 application for Cs immobilization, *J. Nucl. Mater.*, 493 (2017) 168-179.

1848 [264] E. Ofer-Rozovsky, M.A. Haddad, G. Bar-Nes, E.J.C. Borojovich, A. Binyamini, A. Nikolski,
1849 A. Katz, Cesium immobilization in nitrate-bearing metakaolin-based geopolymers, *J. Nucl. Mater.*,
1850 514 (2019) 247-254.

1851 [265] J. Wang, J. Wang, Y. Huang, K. Zhang, Y. Li, X. Wu, Preparation of alkali-activated slag-
1852 fly ash-metakaolin hydroceramics for immobilizing simulated sodium-bearing waste, *J. Am.*
1853 *Ceram. Soc.*, 98 (2015) 1393-1399.

1854 [266] B.D. Williams, J.J. Neeway, M.M.V. Snyder, M.E. Bowden, J.E. Amonette, B.W. Arey, E.M.
1855 Pierce, C.F. Brown, N.P. Qafoku, Mineral assemblage transformation of a metakaolin-based waste
1856 form after geopolymer encapsulation, *J. Nucl. Mater.*, 473 (2016) 320-332.

1857 [267] V. Cantarel, D. Lambertin, A. Poulesquen, F. Leroux, G. Renaudin, F. Frizon, Geopolymer
1858 assembly by emulsion templating: Emulsion stability and hardening mechanisms, *Ceram. Int.*, 44
1859 (2018) 10558-10568.

1860 [268] C.A. Davy, G. Hauss, B. Planel, D. Lambertin, 3D structure of oil droplets in hardened
1861 geopolymer emulsions, *J. Am. Ceram. Soc.*, 102 (2019) 949-954.

1862 [269] P. Kryvenko, C. Hailin, O. Petropavlovskiy, L. Weng, O. Kovalchuk, Applicability of alkali-
1863 activated cement for immobilization of low-level radioactive waste in ion-exchange resins, *East.*
1864 *Eur. J. Enterpr. Technol.*, 1 (2016) 40-45.

1865 [270] C. Kuenzel, J.F. Cisneros, T.P. Neville, L.J. Vandeperre, S.J.R. Simons, J. Bensted, C.R.
1866 Cheeseman, Encapsulation of Cs/Sr contaminated clinoptilolite in geopolymers produced from
1867 metakaolin, *J. Nucl. Mater.*, 466 (2015) 94-99.

1868 [271] D. Chartier, B. Muzeau, L. Stefan, J. Sanchez-Canet, C. Monguillon, Magnesium alloys and
1869 graphite wastes encapsulated in cementitious materials: reduction of galvanic corrosion using
1870 alkali hydroxide activated blast furnace slag, *J. Hazard Mater.*, 326 (2017) 197-210.

1871 [272] D. Rodrigues, C. Cannes, N. Barré, D. Lambertin, S. Delpech, Role of fluoride ions on the
1872 uranium oxidation mechanism in highly alkaline solutions, *Electrochim. Acta*, 266 (2018) 384-
1873 394.

1874 [273] A. Rooses, D. Lambertin, D. Chartier, F. Frizon, Galvanic corrosion of Mg-Zr fuel cladding
1875 and steel immobilized in Portland cement and geopolymer at early ages, *J. Nucl. Mater.*, 435 (2013)
1876 137-140.

1877 [274] F. Chupin, A. Dannoux-Papin, Y. Ngonon Ravache, J.-B. d'Espinose de Lacaillerie, Water
1878 content and porosity effect on hydrogen radiolytic yields of geopolymers, *J. Nucl. Mater.*, 494
1879 (2017) 138-146.

1880 [275] N. Mobasher, S.A. Bernal, H. Kinoshita, J.L. Provis, Gamma irradiation resistance of early
1881 age Ba(OH)₂-Na₂SO₄-slag cementitious grouts, *J. Nucl. Mater.*, 482 (2016) 266-277.

1882 [276] N. Deng, H. An, H. Cui, Y. Pan, B. Wang, L. Mao, J. Zhai, Effects of gamma-ray irradiation

1883 on leaching of simulated $^{133}\text{Cs}^+$ radionuclides from geopolymer wasteforms, *J. Nucl. Mater.*, 459
1884 (2015) 270-275.

1885 [277] C. Bai, P. Colombo, Processing, properties and applications of highly porous geopolymers:
1886 a review, *Ceram. Int.*, 44 (2018) 16103-16118.

1887 [278] Z. Zhang, J.L. Provis, A. Reid, H. Wang, Geopolymer foam concrete: an emerging material
1888 for sustainable construction, *Constr. Build. Mater*, 56 (2014) 113-127.

1889 [279] C. Bai, T. Ni, Q. Wang, H. Li, P. Colombo, Porosity, mechanical and insulating properties
1890 of geopolymer foams using vegetable oil as the stabilizing agent, *J. Eur. Ceram. Soc.*, 38 (2018)
1891 799-805.

1892 [280] C. Bai, G. Franchin, H. Elsayed, A. Zaggia, L. Conte, H. Li, P. Colombo, High-porosity
1893 geopolymer foams with tailored porosity for thermal insulation and wastewater treatment, *J. Mater.*
1894 *Res.*, 32 (2017) 3251-3259.

1895 [281] Z. Zhang, J.L. Provis, A. Reid, H. Wang, Mechanical, thermal insulation, thermal resistance
1896 and acoustic absorption properties of geopolymer foam concrete, *Cem. Concr. Compos.*, 62 (2015)
1897 97-105.

1898 [282] A. De Rossi, J. Carvalheiras, R.M. Novais, M.J. Ribeiro, J.A. Labrincha, D. Hotza, R.F.P.M.
1899 Moreira, Waste-based geopolymeric mortars with very high moisture buffering capacity, *Constr.*
1900 *Build. Mater*, 191 (2018) 39-46.

1901 [283] A. Hajimohammadi, T. Ngo, P. Mendis, J. Sanjayan, Regulating the chemical foaming
1902 reaction to control the porosity of geopolymer foams, *Mater. Design*, 120 (2017) 255-265.

1903 [284] J.R. Mackechnie, L.A. Bellamy, Thermal performance of variable density wall panels made
1904 using Portland cement or inorganic polymer concrete, *Mater. Struct.*, 48 (2015) 643-651.

1905 [285] M.D.M. Paiva, E.C.C.M. Silva, D.M.A. Melo, A.E. Martinelli, J.F. Schneider, A geopolymer
1906 cementing system for oil wells subject to steam injection, *J. Petrol. Sci. Eng.*, 169 (2018) 748-759.

1907 [286] J. Du, Y. Bu, X. Cao, Z. Shen, B. Sun, Utilization of alkali-activated slag based composite
1908 in deepwater oil well cementing, *Constr. Build. Mater*, 186 (2018) 114-122.

1909 [287] T. Sugama, T. Pyatina, Effect of sodium carboxymethyl celluloses on water-catalyzed self-
1910 degradation of 200°C-heated alkali-activated cement, *Cem. Concr. Compos.*, 55 (2015) 281-289.

1911 [288] R.M. Wimalasinghe, C.A. Weatherly, M.F. Wahab, N. Thakur, D.W. Armstrong,
1912 Geopolymers as a new class of high pH stable supports with different chromatographic selectivity,
1913 *Anal. Chem.*, 90 (2018) 8139-8146.

1914 [289] R.A. Sá Ribeiro, M.G. Sá Ribeiro, W.M. Kriven, A review of particle- and fiber-reinforced
1915 metakaolin-based geopolymer composites, *J. Ceram. Sci. Technol.*, 8 (2017) 307-322.

1916 [290] G.C.H. Doudart de la Grée, V. Caprai, J.E.G. van Dam, H. van As, H.J.H. Brouwers, Q.L.
1917 Yu, Ionic interaction and liquid absorption by wood in lignocellulose inorganic mineral binder
1918 composites, *J. Cleaner Prod.*, 206 (2019) 808-818.

1919 [291] M. Ohno, V.C. Li, An integrated design method of engineered geopolymer composite, *Cem.*
1920 *Concr. Compos.*, 88 (2018) 73-85.

1921 [292] J.-I. Choi, B.Y. Lee, R. Ranade, V.C. Li, Y. Lee, Ultra-high-ductile behavior of a
1922 polyethylene fiber-reinforced alkali-activated slag-based composite, *Cem. Concr. Compos.*, 70
1923 (2016) 153-158.

1924 [293] M.H. Al-Majidi, A. Lampropoulos, A.B. Cundy, Tensile properties of a novel fibre
1925 reinforced geopolymer composite with enhanced strain hardening characteristics, *Compos. Struct.*,

1926 168 (2017) 402-427.

1927 [294] S. Kramar, A. Šajna, V. Ducman, Assessment of alkali activated mortars based on different
1928 precursors with regard to their suitability for concrete repair, *Constr. Build. Mater.*, 124 (2016)
1929 937-944.

1930 [295] G. Franchin, P. Scanferla, L. Zeffiro, H. Elsayed, A. Baliello, G. Giacomello, M. Pasetto, P.
1931 Colombo, Direct ink writing of geopolymeric inks, *J. Eur. Ceram. Soc.*, 37 (2017) 2481-2489.

1932 [296] B. Panda, S. C. Paul, M. J. Tan, Anisotropic mechanical performance of 3D printed fiber
1933 reinforced sustainable construction material, *Mater. Lett.*, 209 (2017) 146-149.

1934 [297] B. Nematollahi, M. Xia, J. Sanjayan, P. Vijay, Effect of type of fiber on inter-layer bond and
1935 flexural strengths of extrusion-based 3D printed geopolymer, *Mater. Sci. Forum*, 939 (2018) 155-
1936 162.

1937 [298] M. Xia, B. Nematollahi, J. Sanjayan, Influence of binder saturation level on compressive
1938 strength and dimensional accuracy of powder-based 3D printed geopolymer, *Mater Sci. Forum*,
1939 939 (2018) 177-183.

1940 [299] O.G. Rivera, W.R. Long, C.A. Weiss Jr, R.D. Moser, B.A. Williams, K. Torres-Cancel, E.R.
1941 Gore, P.G. Allison, Effect of elevated temperature on alkali-activated geopolymeric binders
1942 compared to portland cement-based binders, *Cem Concr. Res.*, 90 (2016) 43-51.

1943 [300] W.D.A. Rickard, G.J.G. Gluth, K. Pistol, In-situ thermo-mechanical testing of fly ash
1944 geopolymer concretes made with quartz and expanded clay aggregates, *Cem Concr. Res.*, 80
1945 (2016) 33-43.

1946 [301] G.J.G. Gluth, W.D.A. Rickard, S. Werner, S. Pirskawetz, Acoustic emission and
1947 microstructural changes in fly ash geopolymer concretes exposed to simulated fire, *Mater. Struct.*,
1948 49 (2016) 5243-5254.

1949 [302] S.M. Park, J.G. Jang, N.K. Lee, H.K. Lee, Physicochemical properties of binder gel in
1950 alkali-activated fly ash/slag exposed to high temperatures, *Cem Concr. Res.*, 89 (2016) 72-79.

1951 [303] G. Habert, C. Ouellet-Plamondon, Recent update on the environmental impact of
1952 geopolymers, *RILEM Tech. Lett.*, 1 (2016) 17-23.

1953 [304] Beyond Zero Emissions, Zero Carbon Industry Plan - Rethinking Cement, Melbourne, 2017.

1954 [305] A. Passuello, E.D. Rodríguez, E. Hirt, M. Longhi, S.A. Bernal, J.L. Provis, A.P. Kirchheim,
1955 Evaluation of the potential improvement in the environmental footprint of geopolymers using
1956 waste-derived activators, *J. Cleaner Prod.*, 166 (2017) 680-689.

1957 [306] D.A. Salas, A.D. Ramirez, N. Ulloa, H. Baykara, A.J. Boero, Life cycle assessment of
1958 geopolymer concrete, *Constr. Build. Mater.*, 190 (2018) 170-177.

1959 [307] J. Dahmen, J. Kim, C.M. Ouellet-Plamondon, Life cycle assessment of emergent masonry
1960 blocks, *J. Cleaner Prod.*, 171 (2018) 1622-1637.

1961 [308] A. Heath, K. Paine, M. McManus, Minimising the global warming potential of clay based
1962 geopolymers, *J. Cleaner Prod.*, 78 (2014) 75-83.

1963 [309] A. Peys, L. Arnout, B. Blanpain, H. Rahier, K. Van Acker, Y. Pontikes, Mix-design
1964 parameters and real-life considerations in the pursuit of lower environmental impact inorganic
1965 polymers, *Waste Biomass Valor.*, 9 (2018) 879-889.

1966 [310] A. Petrillo, R. Cioffi, F. De Felice, F. Colangelo, C. Borrelli, An environmental evaluation:
1967 A comparison between geopolymer and OPC concrete paving blocks manufacturing process in
1968 Italy, *Environ. Progr. Sust. Energy*, 35 (2016) 1699-1708.

- 1969 [311] S.H. Teh, T. Wiedmann, A. Castel, J. de Burgh, Hybrid life cycle assessment of greenhouse
1970 gas emissions from cement, concrete and geopolymer concrete in Australia, *J. Cleaner Prod.*, 152
1971 (2017) 312-320.
- 1972 [312] M. Sandanayake, C. Gunasekara, D. Law, G. Zhang, S. Setunge, Greenhouse gas emissions
1973 of different fly ash based geopolymer concretes in building construction, *J. Cleaner Prod.*, 204
1974 (2018) 399-408.
- 1975 [313] A. Di Maria, M. Salman, M. Dubois, K. Van Acker, Life cycle assessment to evaluate the
1976 environmental performance of new construction material from stainless steel slag, *Int. J. Life
1977 Cycle Assess.*, 23 (2018) 2091-2109.
- 1978 [314] A. Akbarnezhad, M. Huan, S. Mesgari, A. Castel, Recycling of geopolymer concrete, *Constr.
1979 Build. Mater.*, 101 (2015) 152-158.
- 1980 [315] N.A. Chaliasou, A. Heath, K. Paine, J. Calabria Holley, Chemical aspects related to using
1981 recycled geopolymers as aggregates, *Adv. Cem. Res.*, 30 (2018) 361-370.
- 1982 [316] A. Keulen, A. van Zomeren, J.J. Dijkstra, Leaching of monolithic and granular alkali
1983 activated slag-fly ash materials, as a function of the mixture design, *Waste Manag.*, 78 (2018)
1984 497-508.
- 1985 [317] H.A. van der Sloot, D.S. Kosson, N. Impens, N. Vanhoudt, T. Almahayni, H. Vandenhove,
1986 L. Sweeck, R. Wiegiers, J.L. Provis, C. Gascó, W. Schroeyers, 8 - Leaching assessment as a
1987 component of environmental safety and durability analyses for NORM containing building
1988 materials, in: W. Schroeyers (Ed.) *Naturally Occurring Radioactive Materials in Construction*,
1989 Woodhead Publishing, Duxford, UK, 2017, pp. 253-288.
- 1990 [318] J. Labrincha, F. Puertas, W. Schroeyers, K. Kovler, Y. Pontikes, C. Nuccetelli, P. Krivenko,
1991 O. Kovalchuk, O. Petropavlovsky, M. Komljenovic, E. Fidanchevski, R. Wiegiers, E. Volceanov,
1992 E. Gunay, M.A. Sanjuán, V. Ducman, B. Angjusheva, D. Bajare, T. Kovacs, G. Bator, S. Schreurs,
1993 J. Aguiar, J.L. Provis, 7 - From NORM by-products to building materials, in: W. Schroeyers (Ed.)
1994 *Naturally Occurring Radioactive Materials in Construction*, Woodhead Publishing, Duxford, UK,
1995 2017, pp. 183-252.
- 1996 [319] C. Shi, F. He, A. Fernández-Jiménez, P.V. Krivenko, A. Palomo, Classification and
1997 characteristics of alkali-activated cements, *J. Chinese Ceram. Soc.*, 40 (2012) 69-75.
- 1998 [320] X. Pan, C. Shi, X. Hu, Z. Ou, Effects of CO₂ surface treatment on strength and permeability
1999 of one-day-aged cement mortar, *Construction and Building Materials*, 154 (2017) 1087-1095.
- 2000 [321] W. Ashraf, J. Olek, Carbonation behavior of hydraulic and non-hydraulic calcium silicates:
2001 potential of utilizing low-lime calcium silicates in cement-based materials, *J Mater Sci*, 51 (2016)
2002 6173-6191.
- 2003 [322] B. Qian, X. Li, X. Shen, Preparation and accelerated carbonation of low temperature
2004 sintered clinker with low Ca/Si ratio, *J. Cleaner Prod.*, 120 (2016) 249-259.
- 2005 [323] B. Lu, C. Shi, G. Hou, Strength and microstructure of CO₂ cured low-calcium clinker,
2006 *Constr Build Mater*, 188 (2018) 417-423.
- 2007 [324] W. Ashraf, J. Olek, Carbonation activated binders from pure calcium silicates: Reaction
2008 kinetics and performance controlling factors, *Cem Concr Compos*, 93 (2018) 85-98.
- 2009 [325] W. Ashraf, J. Olek, J. Jain, Microscopic features of non-hydraulic calcium silicate cement
2010 paste and mortar, *Cem Concr Res*, 100 (2017) 361-372.
- 2011 [326] W. Ashraf, J. Olek, Elucidating the accelerated carbonation products of calcium silicates

2012 using multi-technique approach, *J. CO₂ Utilization*, 23 (2018) 61-74.

2013 [327] Y. Mu, Z. Liu, F. Wang, X. Huang, Carbonation characteristics of γ -dicalcium silicate for
2014 low-carbon building material, *Constr. Build. Mater.*, 177 (2018) 322-331.

2015 [328] J. Chang, Y. Fang, X. Shang, The role of β -C₂S and γ -C₂S in carbon capture and strength
2016 development, *Mater Struct*, 49 (2016) 4417-4424.

2017 [329] X. Guan, S. Liu, C. Feng, M. Qiu, The hardening behavior of γ -C₂S binder using accelerated
2018 carbonation, *Constr. Build. Mater.*, 114 (2016) 204-207.

2019 [330] S. Liu, Z. Dou, S. Zhang, H. Zhang, X. Guan, C. Feng, J. Zhang, Effect of sodium hydroxide
2020 on the carbonation behavior of β -dicalcium silicate, *Constr. Build. Mater.*, 150 (2017) 591-594.

2021 [331] V. Shah, K. Scrivener, B. Bhattacharjee, S. Bishnoi, Changes in microstructure
2022 characteristics of cement paste on carbonation, *Cem. Concr. Res.*, 109 (2018) 184-197.

2023 [332] C. Shi, F. He, Y. Wu, Effect of pre-conditioning on CO₂ curing of lightweight concrete
2024 blocks mixtures, *Constr. Build. Mater.*, 26 (2012) 257-267.

2025 [333] M. Castellote, L. Fernandez, C. Andrade, C. Alonso, Chemical changes and phase analysis
2026 of OPC pastes carbonated at different CO₂ concentrations, *Mater Struct*, 42 (2009) 515-525.

2027 [334] C. Shi, Y. Wu, Studies on some factors affecting CO₂ curing of lightweight concrete
2028 products, *Resourc Conserv Recyc*, 52 (2008) 1087-1092.

2029 [335] C. Shi, D. Wang, F. He, M. Liu, Weathering properties of CO₂-cured concrete blocks,
2030 *Resourc Conserv Recyc*, 65 (2012) 11-17.

2031 [336] S. Monkman, P.A. Kenward, G. Dipple, M. MacDonald, M. Raudsepp, Activation of cement
2032 hydration with carbon dioxide, *J Sust Cement-Based Mater*, 7 (2018) 160-181.

2033 [337] P. He, C. Shi, Z. Tu, C.S. Poon, J. Zhang, Effect of further water curing on compressive
2034 strength and microstructure of CO₂-cured concrete, *Cem Concr Compos*, 72 (2016) 80-88.

2035 [338] M. Auroy, S. Poyet, P. Le Bescop, J.-M. Torrenti, T. Charpentier, M. Moskura, X. Bourbon,
2036 Comparison between natural and accelerated carbonation (3% CO₂): Impact on mineralogy,
2037 microstructure, water retention and cracking, *Cem Concr Res*, 109 (2018) 64-80.

2038 [339] J.H. Seo, S.M. Park, H.K. Lee, Evolution of the binder gel in carbonation-cured Portland
2039 cement in an acidic medium, *Cem Concr Res*, 109 (2018) 81-89.

2040 [340] L. Mo, D.K. Panesar, Accelerated carbonation – A potential approach to sequester CO₂ in
2041 cement paste containing slag and reactive MgO, *Cem Concr Compos*, 43 (2013) 69-77.

2042 [341] P. He, C.S. Poon, D.C.W. Tsang, Effect of pulverized fuel ash and CO₂ curing on the water
2043 resistance of magnesium oxychloride cement (MOC), *Cem Concr Res*, 97 (2017) 115-122.

2044 [342] L. Mo, D.K. Panesar, Effects of accelerated carbonation on the microstructure of Portland
2045 cement pastes containing reactive MgO, *Cem Concr Res*, 42 (2012) 769-777.

2046 [343] F.P. Glasser, G. Jauffret, J. Morrison, J.-L. Galvez-Martos, N. Patterson, M.S.-E. Imbabi,
2047 Sequestering CO₂ by mineralization into useful nesquehonite-based products, *Front. Energy Res.*,
2048 4 (2016) #3.

2049 [344] N.T. Dung, C. Unluer, Development of MgO concrete with enhanced hydration and
2050 carbonation mechanisms, *Cem Concr Res*, 103 (2018) 160-169.

2051 [345] S.A. Walling, J.L. Provis, Magnesia based cements – a journey of 150 years, and cements
2052 for the future?, *Chem. Rev.*, 116 (2016) 4170-4204.

2053 [346] C. Shi, J. Qian, High performance cementing materials from industrial slags — a review,
2054 *Resourc Conserv Recyc*, 29 (2000) 195-207.

2055 [347] C. Shi, Steel slag—its production, processing, characteristics, and cementitious properties,
2056 J Mater Civil Eng, 16 (2004) 230-236.

2057 [348] P.S. Humbert, J. Castro-Gomes, CO₂ activated steel slag-based materials: A review, J.
2058 Cleaner Prod., 208 (2019) 448-457.

2059 [349] L. Mo, F. Zhang, M. Deng, Mechanical performance and microstructure of the calcium
2060 carbonate binders produced by carbonating steel slag paste under CO₂ curing, Cem Concr Res, 88
2061 (2016) 217-226.

2062 [350] Z. Ghoulleh, R.I.L. Guthrie, Y. Shao, High-strength KOBM steel slag binder activated by
2063 carbonation, Constr Build Mater, 99 (2015) 175-183.

2064 [351] L. Mo, F. Zhang, M. Deng, F. Jin, A. Al-Tabbaa, A. Wang, Accelerated carbonation and
2065 performance of concrete made with steel slag as binding materials and aggregates, Cem Concr
2066 Compos, 83 (2017) 138-145.

2067 [352] S. Monkman, Y. Shao, C. Shi, Carbonated ladle slag fines for carbon uptake and sand
2068 substitute, J. Mater. Civil Eng., 21 (2009) 657-665.

2069 [353] N.L. Ukwattage, P.G. Ranjith, M. Yellishetty, H.H. Bui, T. Xu, A laboratory-scale study of
2070 the aqueous mineral carbonation of coal fly ash for CO₂ sequestration, J. Cleaner Prod., 103 (2015)
2071 665-674.

2072 [354] A. Dindi, D.V. Quang, L.F. Vega, E. Nashef, M.R.M. Abu-Zahra, Applications of fly ash for
2073 CO₂ capture, utilization, and storage, J. CO₂ Utilization, 29 (2019) 82-102.

2074 [355] Z. Wei, B. Wang, G. Falzone, E.C. La Plante, M.U. Okoronkwo, Z. She, T. Oey, M. Balonis,
2075 N. Neithalath, L. Pilon, G. Sant, Clinkering-free cementation by fly ash carbonation, J. CO₂
2076 Utilization, 23 (2018) 117-127.

2077 [356] Y. Shao, M. Mahoutian, Low temperature synthesis of cement from ladle slag and fly ash,
2078 J.Sust Cement-Based Mater, 5 (2016) 247-258.

2079 [357] C.W. Hargis, J. Moon, B. Lothenbach, F. Winnefeld, H.-R. Wenk, P.J.M. Monteiro, Calcium
2080 sulfoaluminate sodalite (Ca₄Al₆O₁₂SO₄) crystal structure evaluation and bulk modulus
2081 determination, J. Am. Ceram. Soc., 97 (2014) 892-898.

2082 [358] L. Zhang, M. Su, Y. Wang, Development of the use of sulfo- and ferroaluminate cements in
2083 China, Adv. Cem. Res., 11 (1999) 15-21.

2084 [359] E. Gartner, H. Hirao, A review of alternative approaches to the reduction of CO₂ emissions
2085 associated with the manufacture of the binder phase in concrete, Cem Concr Res, 78 (2015) 126-
2086 142.

2087 [360] E. Gartner, T. Sui, Alternative cement clinkers, Cem Concr Res, 114 (2018) 27-39.

2088 [361] T. Hanein, I. Galan, A. Elhoweris, S. Khare, S. Skalamprinos, G. Jen, M. Whittaker, M.S.
2089 Imbabi, F.P. Glasser, M.N. Bannerman, Production of belite calcium sulfoaluminate cement using
2090 sulfur as a fuel and as a source of clinker sulfur trioxide: pilot kiln trial, Adv. Cem. Res., 28 (2016)
2091 643-653.

2092 [362] L. Zhang, F.P. Glasser, Investigation of the microstructure and carbonation of C \bar{S} A-based
2093 concretes removed from service, Cem Concr Res, 35 (2005) 2252-2260.

2094 [363] F. Winnefeld, B. Lothenbach, Hydration of calcium sulfoaluminate cements —
2095 Experimental findings and thermodynamic modelling, Cem Concr Res, 40 (2010) 1239-1247.

2096 [364] C.W. Hargis, A.P. Kirchheim, P.J.M. Monteiro, E.M. Gartner, Early age hydration of
2097 calcium sulfoaluminate (synthetic ye'elimitite, C₄A₃ \bar{S}) in the presence of gypsum and varying

2098 amounts of calcium hydroxide, *Cem Concr Res*, 48 (2013) 105-115.

2099 [365] H. Beltagui, G. Jen, M. Whittaker, M.S. Imbabi, The influence of variable gypsum and water
2100 content on the strength and hydration of a belite-calcium sulphoaluminate cement, *Adv. Appl.*
2101 *Ceram.*, 116 (2017) 199-206.

2102 [366] A. Cuesta, G. Álvarez-Pinazo, S.G. Sanfélix, I. Peral, M.A.G. Aranda, A.G. De la Torre,
2103 Hydration mechanisms of two polymorphs of synthetic ye'elimite, *Cem Concr Res*, 63 (2014)
2104 127-136.

2105 [367] G. Álvarez-Pinazo, I. Santacruz, M.A.G. Aranda, Á.G. De la Torre, Hydration of belite–
2106 ye'elimite–ferrite cements with different calcium sulfate sources, *Adv. Cem. Res*, 28 (2016) 529-
2107 543.

2108 [368] M. García-Maté, I. Santacruz, Á.G. De la Torre, L. León-Reina, M.A.G. Aranda,
2109 Rheological and hydration characterization of calcium sulfoaluminate cement pastes, *Cem Concr*
2110 *Compos*, 34 (2012) 684-691.

2111 [369] M. García-Maté, A.G. De la Torre, L. León-Reina, E.R. Losilla, M.A.G. Aranda, I.
2112 Santacruz, Effect of calcium sulfate source on the hydration of calcium sulfoaluminate eco-
2113 cement, *Cem Concr Compos*, 55 (2015) 53-61.

2114 [370] V. Morin, P. Termkhajornkit, B. Huet, G. Pham, Impact of quantity of anhydrite, water to
2115 binder ratio, fineness on kinetics and phase assemblage of belite-ye'elimite-ferrite cement, *Cem*
2116 *Concr Res*, 99 (2017) 8-17.

2117 [371] M.T. Blanco-Varela, A. Palomo, F. Puertas, T. Vázquez, CaF₂ and CaSO₄ in white cement
2118 clinker production, *Adv Cem Res*, 9 (1997) 105-113.

2119 [372] J.D. Zea-Garcia, I. Santacruz, M.A.G. Aranda, A.G. De la Torre, Alite-belite-ye'elimite
2120 cements: Effect of dopants on the clinker phase composition and properties, *Cem Concr Res*, 115
2121 (2019) 192-202.

2122 [373] N. Chitvoranund, F. Winnefeld, C.W. Hargis, S. Sinthupinyo, B. Lothenbach, Synthesis and
2123 hydration of alite-calcium sulfoaluminate cement, *Adv Cem Res*, 29 (2017) 101-111.

2124 [374] D. Londono-Zuluaga, J.I. Tobón, M.A.G. Aranda, I. Santacruz, A.G. De la Torre, Clinkering
2125 and hydration of belite-alite-ye'elimite cement, *Cem Concr Compos*, 80 (2017) 333-341.

2126 [375] D. Londono-Zuluaga, J.I. Tobón, M.A.G. Aranda, I. Santacruz, A.G. De la Torre, Influence
2127 of fly ash blending on hydration and physical behavior of belite–alite–ye'elimite cements, *Mater*
2128 *Struct*, 51 (2018) #128.

2129 [376] T. Duvallet, Y. Zhou, K.R. Henke, T.L. Robl, R. Andrews, Effects of ferrite concentration
2130 on synthesis, hydration and mechanical properties of alite-calcium sulfoaluminate-ferrite cements,
2131 *J Sust Cement-Based Mater*, 6 (2017) 85-110.

2132 [377] M. Ben Haha, F. Bullerjahn, M. Zajac, On the reactivity of ternesite, 14th International
2133 Congress on the Chemistry of Cement, Beijing, 2015.

2134 [378] M. Montes, E. Pato, P.M. Carmona-Quiroga, M.T. Blanco-Varela, Can calcium aluminates
2135 activate ternesite hydration?, *Cem Concr Res*, 103 (2018) 204-215.

2136 [379] M.T. Blanco-Varela, P.M. Carmona-Quiroga, Ternesite as a component of sulfobelitic
2137 cements, *MATEC Web Conf.*, 149 (2018) #01011.

2138 [380] T. Hanein, I. Galan, F.P. Glasser, S. Skalamprinos, A. Elhoweris, M.S. Imbabi, M.N.
2139 Bannerman, Stability of ternesite and the production at scale of ternesite-based clinkers, *Cem.*
2140 *Concr. Res.*, 98 (2017) 91-100.

2141 [381] I. Galan, T. Hanein, A. Elhoweris, M.N. Bannerman, F.P. Glasser, Phase compatibility in
2142 the system $\text{CaO-SiO}_2\text{-Al}_2\text{O}_3\text{-SO}_3\text{-Fe}_2\text{O}_3$ and the effect of partial pressure on the phase stability,
2143 *Ind. Eng. Chem. Res.*, 56 (2017) 2341-2349.

2144